Photophysicochemical properties and *in vitro* photodynamic therapy activities of zinc phthalocyanine conjugates with biomolecules and single-walled carbon nanotubes

A thesis submitted in fulfilment of the requirements for the degree of

DOCTOR OF PHILOSOPHY

Of

RHODES UNIVERSITY

By

RACHEAL ODIRI OGBODU

January 2015

DEDICATION

To the TRIUNE GOD: whose LOVE sought me, whose BLOOD bought me and GRACE keeping me in His FAMILY

To my Treasured Mother:

Hannah Omokri Ogbodu

To my Dearest Brother:

Daniel Ogaga Ogbodu

ACKNOWLEDGMENTS

"Being confident of this very thing, that he (God) which hath begun a good work in me will perform it until the day of Jesus Christ". Philippians 1:6

My profound gratitude goes to Almighty God for everything; His mercies, grace, love, wisdom, strength, intuition, understanding and knowledge, throughout the program and still counting.

My sincere appreciation goes to my supervisor, Distinguished Prof Tebello Nyokong for her constructive and positive criticism, promptness and supervision of this research work.

I am deeply indebted to my treasured mother and dearest brother for their; support, prayers, sacrifice, encouragement, understanding, love, faith: what more can I say, for everything. I cannot but say a big thank you to big daddy and mummy Umukoro, daddy and mummy Renew, Pastor Adeshina, all my spiritual leaders and "*loved ones*" whose prayers, love, care, concern and words of encouragement kept me throughout this program and still counting.

My gratitude goes to my bible study family in South Africa (Bola, David, Odun, Stephen, Moreen, Audacity, Gugu, Abram, Racheal, Mhlangulele among others) for time spent together sharing the ever living word of God. I also want to thank my dearest friends Dorcas Egede and Oluwasegun Awolope for always being there for me.

I want to thank the S22 family and colleagues for making the laboratory and research road pliable and my big friend in the lab: Adedayo Fashina and mentor Phindile for always being there. I wish you all well, you will forever be remembered. My utmost appreciation also goes to the following persons: Dr Antune, Dr Britton, Dr Mack, Dr Amuhaya, members of staffs and postgraduate students in the Chemistry department of Rhodes University, South Africa.

Financial and post graduate fellowship fund from the Organization for Women in Science for the Developing World (OWSD) is gratefully acknowledged.

ABSTRACT

The synthesis, photophysicochemcial properties, *in vitro* dark toxicity and photodynamic therapy (PDT) activities of different derivatives of zinc phthalocyanine (ZnPc) conjugates with biomolecules (folic acid, bovine serum albumin (BSA), ascorbic acid, uridine or spermine) and single-walled carbon nanotubes (SWCNTs) are presented in this work. The fluorescence quantum yields (Φ_F) of the ZnPc derivatives or ZnPc-biomolecule conjugates remained relatively the same as compared to the precursor Pcs. Slight increases were observed in the Φ_F values of conjugates containing substituents such as pyrene, folic acid or BSA with intrinsic fluorescence properties.

The triplet quantum yield (Φ_T) values for some ZnPc conjugates increases compared to the precursor ZnPcs due to extended π conjugation (for the conjugate with pyrene) and the presence of phenyl ring that support spin-orbit charge transfer intersystem crossing to triplet state. While some conjugates showed decreases in the Φ_T values compared to precursor ZnPcs due to the presence of substituents that could quench photo-excited state properties. The singlet oxygen quantum yield (Φ_Δ) values follow the trends of the triplet quantum yield values. The conjugates containing BSA also show increases in the Φ_Δ values without corresponding increases in Φ_T values due to the ability of BSA to generate free radicals including singlet oxygen.

The presence of SWCNTs decreases the photophysicochemcial properties of some ZnPc-SWCNT conjugates compared to the precursor ZnPcs due to photo-induced electron transfer from an excited Pc complex (electron donor) to SWCNTs (electron acceptor). However, increases were observed in some ZnPc-SWCNT conjugates as a result of fast charge recombination process due to highly short-lived radical ion pair produced. These phenomena

affected the Φ_F values, Φ_T values, and the Φ_Δ values. Increases or decreases in Φ_T values resulted in corresponding increases or decreases in Φ_Δ values.

The cytotoxicity viability tests show that all the tested ZnPc and ZnPc-SWCNT conjugates were relatively not toxic when gradient concentrations of respective complexes were treated *in vitro* on either A375 melanoma or MCF-7 breast cancer cells. All the ZnPc conjugates except the ones with ascorbic acid enhanced PDT effects. Ascorbic acid suppresses the PDT effects of Pc complexes due to its ability to reduce oxidative deoxyribonucleic acid (DNA) damage and its potent reducing properties. ZnPc-SWCNT conjugates showed relatively the same phototoxicity as the precursor ZnPc conjugates contradicting the low singlet oxygen quantum yields observed for the former. The findings from this work show the importance of combination therapy which gives the advantage of a dual modality drug protocol, where the ZnPc derivatives are the photodynamic agents and SWCNTs is the photothermal agent.

CONTENT

LIST OF ABBREVIATIONS

MPcs	=	Metallophthalocyanines
Pc	=	Phthalocyanine
PDT	=	Photodynamic therapy
FA	=	Folic acid
BSA	=	Bovine serum albumin
AA	=	Ascorbic acid
HOMO	=	Highest occupied molecular orbital
LOMO	=	Lowest unoccupied molecular orbital
H_2O_2	=	Hydrogen peroxide
DNA	=	Deoxyribonucleic acid
MCF-7	=	Michigan Cancer Foundation-7
TAP	=	Tetraaminophenoxy
MAP	=	Monoaminophenoxy
OC	=	Octacarboxy
MA	=	Monoamino
MCP	=	Monocarboxyphenoxy
t-Bu	=	Tert-butyl
SWCNTs	=	Single-walled carbon nanotubes
CNTs	=	Carbon nanotubes
PTT	=	Photothermal therapy
XRD	=	X-ray diffraction
TGA	=	Thermal gravimetric analysis

TEM	=	Transmission electron microscopy
F	=	Fluorescence
P	=	Phosphorescence
IC	=	Internal conversion
VR	=	Vibrational relaxation
ISC	=	Intersystem crossing
Et	=	Electron transfer
S_1	=	Singlet excited state
T_1	=	Triplet excited state
TCSPC	=	Time-correlated single-photon counting
Ket	=	Photo-induced energy transfer rate constant
PET Eff.	=	Electron transfer efficiency
DPBF	=	1,3-diphenylsobenzofuran
DABCO	=	1,4-diazabicyclo-octane
ADMA	=	Tetrasodium-α,α-(anthracene-9,10-diyl) dimethylmalonate
NaN_3	=	Sodium azide
DMAP	=	Dimethylaminopyridine
TFA	=	Trifluoroactetic acid
EDC	=	1-Ethyl-3-(3-dimethylaminoproplyl) carbodiimide hydrochloride
NHS	=	9,10-N-hydroxysuccinimide
DCC	=	Dicyclohexylcarbodiimide
DMSO	=	Dimethylsulfoxide
DCM	=	Dichloromethane

DMF	=	*N*,*N*-dimethylformamide
EtOH	=	Ethanol
MeOH	=	Methanol
THF	=	Tetrahydrofuran
FT-IR	=	Fourier transformed infrared spectroscopy
ATR	=	Attenuated total reflectance
NMR	=	Nuclear magnetic resonance
UV-Vis	=	Ultra-violet visible spectroscopy
Py	=	1-pyrene-1-carboxaldehyde
DMEM	=	Dulbecco's modified eagle's medium
DPBS	=	Dulbecco's phosphate buffer saline
FBS	=	Fetal bovine serum
NR	=	Neutral red
WST	=	Water soluble tetrazolium
SOCT	=	Spin-orbit charge transfer
RP	=	Radical-pair
ROS	=	Reactive oxygen specie
amu	=	atomic mass unit

LIST OF SYMBOLS

β	=	Peripheral position
α	=	Non-peripheral position
$^3O_2$	=	Molecular oxygen
$^1O_2$	=	Singlet oxygen
τ_F	=	Fluorescence life-time
Φ_F	=	Fluorescence quantum yield
ns	=	Nanoseconds
Q_F	=	Quenching factor
τ_T	=	Triplet life-time
Φ_T	=	Triplet quantum yield
μs	=	Microseconds
ms	=	Milliseconds
Φ_Δ	=	Singlet oxygen quantum yield
ε_s	=	Molar extinction coefficient
S_Δ	=	Energy transfer efficiency

LIST OF FIGURES

LIST OF SCHEMES

LIST OF TABLES

CHAPTER ONE

1. INTRODUCTION

This chapter provides an overview of spectra, photophysical and photochemical properties of phthalocyanine and their conjugates with biological molecules and single-walled carbon nanotubes. The possible applications of the conjugates as photodynamic therapy agents against cancer cells are also presented.

1.1 Metallophthalocyanines (MPcs)

Metallophthalocyanines (MPcs) are two-dimensional 18 π-electron aromatic porphyrin synthetic analogues, consisting of four isoindole subunits linked together through nitrogen atoms (Fig 1.1). The exclusive properties of MPcs which arise from their electronic delocalization and extensive hetero-aromatic π-conjugation have made them one of the most studied compounds. These properties include: thermal and chemical stability, effective singlet oxygen generation, their low toxicity in the absence of light, intense absorption in the red region of the visible spectrum, as well as selective localization in tumors [1-7]. MPcs have found applications in various fields including as electrochemical sensors [8], in nonlinear optics [9] and more importantly for this work as photosensitizers in photodynamic therapy (PDT) [10-12]. The physical, electronic and optical properties of MPc complexes can be further modified by introducing substituents to the peripheral (β) or non-peripheral (α) position of the phthalocyanine ring [13-16]. This work focuses on the synthesis, photophysical and photochemical properties of β-substituted zinc phthalocyanine (ZnPc) derivatives and their conjugates with molecules of biological importance for applications in PDT. ZnPc was chosen because its derivatives are in clinical trials [10] and the presence of biological molecules, such as; folic acid (FA), bovine serum albumin (BSA), ascorbic acid (AA), uridine and spermine in ZnPc structure will impart specificity and selectivity of the ZnPc to cancer cells as well as improve PDT effect.

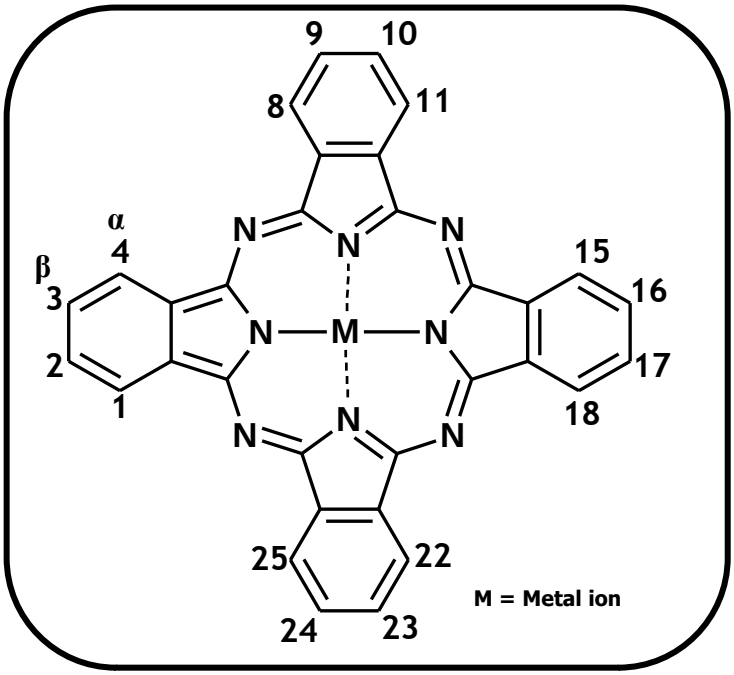

Fig. 1.1: General structure of Metallophthalocyanine.

1.1.1 Spectra properties of metallophthalocyanines (MPcs)

Metallophthalocyanines have two characteristics peaks, known as the Q-band (the most intense band) and the B-band (consisting of two bands). The Q-band is from 650 nm and can go beyond 1000 nm, while the B-band is between 300 - 400 nm, (Fig. 1.2) [17,18]. Using Gouterman's four orbital model [19] the Q-band is due to the transition between the ground state a_{1u} highest occupied molecular orbital (HOMO) to e_g lowest unoccupied molecular orbital (LUMO), while the B-bands correspond to the a_{2u} to e_g and b_{2u} to e_g transitions. Symmetrically substituted MPc are characterized by a single Q-band while unmetallated Pcs and unsymmetrically substituted MPcs might display split Q-band depending on the solvent [20].

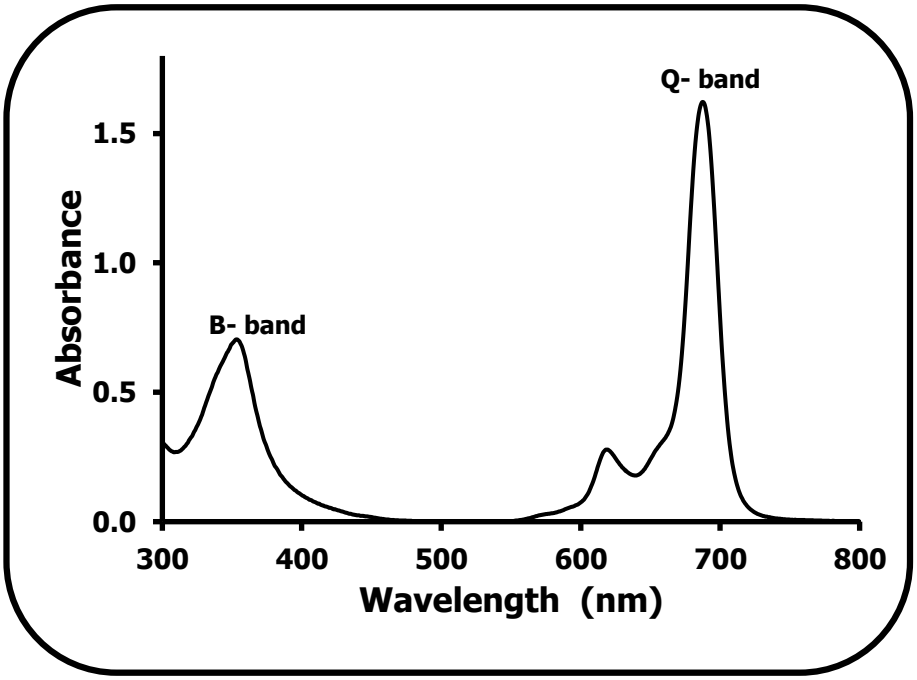

Fig. 1.2: Typical electronic absorption spectra of metallophthalocyanine.

1.1.2 General synthesis of symmetrical and unsymmetrical A_3B type MPcs

Metallophthalocyanines can be substituted in 16 possible positions around the ring as shown in Fig. 1.1. Positions 1(4), 8(11), 15(18) and 22(25) are the non-peripheral (α) positions, while positions 2(3), 9(10), 16(17) and 23(24) are the peripheral (β) positions. Substitution on one (or two) β position results in tetra (or octa) substituted symmetrical MPcs. The general synthesis of symmetrical metal free Pcs, involves the condensation of a mono (or di-) substituted phthalonitrile for tetra (or octa) substituted Pcs respectively [21]. The synthetic route for tetra-substituted Pc at the β position is shown in Scheme 1.1.

In recent years there has been increasing interest in unsymmetrical MPc derivatives, which provides one point of co-ordination, whilst exhibiting unique set of properties required for use in

specific practical applications; such as PDT, materials science and optical limiting applications [22]. Statistical condensation of two differently substituted phthalonitriles is widely employed in the synthesis of A_3B-type unsymmetrical MPcs. The desired MPcs bear one different (B) isoindole subunit and three identical (A) subunits. The condensation of A and B isoindole subunits often result in a mixture of six compounds (Scheme 1.2). The common mole ratio of A and B is 3:1, a larger mole ratio of 9:1 or higher could be employed due to different reactivity of the substituents [23,24]. Both symmetrical and the A_3B-type unsymmetrical ZnPcs conjugates with different biological molecules (FA, AA, BSA, uridine or spermine) were synthesized in this work.

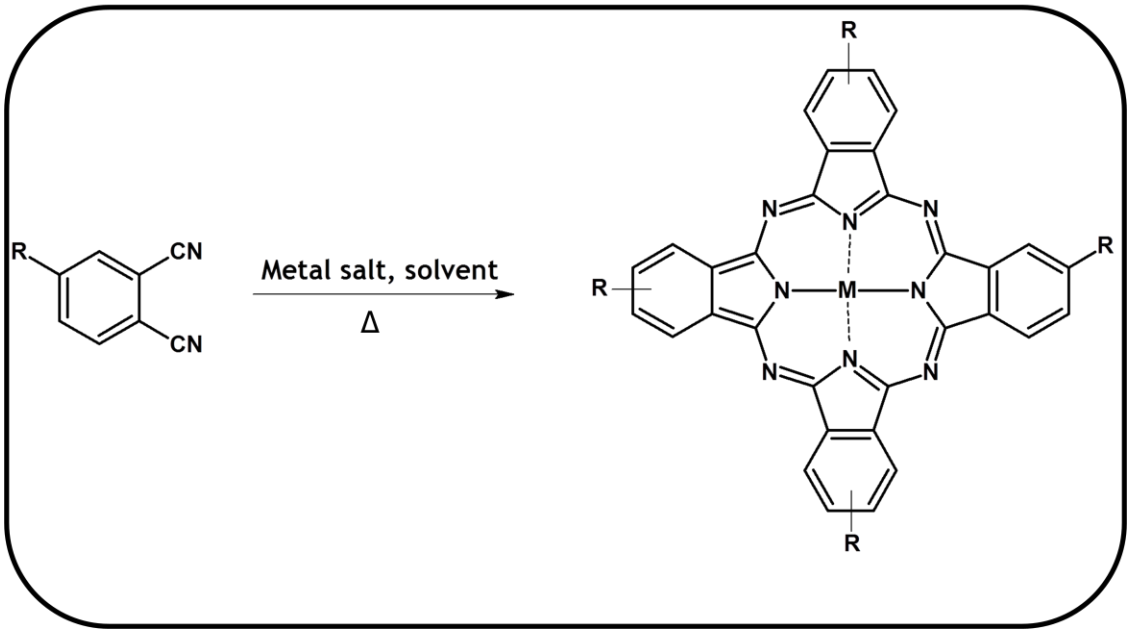

Scheme 1:1: Synthetic route for tetra-substituted Pcs (peripheral position).

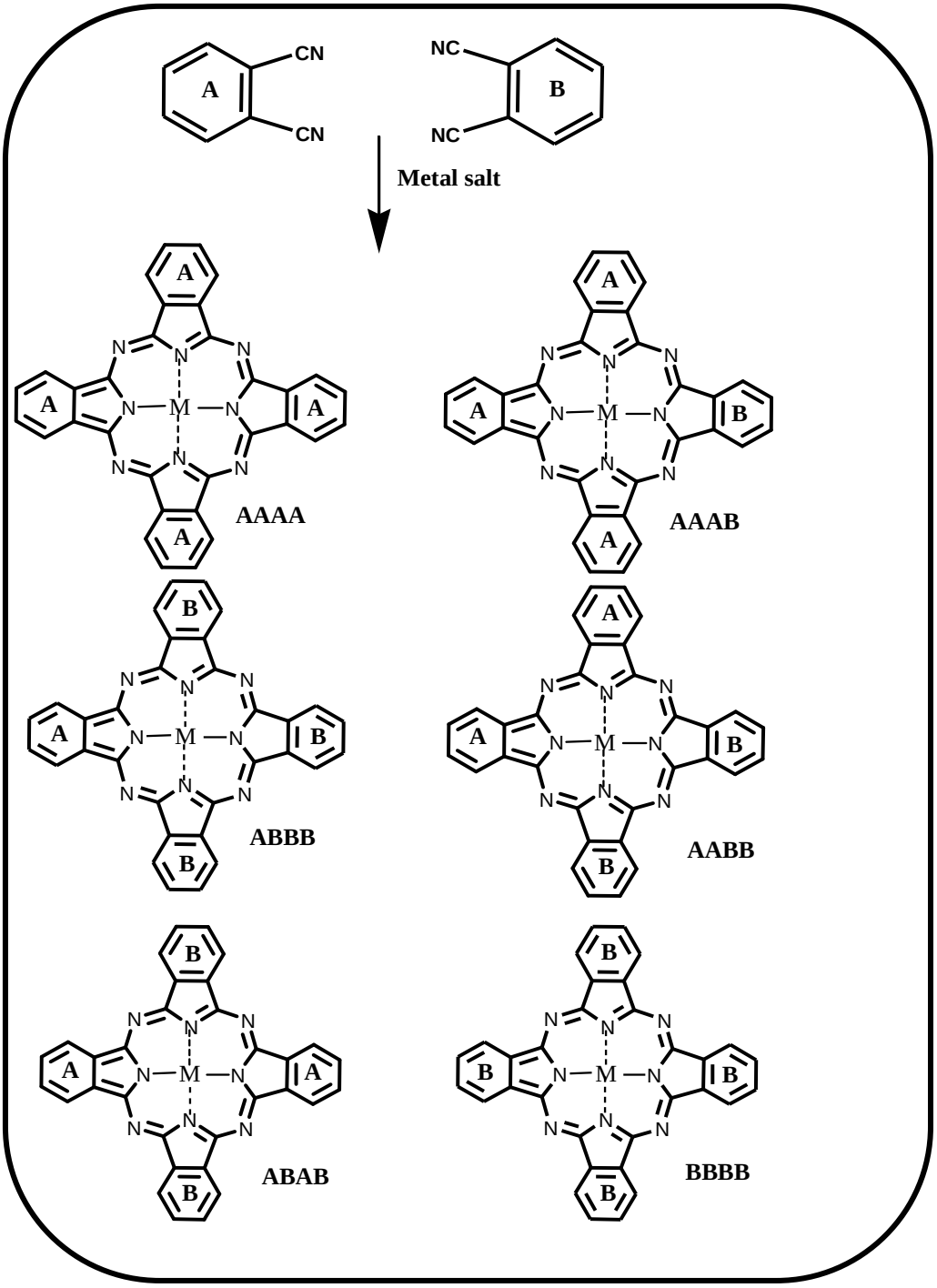

Scheme 1.2: Statistical condensation of two phthalonitriles to give six possible MPc products. (A) 1,2-dicyanobenzene and (B) substituted ring.

1.1.3 Use of metallophthalocyanines in photodynamic therapy

Photodynamic therapy (PDT) has continued to gain attention as an effective treatment approach for some cancers. PDT involves administration of a tumor localizing photosensitizing agent, followed by activation of the photosensitizer by light of a specific wavelength. This then results in a sequence of photochemical processes that cause irreversible photo-damage to tumor cells [8,25]. Some MPcs have been reported to show long triplet life-times and high triplet quantum yields and hence can effectively interact with ground state molecular oxygen ($^3O_2$) to generate singlet oxygen ($^1O_2$) (the chief cytotoxic species responsible for cancerous cells destruction) [7,8,10]. Thus, MPcs (containing metals such as zinc, aluminum, silicon) are good candidates as photosensitizers for PDT. Examples of MPcs derivatives containing Zn, Al or Si metal in clinical trials for PDT are shown in Fig. 1.3.

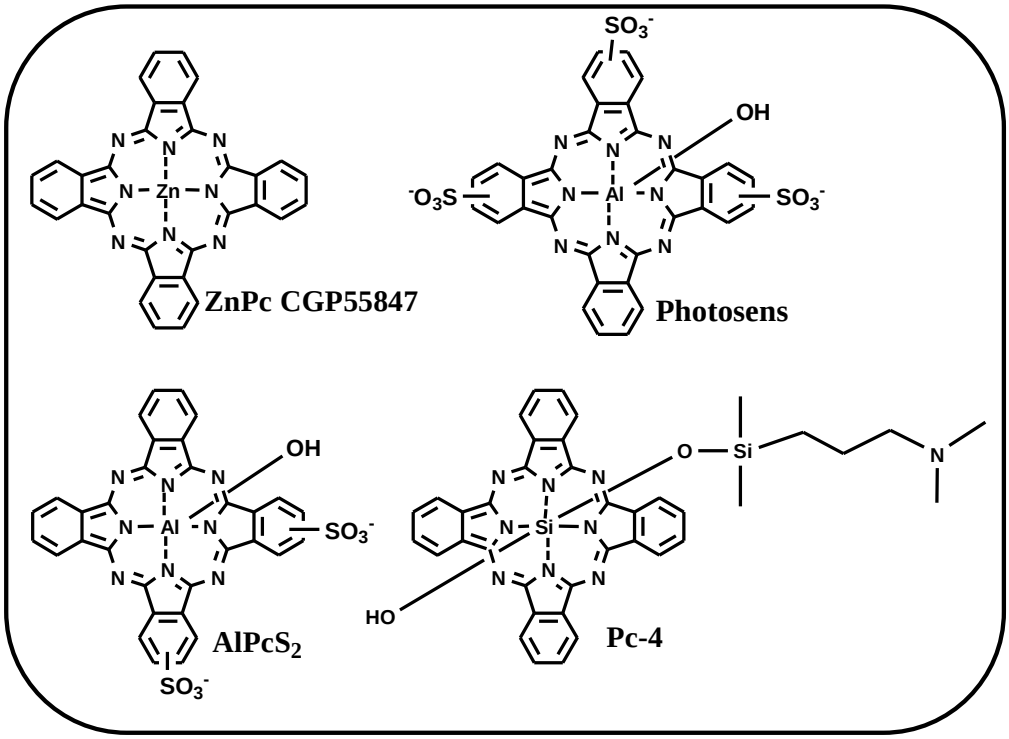

Fig. 1.3: MPc derivatives in clinical trials.

1.1.4 Use of MPc-biomolecule conjugates in photodynamic therapy-overview

One of the ways to improve MPcs in selective tumor destruction in PDT is to develop targeting strategies which include conjugating MPcs to compounds such as biomolecules that are over-expressed in cancer cells [26-28].

Folate receptors are over expressed in a number of cancer cells, including malignancies of the ovary, brain, kidney, breast, colon and lung [29-31], thus the presence of folic acid (FA) in MPc will improve solubility, specificity and selectivity of MPc to tumor cells in PDT.

Ascorbic acid (AA) has a long history in the treatment of cancer. Cameron et al [32-34] showed that patients who received ascorbate survived 300 days longer than controls. Studies have shown that the intravenous administration of ascorbate in pharmacological concentrations can selectively kill cancer cells [35-38] as a result of its ability to generate hydrogen peroxide (H_2O_2) that can further produce free radicals and singlet oxygen. Ascorbic acid is a well-known antioxidant and would be expected to quench singlet oxygen and other reactive oxygen species (ROS) required for PDT. The combination of AA and MPc will be examined.

Studies have shown that uridine has anticancer properties [39-43]. Haakensen et al [44] also showed that uridine 5′-diphospho-glucuronosyltransferase is over expressed in breast cancer. Uridine will improve the potency of MPc in PDT.

Bovine serum albumin (BSA) belongs to the family of serum albumins which are the major soluble protein constituent of the circulatory system, and has several physiological functions including use as transport and depot protein for varieties of compounds [45]. Studies have shown that albumin binding proteins (ABPs) interact with normal endothelial and tumor cells [46]. Thus, BSA may improve the selectivity of MPc to cancer cells.

Spermines are found in nature and have been shown to have a variety of biological functions [47-50]. Spermine is an example of polyamines, which are essential for cell growth due to their ability to bind strongly to deoxyribonucleic acid (DNA) through electrostatic interactions and thus, positively affect replication, transcription of cells, among other functions [51]. Rapidly proliferating tumor cells contain high concentration of polyamines [52]. Thus, the linking of spermine to an anticancer agent such as MPc, will facilitate both uptake of the conjugate and its targeting to DNA.

The PDT activity of some ZnPc derivatives and biomolecule conjugates against different cancer cell lines are shown in Table 1.1 [53-60]. The photophysical, photochemical properties and cell studies of ZnPc covalently linked to folic acid have been reported [60,61], however the Pc involved was tetra- substituted. In this work a more defined binding is achieved by linking a mono-substituted ZnPc to folic acid. The photophysical properties of octa carboxy ZnPc chemically linked to BSA was also studied in the current work instead of the unsubstituted ZnPc adsorbed on single-walled carbon nanotubes (SWCNT-COOH) and linked to BSA reported in literature [53] Table 1.1. In the reported conjugate, there was no direct link between BSA and the Pc while there is a direct link in this work. There are no reports on pyrene, spermine, uridine or AA conjugates with MPcs.

All the biomolecules conjugated to MPc used in this work are either over-expressed in tumors or are needed for cell proliferation. The photophysical and photochemical properties (such as triplet life-times and quantum yields, fluorescence life-times and quantum yields, singlet oxygen quantum yields), cytotoxicity and PDT activities on either A375 melanoma cells or MCF-7 breast cancer cells of mono-substituted ZnPc derivatives conjugated to biomolecules such as folic acid, spermine, uridine and ascorbic acid are reported for the first time.

Table 1.1: PDT activities of some ZnPc derivatives on different cancer cell lines

ZnPc -Conjugates	Cancer cell line	REF
Unsubstituted ZnPc adsorbed on SWCNT-COOH and linked to BSA	5RP7 cells (rat fibroblasts transformed by the c-Ha-ras oncogene)	[53]
ZnPc differently substituted with benzo-units	HCT116 cell line (human colon adenocancer)	[54]
ZnPc coupled to boron (tetra)	B16F1 melanotic melanoma cells	[55]
ZnPc substituted with 3-aminopropyloxy (octa)	MCF-7c3 breast cancer cells	[56]
di-ZnPc substituted with 11,11'dithiodiundecyl and linked to antibody polyethylene glycol-gold nanoparticle conjugate	SK-BR-3 and MDA-MB 231 Breast cancer cell lines and MCF-10A normal mammary epithelial cells	[57]
ZnPc substituted with 1,6-hexanedithiol (tetra) and linked to gold nanoparticles	MCF-7 breast cancer cells and healthy fibroblast cells	[58]
ZnPc differently substituted with sulphonate and phthalimidomethyl group	HCC HepG2, BGC823 and AGS gastric cancer, SH-SY5Y neuroblastoma cells, GES-1 normal noncancerous gastric epithelial cells and HELF embryonic lung fibroblast cells. All from human	[59]
ZnPc linked to folic acid (tetra)	Human nasopharyngeal epidermal cancer	[60]

tetra = tetra substituted, octa = octa substituted

1.2 Metallophthalocyanines (MPc-biomolecule conjugates) synthesized in this work

This work focuses on the synthesis of ZnPc derivatives, since they have been reported to show desirable photophysical and photochemical properties ideal for PDT [62-64], the ZnPcs derivatives used in this work are substituted in the peripheral positions. The structures of ZnPc (or ZnPc-biomolecule conjugates) use in this work are shown in Table 1.2. The synthesis of complexes **1** [65], **4** [66], **8** [67], **10** [68], **12** [69] and **13** [70] have been reported in literature; while **2**, **3**, **5**, **6**, **7**, **9** and **11** are reported for the first time in this work. The synthetic routes adopted are known in literature, using the carbodiimide chemistry method [53,61,71,72].

Complex **2** (ZnMAPc-Py) contains pyrene (Py) which is not a biological molecule but a fluorescent material. The linking of fluorescent pyrene to a Pc may influence the fluorescence characteristics on the aromatic structure [73,74]. On the other hand, it has been reported [75] that aromatic groups that are part of the Pc pi (π) system can enhance intersystem crossing, this would result in enhanced singlet oxygen production. In this work pyrene forms part of the Pc π conjugation, it was shown to improve the triplet quantum yields, singlet oxygen quantum yields while at the same time it positively influences the fluorescence behaviour of the conjugates.

The synthesized complexes are represented as: Zinc monoamino Pc (ZnMAPc (**1**)), ZnMAPc linked to pyrene (ZnMAPc-Py (**2**)), ZnMAPc linked to folic acid (ZnMAPc-FA (**3**)), Zn monocarboxyphenoxy Pc (ZnMCPPc (**4**)), ZnMCPPc linked to spermine (ZnMCPPc-spermine (**5**)), ZnMCPPc linked to uridine (ZnMCPPc-uridine (**6**)), ZnMCPPc linked to ascorbic acid (ZnMCPPc-AA (**7**)), Zn tetracarboxyphenoxy Pc ZnTCPPc (**8**) linked to ascorbic acid (ZnTCPPc-AA (**9**)), Zn octacarboxy Pc ZnOCPc (**10**) linked to bovine serum albumin (ZnOCPc-BSA (**11**)), Zn monoaminophenoxy Pc (ZnMAPPc (**12**)), Zn tetraaminophenoxy Pc (ZnTAPPc (**13**)).

Table 1.2: List and structures of ZnPc (or ZnPc-biomolecule conjugates) studied

ZnPcs	STRUCTURE	STUDIES
R = H_2 ZnMAPc (**1**) R= Py ZnMAPc-Py (**2**)	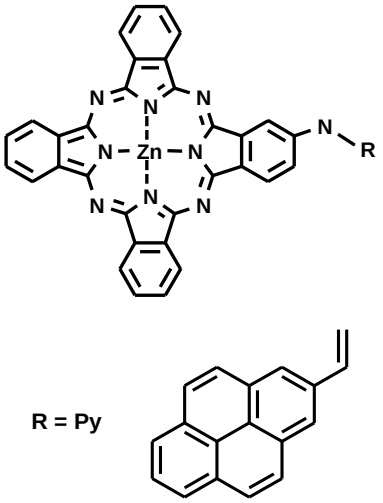	**Photophysical and photochemical studies:** fluorescence quantum yields and life-times, triplet quantum yields and life-times and singlet oxygen quantum yields
ZnMAPc-FA (**3**)	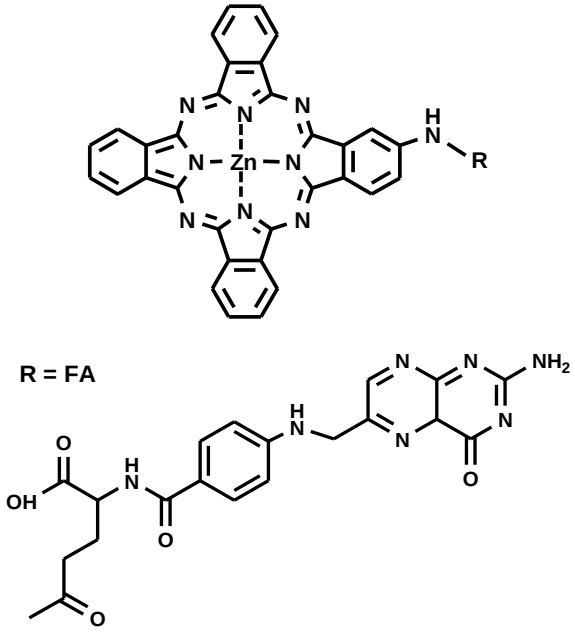	**Photophysical and photochemical studies:** fluorescence quantum yields and life-times, triplet quantum yields and life-times and singlet oxygen quantum yields **Cell studies:** cytotoxicity and PDT effects on A375 melanoma cells and MCF-7 breast cancer cells

MAPc = monoamino Pc, FA = folic acid, Py = pyrene

Table 1.2 contd.

ZnPcs	STRUCTURE	STUDIES
R = OH ZnMCPPc (**4**) R= spermine ZnMCPPc-spermine (**5**) R= uridine ZnMCPPc-uridine (**6**) R = AA ZnMCPPc-AA (**7**)	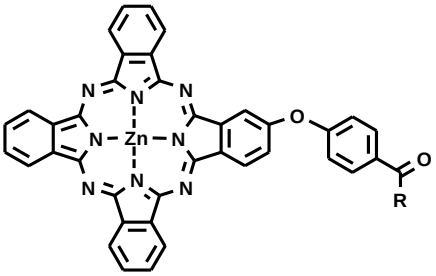 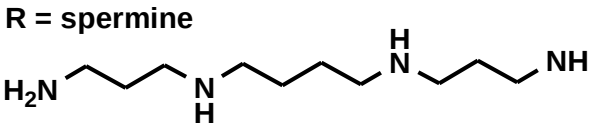 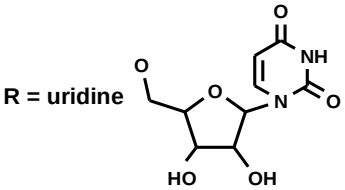 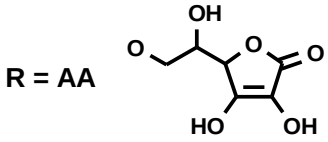	**Photophysical and photochemical studies:** fluorescence quantum yields and life-times, triplet quantum yields and life-times and singlet oxygen quantum yields **Cell studies:** cytotoxicity and PDT effects on MCF-7 breast cancer cells
ZnTCPPc (**8**)	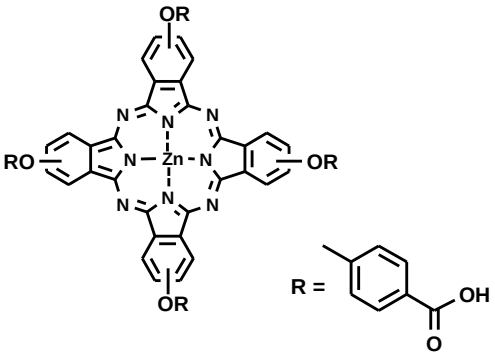	**Photophysical and photochemical studies:** fluorescence quantum yields and life-times, triplet quantum yields and life-times and singlet oxygen quantum yields

MCPPc = monocarboxyphenoxy Pc, TCPPc = tetracarboxyphenoxy Pc, AA = ascorbic acid

Table 1.2 contd.

ZnPcs	STRUCTURE	STUDIES
ZnTCPPc-AA (**9**)	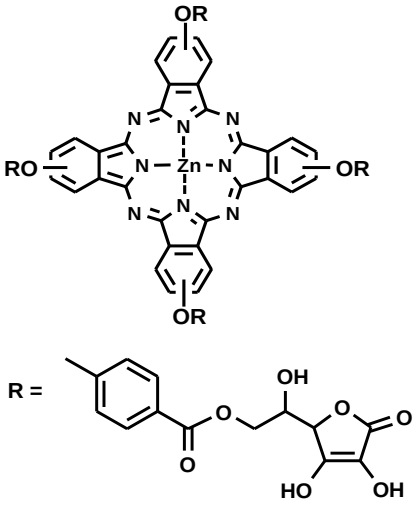	**Photophysical and photochemical studies:** fluorescence quantum yields and life-times, triplet quantum yields and life-times and singlet oxygen quantum yields
R = OH ZnOCPc (**10**)	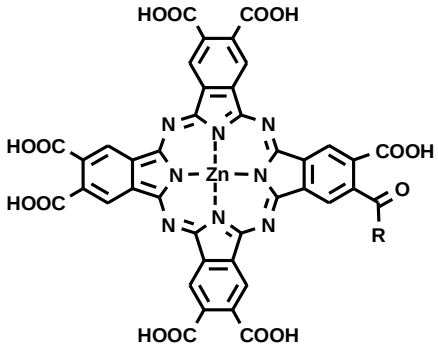	
R = BSA ZnOCPc-BSA (**11**)	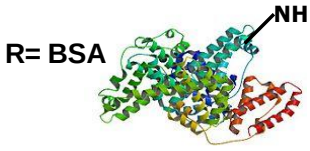	
ZnMAPPc (**12**)	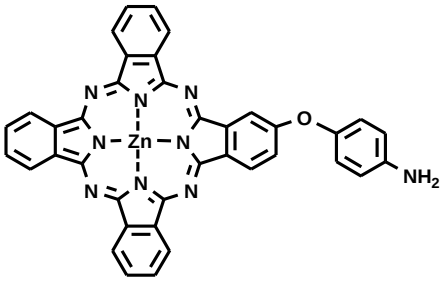	

OCPc = octacarboxy Pc, MAPPc = monoaminophenoxy Pc, BSA = bovine serum albumin, TCPPc = tetracarboxyphenoxy Pc, AA = ascorbic acid

Table 1.2 contd.

ZnPcs	STRUCTURE	STUDIES
ZnTAPPc (**13**)	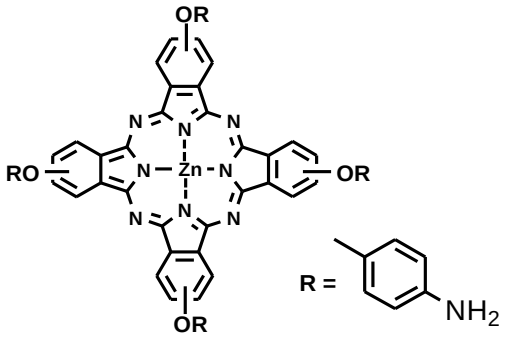	**Photophysical and photochemical studies:** fluorescence quantum yields and life-times, triplet quantum yields and life-times and singlet oxygen quantum yields

TAPPc = tetraaminophenoxy Pc

1.3 Single-walled carbon nanotubes (SWCNTs)

Single-walled carbon nanotubes (SWCNTs) are graphene sheets rolled up into a nanoscale-tube, with diameters ranging from 0.4 - 2 nm and lengths of several microns (Fig.1.4) [76-79]. SWCNTs consist entirely of elemental carbon in the sp^2 hybridization. They are one-dimensional nano materials that readily accept charge when interfaced with excited-state electron donors via functionalization [80]. The properties of SWCNTs can be tuned via functionalization which could be achieved by either covalent or non-covalent interaction. Covalent functionalization involves the introduction of functional groups to either the ends or the side wall of the SWCNTs by creating defect sites through oxidation. This process affects the extended π system of the SWCNTs backbone, thus influencing its electronic properties [13-16,81]. Non-covalent functionalization (adsorption), on the other hand, involves interaction between aromatic groups and the sidewalls of the SWCNTs [82-84], and this has the major advantage of preserving the properties of SWCNTs since the carbon backbone is not affected. Functionalized SWCNTs have

the additional advantage of increasing drug specificity and increasing their solubility in aqueous media (such as blood). Unlike unfunctionalized SWCNTs which have hydrophobic surface [85], functionalized SWCNTs have the ability to move across cellular membranes with less cytotoxic effects compared to the unfunctionalized SWCNTs [86]. All the SWCNTs used in this work were functionalized either through chemical linking or adsorption of MPcs (or MPc-biomolecule conjugates). Their photophysical and photochemical properties were studied, and the cytotoxicity and PDT effects of some selected MPc-SWCNT conjugates were tested on either A375 melanoma cells or MCF-7 breast cancer cells.

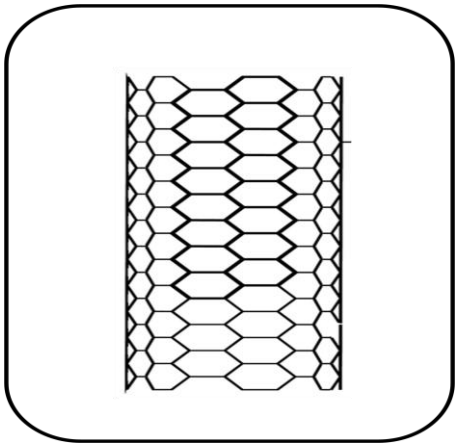

Fig. 1.4: Diagrammatic representation of SWCNTs.

1.3.1 Applications of single-walled carbon nanotubes in photothermal (PTT) and photodynamic therapy (PDT)

SWCNTs have emerged as a potential delivery systems for therapeutic molecules due to their remarkable properties which include their high aspect ratio, hollow and cage like interior [87], and high surface area [80], through which drugs can be anchored and transported into the cells. SWCNTs absorb light in the near infrared region and they may induce cell death by a localized

heating effect known as photothermal therapy (PTT) [88]. SWCNTs have being widely applied in either PTT or in combined cancer therapy (PDT and PTT). Zhang et al [53] have reported on the double cancer therapy system using PDT and PTT on cancer cell line, where unsubstituted ZnPc is the PDT agent and SWCNTs is the PTT agent. SWCNTs have been used in the treatment of melanoma cells [89] as PTT agents.

1.3.2 Synthesis of MPc-SWCNT (or MPc-biomolecule-SWCNT) conjugates

Metallophthalocyanines used in this work, were either linked or adsorbed on SWCNT-COOH according to literature methods. The adsorption was through π-π interaction between the MPc and SWCNTs [71]. All the ZnPc-SWCNTs derivatives (**14 - 28**) studied are reported for the first time and they are listed in Table 1.3.

Table 1.3: List of ZnPcs (or ZnPc-biomolecule conjugates) linked to (or adsorbed on) SWCNTs

ZnPc (or ZnPc conjugate)	**SWCNTs type**	**Abbreviation**	**STUDIES**
ZnMAPc-FA (**3**)	SWCNTs	ZnMAPc-FA-SWCNT (adsorbed) (**14**)	**Photophysical and photochemical studies:** fluorescence quantum yields and life-times, triplet quantum yields and life-times and singlet oxygen quantum yields **Cell studies:** cytotoxicity and PDT effects on MCF-7 breast cancer cells **3** and **14** were also tested on A375 melanoma cells
ZnMCPPc (**4**)	SWCNT-COOH	ZnMCPPc-SWCNT (adsorbed) (**15**)	
ZnMCPPc-spermine (**5**)	SWCNT-COOH	ZnMCPPc-spermine-SWCNT (adsorbed) (**16**)	
ZnMCPPc-uridine (**6**)	SWCNT-COOH	ZnMCPPc-uridine-SWCNT (adsorbed) (**17**)	
ZnMCPPc-AA (**7**)	SWCNT-COOH	ZnMCPPc-AA-SWCNT (adsorbed) (**18**)	
ZnMAPc (**1**)	SWCNT-COOH	ZnMAPc-SWCNT (linked) (**19**)	**Photophysical and photochemical studies:** fluorescence quantum yields and life-times, triplet quantum yields and life-times and singlet oxygen quantum yields
ZnMAPc-Py (**2**)	SWCNTs	ZnMAPc-Py-SWCNT (adsorbed) (**20**)	
ZnTCPPc (**8**)	SWCNT-COOH	ZnTCPPc-SWCNT (adsorbed) (**21**)	
ZnTCPPc-AA (**9**)	SWCNT-COOH	ZnTCPPc-AA-SWCNT (adsorbed) (**22**)	
ZnOCPc (**10**)	SWCNT-COOH	ZnOCPc-SWCNT (adsorbed) (**23**)	

Table 1.3 contd.

ZnPc (or ZnPc conjugate)	**SWCNTs type**	**Abbreviation**	**STUDIES**
ZnOCPc-BSA (**11**)	SWCNT-COOH	ZnOCPc-BSA-SWCNT (adsorbed) (**24**)	**Photophysical and photochemical studies:** fluorescence quantum yields and life-times, triplet quantum yields and life-times and singlet oxygen quantum yields
ZnMAPPc (**12**)	SWCNT-COOH	ZnMAPPc-SWCNT (linked) (**25**)	
ZnMAPPc (**12**)	SWCNT-COOH	ZnMAPPc-SWCNT (adsorbed) (**26**)	
ZnTAPPc (**13**)	SWCNT-COOH	ZnTAPPc-SWCNT (linked) (**27**)	
ZnTAPPc (**13**)	SWCNT-COOH	ZnTAPPc-SWCNT (adsorbed) (**28**)	

ZnTAPPc and ZnMAPPc were linked to and adsorbed on SWCNTs, All the ZnPc-biomolecule derivatives were adsorbed onto SWCNTs.

1.4 Photophysical and photochemical parameters

The photophysical and photochemical properties of MPcs are fundamental in their applications, especially in PDT. The photophysicochemical properties of MPcs depend on their electronic properties at the photo-excited state. The Jablonski diagram [90-92] (Fig. 1.5) closely explains the electronic properties of a photo-excited MPcs molecule through radiative (fluorescence (F), phosphorescence (P)) and non-radiative (internal conversion (IC), vibrational relaxation (VR), intersystem crossing (ISC)) processes [91]. The MPcs studied in this work contained zinc as the central metal in order to encourage intersystem crossing to triplet state (long-lived), where the

molecule can interact with molecular oxygen ($^3O_2$) to generate singlet oxygen ($^1O_2$) which is of particular importance in PDT.

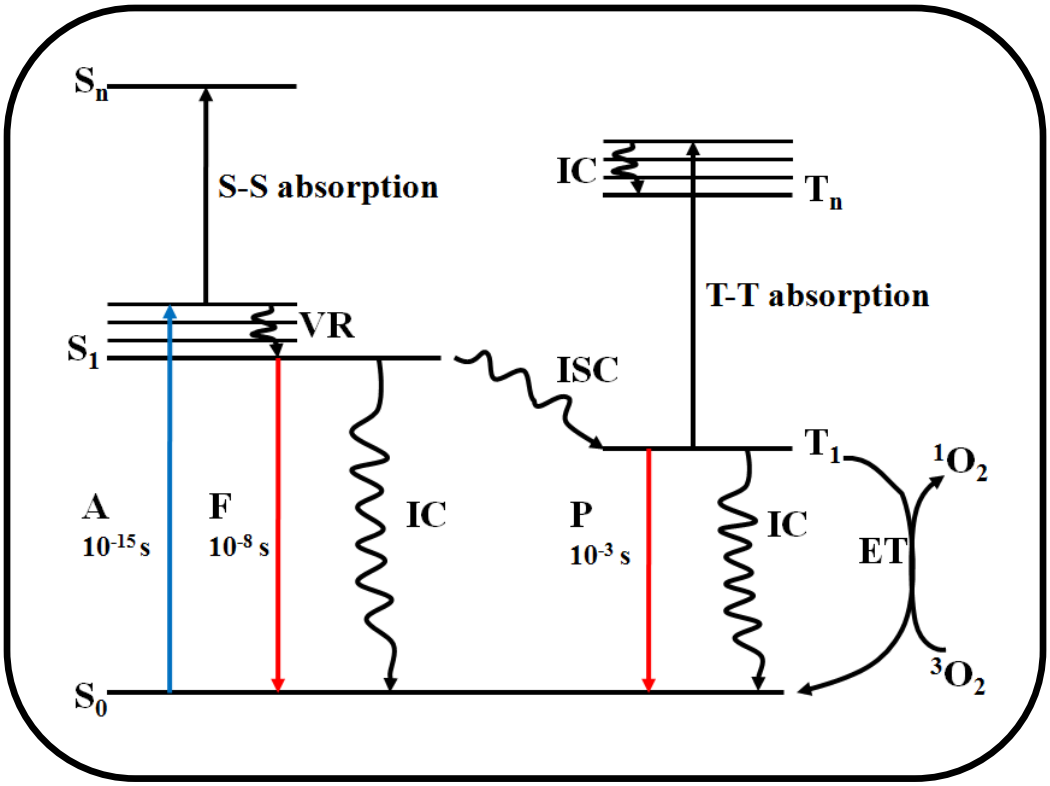

Fig. 1.5: A modified Jablonski diagram showing the transition between the singlet ground state (S_0) and electronic excited states (S_1 and T_1). A = absorption, F = fluorescence, VR = vibrational relaxation, IC = internal conversion, ISC = intersystem crossing, P = phosphorescence. S_1 = singlet excited state and T_1 = triplet excited state, ET = electron transfer.

1.4.1 Fluorescence quantum yield (Φ_F) and life-time (τ_F)

The fluorescence intensity, life-times (τ_F) and quantum yields (Φ_F) of an MPc molecule are dependent on several factors such as: nature of the central metal atom, aggregation, solvent

properties, concentration, excitation wavelength, substituent type and photo-induced energy transfer [10]. To eliminate most of these factors, this work focuses on the use of zinc as the only central metal, the complexes were excited at approximately the same wavelength (610 nm) and absorbance of 0.05 for the Φ_F measurements. All studies were done in dimethylsuphoxide (DMSO) except for complexes **10**, **11**, **23** and **24** which were carried out in pH 9 buffer.

Fluorescence quantum yields (Φ_F) is defined by the ratio of the number of fluorescing molecules to the number of photons absorbed. The Φ_F values of all the complexes were determined using a comparative method [93,94], where the emission spectrum of a sample is compared with that of a standard (unsubstituted ZnPc was employed) on excitation at the same wavelength. The fluorescence quantum yield (Φ_F) was calculated according to Equation 1.1.

$$\Phi_F = \Phi_F^{std} . \frac{F . A_{std} . n^2}{F_{std} . A . n_{std}^2} \qquad 1.1$$

where Φ_F^{std} is the fluorescence quantum yield of the standard (Φ_F^{std} = 0.2 [95]), F and F_{std} refer to the areas under the fluorescence emission curves of the sample (MPc) and standard respectively, A and A_{std} are the absorbance of the sample and standard respectively at the excitation wavelength, n and n_{std} are the refractive indices of the solvents used for the sample and standard respectively.

Fluorescence life-time (τ_F) is defined as the average time a molecule spends in its excited state before returning to the ground state through fluorescence. The τ_F of all the complexes studied in this work were determined using the time-correlated single-photon counting (TCSPC) techniques [96,97], a typical fluorescence decay curve is shown in Fig. 1.6. The absorbance at the Q-band maxima of the studied complexes was between 0.05 and 0.1, this was done to ensure a low concentration and the complexes were excited at their emission maxima.

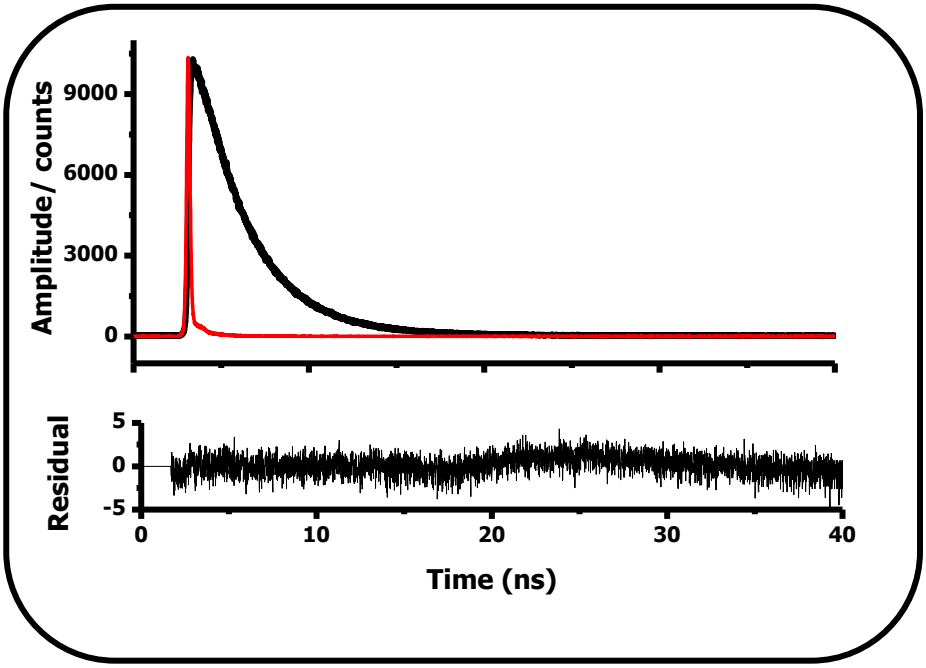

Fig. 1.6: Fluorescence decay curve of ZnTAPc-FA [61].

1.4.2 Energy transfer study

Non-radiative energy transfer often occurs from a photo-excited donor fluorophore after the absorption of a higher energy photon to an acceptor of different species which is in close proximity [98-100]. Energy transfer from ZnPc derivatives to SWCNTs was studied in this work. The quenching factor (Q_F), photo-induced energy transfer rate constant (Ket) and electron transfer efficiency (PET Eff.) [101] can be calculated from the fluorescence quantum yields and life-times of the donor (Pc) in the absence and presence of the acceptor (SWCNTs) using Equations 1.2 - 1.4.

$$Q_F = \frac{\Phi_{F(D)}}{\Phi_{F(A)}} \qquad 1.2$$

$$Ket = \left(\tau_{F\,(A)}\right)^{-1} - \left(\tau_{F(D)}\right) - 1 = \frac{\left(\frac{\Phi_{F\,(D)}}{\Phi_{F\,(A)}}\right) - 1}{\tau_{F(D)}} \qquad 1.3$$

$$\text{PET Eff.} = \left(1 - \left(\frac{\Phi_{F\,(A)}}{\Phi_{F\,(D)}}\right)\right) \quad ` \quad 1.4$$

where Φ_F and τ_F are the fluorescence quantum yield and life-time of the acceptor (A) or donor (D) respectively.

1.4.3 Triplet quantum yield (Φ_T) and life-time (τ_T)

Laser flash photolysis is a technique that can be used to study the properties of molecules at the triplet excited state. The technique involves the introduction of intense pulse of light from a laser source into an MPc molecule, this generates a time-evolved electronic absorption from the $T_1 - T_n$ state, from which the time spent (τ_T) and the population **(**Φ_T) of the triplet state can be calculated [102,103]. A typical triplet decay curve is shown in Fig. 1.7 [65].

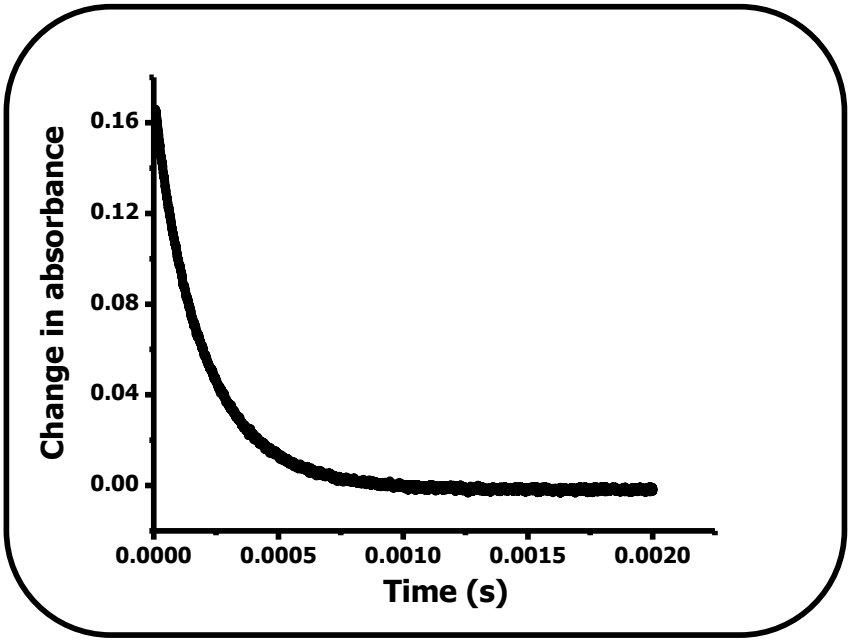

Fig. 1.7: Triplet decay curve for ZnMAPc [65].

High Φ_T are accompanied by low Φ_F, this however, depends on the nature of the central metal. The triplet life-time (τ_T) is the average time an excited MPc molecule remains in the T_1 state. The molecule is long-lived in the triplet state due to forbidden $T_1 \rightarrow S_0$ transition. The typical life-times of an MPcs molecule range between microseconds (μs) and milliseconds (ms). τ_T can be determined by fitting the triplet decay curves (Fig. 1.7) using OriginPro 8.0 software, this method was used in this work.

The triplet quantum yield (Φ_T) can be determined with reference to a standard with known Φ_T value according to Equation 1.5.

$$\Phi_T = \Phi_T^{std} . \frac{\Delta A_T . \varepsilon_T^{std}}{\Delta A_T^{std} . \varepsilon_T} \qquad 1.5$$

where Φ_T^{std} is the triplet quantum yield of the standard (Φ_T^{std} = 0.65 [103]), ΔA_T and ΔA_T^{std} are the changes in the triplet state absorption of the sample and standard respectively, ε_T and ε_T^{std} refer to the triplet state molar extinction coefficients of the sample and standard respectively. ε_T and ε_T^{std} were determined using Equation 1.6 [103].

$$\varepsilon_T = \varepsilon_s . \frac{\Delta A_T}{\Delta A_s} \qquad 1.6$$

where ε_s is the singlet state molar extinction coefficient of the sample.

1.4.4 Singlet oxygen quantum yield (Φ_Δ)

Photosensitization is the method of generating singlet oxygen ($^1O_2$), which is a highly reactive cytotoxic oxidative species involved in photo-induced oxidative processes. $^1O_2$ is responsible for tumor necrosis in PDT. Singlet oxygen is formed through an energy transfer process between excited triplet state (T_1) of MPc (^{3}MPc*) and ground state molecular oxygen ($^3O_2$), Fig 1.5. The

efficiency of singlet oxygen generation depend on; triplet quantum yield (Φ_T), triplet life-time (τ_T), energy transfer efficiency (S_Δ), nature of central metal, type of substituent on the MPc and their enhancing or quenching abilities [10,104].

The mechanism of singlet oxygen generation can either be through type I or type II. Type I mechanism (Scheme 1.3) usually occurs in oxygen poor environment and it involves hydrogen atom abstraction, which initiates free radical formulation. Type II (Scheme 1.4) mechanism involves energy transfer between excited T_1 state of an MPc molecule and molecular oxygen, it is prevalent in oxygen-rich or air saturated environments and is most predominant mechanism in PDT [10].

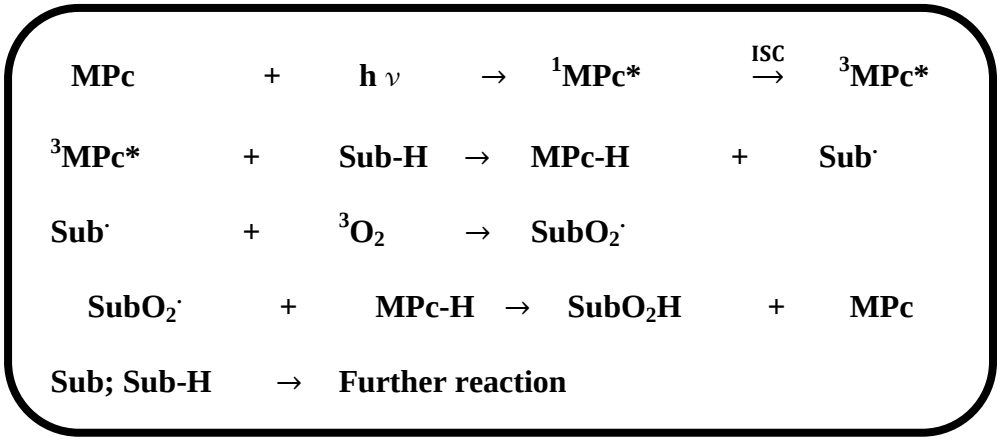

Scheme 1.3: Type I photoreaction mechanism in a metallophthalocyanine photosensitizer.

ISC = intersystem crossing

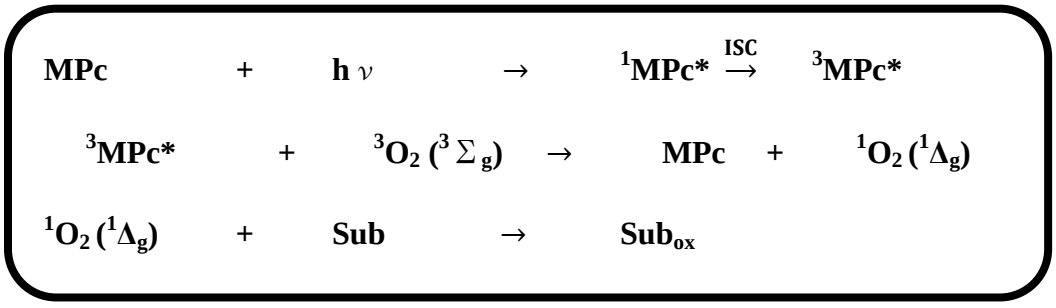

Scheme 1.4: Type II photoreaction mechanism in a metallophthalocyanine photosensitizer.

ISC = intersystem crossing

Singlet oxygen quantum yield (Φ_Δ) is defined as the number of singlet oxygen molecules produced per quanta of light absorbed. Φ_Δ can be determined using a relative method by comparing the Φ_Δ of the sample to that of a standard whose Φ_Δ is known. The experiment can be performed either through a chemical method or through the detection of singlet oxygen characteristic phosphorescence at 1270 nm [105]. Both methods involve the use of a singlet oxygen quenchers, which include, 1,3-diphenylsobenzofuran (DPBF), 1,4-diazabicyclo-octane (DABCO), tetrasodium α,α-(anthracene-9,10-diyl) dimethylmalonate (ADMA) and sodium azide (NaN_3); the latter two are often used in aqueous conditions, while the former are employed in organic solvents [106,107].

The chemical method of singlet oxygen generation involves the spectroscopic monitoring of the absorption decay of the quencher over a period of time, following irradiation of the mixture of the photosensitizer and the singlet oxygen quencher. The Φ_Δ value can be calculated using Equation 1.7.

$$\Phi_\Delta = \Phi_\Delta^{std} . \frac{R . I_{abs}^{std}}{R^{std} . I_{abs}} \qquad 1.7$$

where Φ_Δ^{std} is the singlet oxygen quantum yield of the standard (Φ_Δ^{std} = 0.67 [75]), R and R^{std} are the singlet oxygen quencher (for example, DPBF) photo-bleaching rates in the presence of the respective MPc complexes under investigation and the standard respectively, I_{abs} and I_{abs}^{std} are the rates of light absorption by the MPc and standard respectively.

Alternatively, the dynamic course of $^1O_2$ concentration can be clearly recorded according Equation 1.8 as theoretically described in literature [108], following the detection of singlet oxygen characteristic phosphorescence at 1270 nm [105].

$$I = A . \frac{\tau_D}{\tau_T - \tau_D} \left[\exp\left(\frac{t}{\tau_T}\right) - \exp\left(\frac{-t}{\tau_D}\right) \right] \qquad 1.8$$

where I is the phosphorescence signal intensity of $^1O_2$ at time t, τ_D is the life-time of $^1O_2$, τ_T is the life-time of MPc at triplet state, and A is a coefficient involved in sensitizer concentration and $^1O_2$ quantum yield.

The $^1O_2$ quantum yield (Φ_Δ) can be determined using Equation 1.9

$$\Phi_\Delta = \Phi_\Delta^{std} . \frac{A . OD^{std}}{A^{std} . OD} \quad 1.9$$

where Φ_Δ^{std} is the singlet oxygen quantum yield of the standard, A and A^{std} refer to the coefficient for the sample and standard respectively, OD and OD^{std} are the optical densities or absorbance of the sample and standard respectively at the excitation wavelength. A typical singlet oxygen phosphorescence decay curve for MPcs is shown in Fig. 1.8 [109].

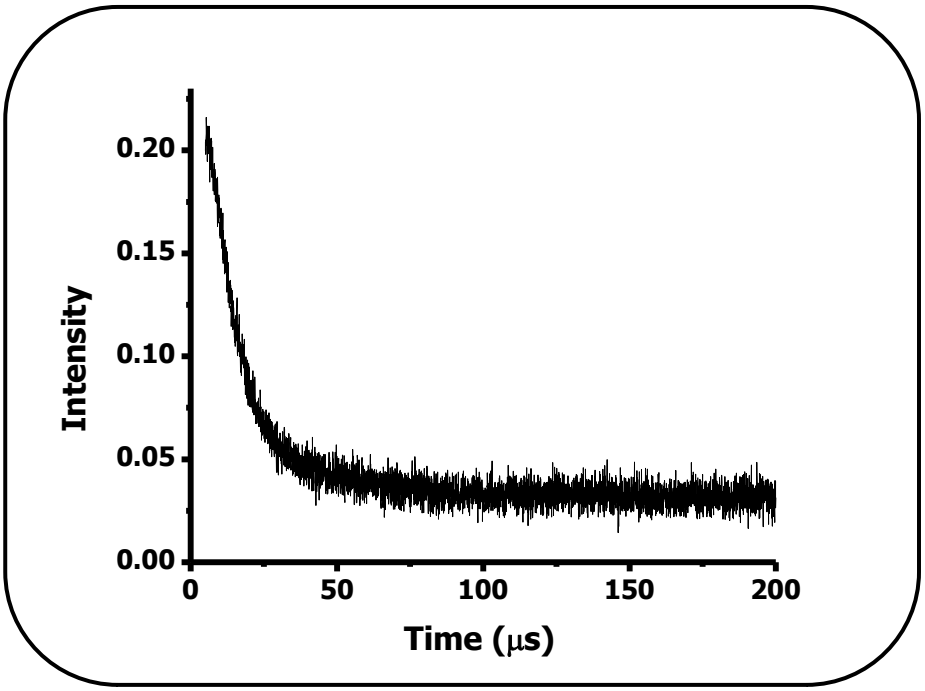

Fig. 1.8: Typical singlet oxygen phosphorescence decay signal for MPcs [109].

Both the chemical and the phosphorescence decay signal methods were used in quantifying of the singlet oxygen quantum yields of the complexes studied in this work.

The photophysical and photochemical parameters of some zinc Pc derivatives [75,102,109-114] are shown in Table 1.4. In general, ZnPc have low fluorescence quantum yields, high triplet and singlet oxygen quantum yields depending on the solvents. ZnPc-biomolecule conjugates studied in this work will be shown to improve the triplet and singlet oxygen quantum yields as compared to the precursor Pc alone.

Table 1.4: Photophysical and photochemical parameters of some ZnPc derivatives

MPc	**Solvent**	**Φ_F**	**τ_T (μs)**	**Φ_T**	**Φ_Δ**	**REF**
ZnPc	DMSO	0.18	350	0.65	0.67	[95],[102]
ZnOCPc	Buffer pH 9	0.15	62	0.34	0.21	[109]
ZnTCPPc	DMSO	0.10	238	0.49	0.10	[110]
$ZnPc(Br)_4$	DMSO	0.29	96	0.59	0.35	[111]
$ZnPc(Cl)_4$	DMSO	0.17	216	0.76	0.41	[111]
$ZnPc(I)_4$	DMSO	0.088	55	0.86	0.54	[111]
ZnPc (*t*-Bu)$_3$(OH)$_2$	Benzene	0.18	176	0.038	-	[112]
ZnPc(*t*-Bu)$_4$	Benzene	0.37	41	0.24	-	[112]
ZnPc(SO3Na)4	H_2O	0.32	245	0.56		[113]
ZnPc-β-(Benzyloxyphenoxy)$_4$	DMSO	0.23	-	0.60	0.52	[114]

t-Bu = tert-butyl

1.5 Summary of aim of thesis

The aims of this thesis can be summarized as follows:

1. Synthesis of zinc phthalocyanine derivatives (octa, tetra and low symmetry) alone and covalently conjugated to pyrene, folic acid, ascorbic acid, bovine serum albumin, uridine or spermine.
2. Adsorption (or linking) of zinc phthalocyanine derivatives on single-walled carbon nanotubes (SWCNTs).
3. Spectroscopic (ground state electronic absorption and fluorescence), photophysical and photochemical (triplet quantum yield, triplet life-time, singlet oxygen quantum yield, fluorescence quantum yield and life-time) studies.
4. Cytotoxicity and photodynamic effects of zinc phthalocyanine derivatives in the presence of biomolecules and single-walled carbon nanotubes, when alone or in combination.

CHAPTER TWO

2. EXPERIMENTAL

This chapter provides information on the materials, instrumentation, synthetic procedures and the protocol for cytotoxicity and photodynamic therapy activities of the synthesized complexes.

2.1 Material

2.1.1 Synthesis, photophysical and photochemical reagents

Folic acid, uridine, ascorbic acid, spermine, 1-pyrene-1-carboxaldehyde, bovine serum albumin, diphenylisobenzofuran (DPBF), dimethylaminopyridine (DMAP), trifluoroactetic acid (TFA), triethylamine, sephadex LH-20 microbeades, dicyclohexylcarbodiimide (DCC), 1-ethyl-3-(3-dimethylaminoproplyl) carbodiimide hydrochloride (EDC), 9,10-N-hydroxysuccinimide (NHS), cultures of human skin melanoma (A375) cell line, trypan blue and unsubstituted zinc phthalocyanine (employed as standard) were obtained from Sigma-Aldrich®. Single-walled carbon nanotubes (SWCNTs, 1-5 nm in diameter and 1-5 μm in length) were obtained from Nanolab. Cultures of MCF-7 breast cancer cells were obtained from Cellonex®. Trypsin, Dulbecco's phosphate-buffered saline (DPBS) and Dulbecco's modified Eagle's medium (DMEM) were obtained from Lonza®, 10% (v/v) heat-inactivated fetal calf serum (FCS), 100μg/mL-penicillin-100 unit/mL-streptomycin-amphotericin B mixture were obtained from Biowest®. 2',3'-O-isopropylideneuridine was synthesized according to [115].

2.1.2 Solvents

Dimethylsulfoxide (DMSO), chloroform, dichloromethane (DCM), *N*,*N*-dimethylformamide (DMF), n-pentanol, ethanol (EtOH), hexane, methanol (MeOH), tetrahydrofuran (THF), toluene, nitric acid (55 %), sulfuric acid (98 %) and thionyl chloride were purchased from SAARCHEM.

2.2 Instrumentation

1. Mass spectra data were collected with a Bruker AutoFLEX III Smart beam TOF/TOF mass spectrometer. The spectra were acquired using either α-cyano-4-hydroxycinnamic acid or dithranol as the MALDI matrix, and a 355 nm Nd:YAG laser as the ionizing source.
2. Elemental analyses were carried out on a Vario EL III MicroCube CHNS instrument analyzer.
3. FTIR spectra were obtained on a Perkin-Elmer spectrum 100 with universal attenuated total reflectance (ATR) sampling accessory.
4. Proton-nuclear magnetic resonance spectra (^{1}H NMR) were recorded in deuterated solvent (DMSO-d_6, DMF-d_7 or D_2O) using either Bruker EMX400 MHz NMR spectrometer or a Bruker ADVANCE II 600 MHz spectrometer.
5. Thermal gravimetric analysis (TGA) were recorded on a Shimadzu DTG-TG 60H with a gas flow of 120 ml/min and operated under nitrogen atmosphere.
6. Transmission electron microscopy (TEM) images were obtained using a Zeiss Libra TEM 120 model operated at 90 kV.
7. X-ray diffraction (XRD) patterns were recorded using a Cu kα radiation (λ = 1.5405 Å, nickel filter), on a Bruker D8 Discover equipped with a proportional counter. Scanning was at 10 min^{-1} with a filter time-constant of 2.5 s per step and a slit width of 6.0 nm. The data were obtained in the range from $2\theta = 5^o$ to 100^o. A zero background silicon wafer slide was used for sample placement. The data analysis was carried out using Eva (evaluation curve fitting) software. Subtraction of spline fitted to the curved background

was used for baseline correction of each diffraction pattern and the full-width at half maximum value was obtained from the fitted curve.

8. Raman spectra were obtained with a Bruker Vertex 70- Ram II spectrometer (equipped with a 1064 nm Nd:YAG laser and liquid nitrogen cooled germanium detector). Solid samples diluted with KBr were used.
9. Ground state electronic absorption spectra were recorded on a Shimadzu UV-Vis 2550 spectrophotometer.
10. Emission spectra were recorded on a Varian Eclipse spectrofluorimeter. The slit width (each 5 nm) was kept constant for all the experiments.
11. Fluorescence life-times were measured using a time correlated single photon counting setup (TCSPC), Fig. 2.1, (Fluo Time 200, Picoquant GMbH) with a diode laser as excitation source (LDH-P-670 driven by PDL 800-B, 670 nm, 20 MHz repetition rate, Picoquant GmbH). Fluorescence was detected under the magic angle with a peltier cooled photomultiplier tube (PMT) (PMA-C 192-N-M, Picoquant GmbH) and integrated electronics (PicoHarp 300E, Picoquant GmbH). A monochromator with a spectra width of about 4 nm was used to select the required measured emission wavelength. The response function of the system, which was with a scattering Ludox solution (DuPont), had a full width at half-maximum (FWHM) of about 300 ns. The ratio of stop to start pulses was kept low (below 0.05) to ensure good statistics. All fluorescence decay curves were measured at the maximum emission peak. The data were analyzed with the program FluoFit (Picoquant GmbH). The support plane approach [99] was used to estimate the errors of the decay times.

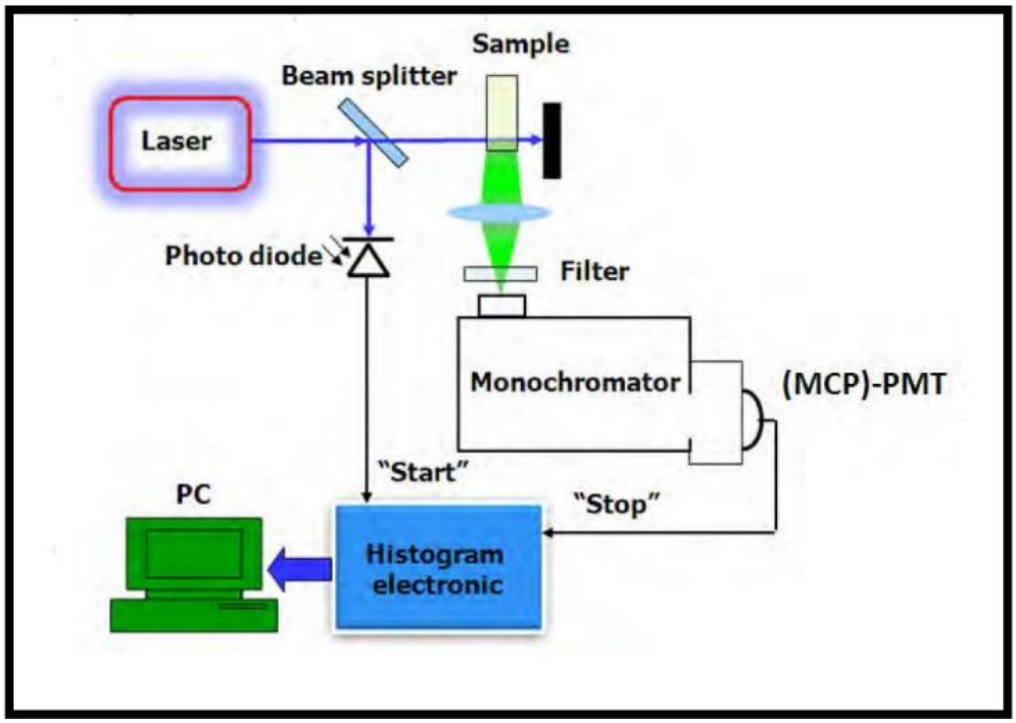

Fig. 2.1: Schematic diagram of time-correlated single photon counting (TCSPC) setup. (MCP)-PMT = (Multi channel plate detector)-Photomultiplier tube, PC = Personal computer.

12. Laser flash photolysis (Fig. 2.2) experiments were performed to determine the triplet decay kinetics and transient absorption spectra. Light pulses were produced by a Quanta-Ray Nd:YAG laser providing 100 mJ, 9 ns pulses of laser light at 10 Hz, pumping a Lambda Physik FL 3002 dye (Pyridin 1 dye in methanol). Single pulse energy ranged from 1 to 3 mJ. The analyzing beam source was from a Thermo Oriel 66902 xenon arc lamp, and a photomultiplier tube (Hamamatsu) mounted to a monochromator was used as a detector. Signals were recorded with a two-channel 300 MHz digital real time oscilloscope (Tektronix TDS 3032C); the kinetic curves were averaged over 256 laser pulses. OriginPro 8.0 was used to fit the kinetic curves in order to determine the triplet life-times.

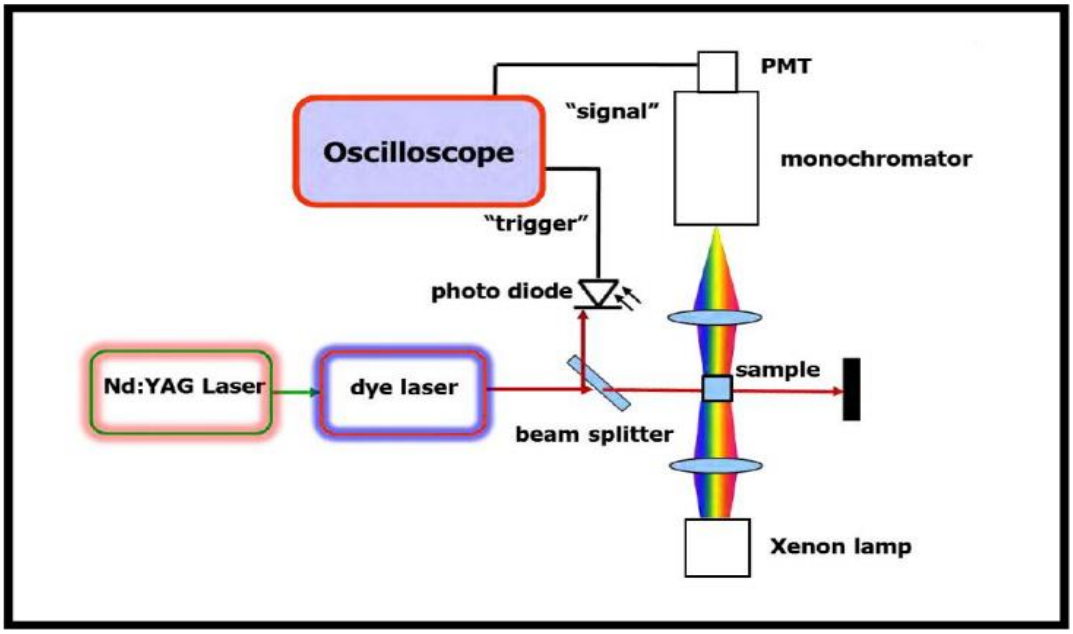

Fig. 2.2: Schematic diagram for a laser flash photolysis setup. PMT = Photomultiplier tube.

13. Time resolved phosphorescence decay of singlet oxygen at 1270 nm was used to determine singlet oxygen quantum yield in either DMSO or pH 9 buffer. The dynamic phosphorescence decay of singlet oxygen ($O_2(^1\Delta_g)$), was demonstrated using time resolved phosphorescence of $O_2(^1\Delta_g)$ at 1270 nm. For these studies an ultra sensitive germanium detector (Edinburgh Instruments, EI-P) combined with a 1000 nm long pass filter (Omega, RD 1000 CP) and a 1270 nm band-pass filter (Omega, C1275, BP50) was used to detect $O_2(^1\Delta_g)$ phosphorescence under the excitation using Quanta-Ray Nd:YAG laser providing 400 mJ, 90 ns pulses of laser light at 10 Hz pumping a Lambda-Physik FL3002 dye laser (Pyridin 1 dye in methanol), with a pulse period of 7 ns and repetition rate of 10 Hz, Fig. 2.3. The near-infrared phosphorescence of the samples were focused onto the germanium detector by a lens (Edmund, NT 48-157) with detection direction

perpendicular to the excitation laser beam. The detected signals were averaged with a digital oscilloscope (Tektronics, TDS 360) to show the dynamic decay of $O_2(^1\Delta_g)$.

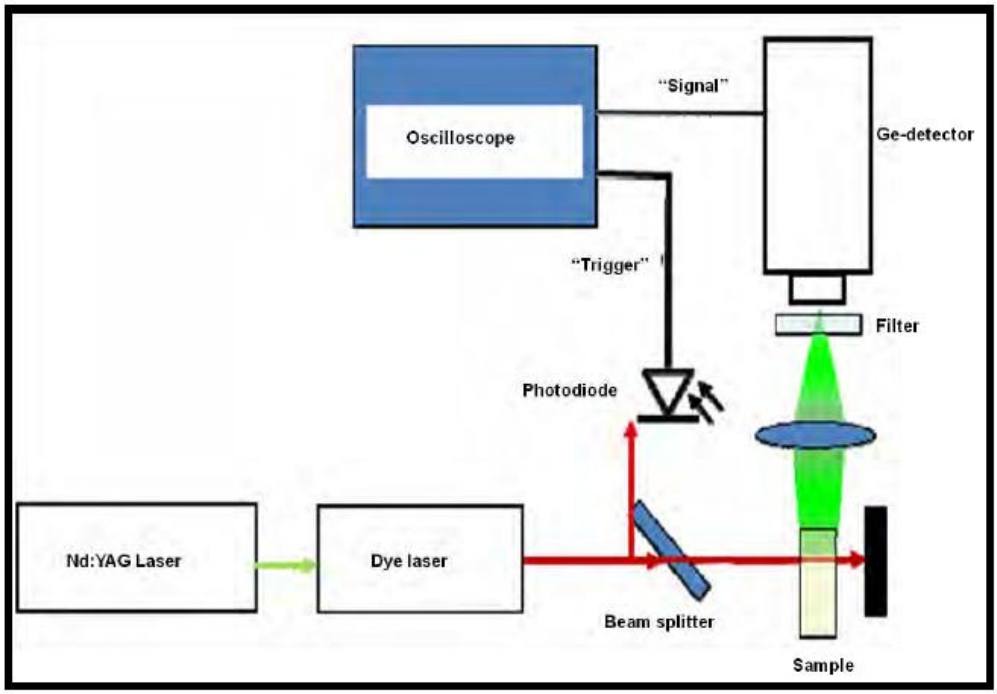

Fig. 2.3: Schematic diagram for the singlet oxygen detection setup using its phosphorescence.

14. Photo-irradiation for the PDT effects of the complexes were performed using a general electric quartz lamp (300 W); 600 nm glass (Schott) to filter off ultra-violet radiation. Light intensities were measured with a POWER MAX 5100 (Mole-electron detector incorporated) power meter and were found to be 4.3 $\times$ 10^{15} photons cm^{-2} s^{-1}. The above set up was also used for the determination of singlet oxygen using the chemical method. A water filter was used to filter off far infrared radiation and an interference filter (Intor, 670 nm with a band width of 40 nm) was placed in the light path just before the cell containing the sample for singlet oxygen studies. Light intensities were found to be 2.97 x 10^{16} photons s^{-1} cm^{-2}. To avoid chain reactions induced by DPBF in the presence of singlet oxygen [116], the concentration of quencher was lowered to ~3 x 10^{-5} mol dm^{-3}.

Solutions of photosensitizer (absorbance = 1 at the irradiation wavelength) containing DPBF were prepared in the dark and irradiated in the Q-band region. DPBF degradation at 417 nm was monitored during irradiation to quantify the singlet oxygen quantum yield with reference to a standard.

15. The cultured cells were incubated in a Heal Force® incubator, the cells were viewed using a Zeiss AxioVert.A1 fluorescence LED (FL-LED) inverted microscope, the absorbance of WST-1 and neutral red assay (cell proliferation reagents) for determining cell viability was read using a Synergy 2 multi-mode microplate reader (BioTek®) at an excitation of 450 nm.

2.3 Synthesis of MPc derivatives and MPc-biomolecule conjugates

The precursor MPcs used in this work are not new, hence details are not provided. The unsymmetrical MPcs: ZnMAPc (**1**) [65], ZnMCPPc (**4**) [66], and ZnMAPPc (**12**) [69] and the symmetrical MPcs: ZnTCPPc (**8**) [67], ZnOCPc (**10**) [68], and ZnTAPPc (**13**) [70] were synthesized according to literature.

The substituents employed in the following sections are pyrene, FA, AA, uridine, spermine and BSA. All except pyrene are biomolecules.

2.3.1 Synthesis of zinc phthalocyanine-pyrene (ZnMAPc-Py (2)) conjugate (Scheme 3.1)

A mixture of zinc monoamino phthalocyanine (ZnMAPc (**1**)) (20 mg, 0.034 mmol) and 7.83 mg (0.034 mmol) of 1-pyrene-1-carboxaldehyde (Py) was refluxed in 5 ml of ethanol at 75 °C for 24 h at room temperature. The product was precipitated out using cold ethanol, followed by

centrifugation to give **2** (Scheme 3.1). Unreacted **1** and Py were removed by repeated centrifugation and dispersion in ethanol.

ZnMAPc-Py (**2**): Yield, 54% (14.8 mg), UV-Vis (DMSO), λ_{max} (nm) (log ε): 679 (5.2), 616 (4.7), 392 (5.0), 362 (5.5). Anal. Calc. for $C_{49}H_{25}N_9Zn$: C, 72.29; H, 3.56; N, 14.74. Found: C, 71.93; H, 3.62; N, 14.85; MALDI-TOF-MS (m/z): amu 805. Found: 807. $[M+2H]^+$. IR [(ATR) ν_{max}/cm^{-1}]: 3048 - 2922 (C-C str.), 1690 - 1606 (–C=N). ^1H NMR (600 MHz, DMSO-d_6): δ/ppm: 10.1 (m, 1H, –CH=N–); 9.5 - 9.3 (m, 8H), 8.6 - 7.8 (m, 16H).

2.3.2 Synthesis of ZnMAPc-folic acid (ZnMAPc-FA (3)) conjugate (Scheme 3.2)

Folic acid (10 mg, 0.031 mmol) in a solvent mixture of H_2O and DMF (1:9) was stirred together with DCC (10 mg, 0.048 mmol) and NHS (5.5 mg, 0.048 mmol) for 24 h. Then, ZnMAPc (10 mg, 0.017 mmol) dissolved in DMF, was added and the solution was further stirred at room temperature for 48 h, according to a modified procedure [66]. The solids were precipitated out of solution using ethanol, obtained by centrifugation and repeatedly washed with ethanol.

ZnMAPc-FA (**3**): Yield, 50%, UV-Vis (DMSO) λ_{max} (nm) (log ε): 683 (5.3), 615 (4.6), 355 (5.1). Anal. Calc. for $C_{51}H_{36}N_{16}O_5Zn.H_2O$: C, 60.1; H, 3.56; N, 22.01. Found: C, 59.07; H, 4.06; N, 22.55%. MALDI-TOF-MS (m/z): 1036 amu, Found: 1037 $[M+H]^+$, IR [(ATR) ν_{max}/cm^{-1}]: 3225 - 3071 (N-H str.), 1689 (C=O amide), 1603 (N-H bend). ^1H NMR (400 MHz, DMF-d_7): δ/ppm: 4.5 - 4.6 (m, FA), 6.7 (br, FA-NH_2), 7.0 - 7.2 (m, Pc-H, FA), 8.8 (m, Pc-H). The ^1H for Pc-H and Pc-FA are not integrated due to aggregation.

2.3.3 Synthesis of ZnMCPPc-spermine (5) conjugate (Scheme 3.3)

Zinc monocarboxyphenoxy phthalocyanine (ZnMCPPc (**4**)) (0.1 g, 0.14 mmol) was stirred with 0.03 g (0.15 mmol) of DCC for 24 h in DMF to activate the carboxy group of the Pc substituent. After this time, 0.028 g (0.014 mmol) of spermine dissolved in 1 ml of DMF was added, and the mixture further stirred for 48 h at room temperature. The reaction mixture was poured into 20 ml of DCM and extracted with 20 ml of distilled water three times. The organic layers were combined and dried in vacuo. The resulting product was washed with methanol to obtain a powdered sample. The solid product was purified by silica gel column chromatography using the solvent mixture of THF and methanol (95:5 v/v) as eluent.

ZnMCPPc-spermine (**5**): Yield, 54 % (0.07 g), UV-Vis (DMSO), λ_{max} (nm) (log ε): 675 (5.5), 607 (4.7), 346 (5.1). Anal. Calc. for $C_{49}H_{44}N_{12}O_2Zn$: C, 65.51; H, 4.94; N, 18.71. Found: C, 65.52; H, 5.00; N, 18.39 %. MALDI-TOF-MS (m/z): 898 amu, Found: 898 $[M]^+$. IR [(ATR) ν_{max}/cm^{-1}]; 3412 - 3139 (N-H str.), 1646 (C=O, amide), 1599 (N-H bend), 1086 and 1053 (C-O-C str.). ^{1}H NMR (600 MHz, DMSO-d_6): 9.10 - 8.87 (m, 7H, Ar-H), 8.14 - 7.95 (m, 8H, Ar-H), 7.75 - 7.68 (2H, Ar-H), 7.49 - 7.43 (2H, Ar-H), 3.22 - 3.20 (m, 2H), 2.86 - 2.73 (m, 10H), 1.63 - 1.61 (m, 4H), 1.36 - 1.17 (m, 4H).

2.3.4 Synthesis of ZnMCPPc-uridine (6) conjugate (Scheme 3.5)

A mixture of ZnMCPPc (**4**) (0.2 g, 0.28 mmol) and DCC (0.06 g, 0.59 mmol) dissolved in 4 ml of DMF was stirred for 24 h under argon at room temperature. DMAP (0.01 g, 0.08 mmol) was then added and the reaction mixture was allowed to stir for 24 h. 2',3'-O-isopropylideneuridine (0.07 g, 0.30 mmol, synthesized according to literature [115]) was added and the mixture was further stirred for 48 h. The reaction mixture was poured into 40 ml of distilled water and

extracted with 40 ml of chloroform three times. The organic layers were combined and dried in vacuo. The solid product (ZnMCPPc-2',3'-O-isopropylideneuridine) was purified by silica gel column chromatography using the solvent mixture of THF and hexane (95:5 v/v) as eluent.

ZnMCPPc-2',3'-O-isopropylideneuridine: Yield, 51 % (0.14 g). Anal. Calc. for $C_{51}H_{34}N_{10}O_8Zn$: C, 62.49; H, 3.50; N, 14.29. Found: C, 62.00; H, 3.15; N, 14.04 %. MALDI-TOF-MS (m/z): 980 amu, Found: 981 $[M+H]^+$; IR [(ATR) ν_{max}/cm^{-1}]: 3322 (O-H str.), 2927 and 2851 (C-H str.), 1773, 1713 and 1625 (C=O), 1228 (O-H bend), 1088 and 1052 (C-O-C); ^{1}H NMR (600 MHz, DMSO-d_6): δ/ppm: 11.30 (s, 1H, N-H),), 8.15 (d, 2H, Ar-H), 8.10 - 8.00 (m, 7H, Ar-H), 7.75 - 7.73 (m, 8H, Ar-H), 7.49 (d, 2H, Ar-H), 7.15 (d, 1H, H-3), 5.58 (d, 1H, H-2), 5.57 (d, 1H, H-1') 4.84 (d, 1H, H-2'), 4.69 (d, 1H, H-3'), 4.01 (d, 1H, H-4'), 3.52 (m, 2H, H-5'), 1.43 (s, 3H, CH_3), 1.23 (s, 3H, CH_3).

To de-protect ZnMCPPc-2',3'-O-isopropylideneuridine, 0.1 g (0.1 mmol) was dispersed in 2 ml of distilled water. This was followed by the slow addition of 4 ml of 50% aqueous trifluoroacetic acid (TFA) at 0 ^oC. The reaction mixture was allowed to warm up to room temperature and stirred for 2 h as described in literature [115]. The de-protected complex was obtained by extracting the reaction mixture using 4 ml of chloroform three times. The organic fractions were combined and dried in vacuo to afford complex **6**. The solid product was purified by silica gel column chromatography using the solvent mixture of THF and hexane (95:5 v/v) as eluent.

ZnMCPPc-uridine (**6**): Yield, 73 % (0.07 g), UV-Vis (DMSO) λ_{max} (nm) (log ε): 674 (5.5), 608 (4.7), 349 (5.0). Anal. Calc. for $C_{48}H_{30}N_{10}O_8Zn$: C, 61.32; H, 3.22; N, 14.90. Found: C, 61.53; H, 3.32; N, 13.32 %. MALDI-TOF-MS (m/z): 940 amu, Found: 940 $[M]^+$. IR [(ATR) ν_{max}/cm^{-1}]; 3058 - 2918 (O-H str.), 1687 and 1596 (C=O), 1224 (O-H bend), 1085 and 1048 (C-O-C); ^{1}H NMR (600 MHz, DMSO-d_6); δ/ppm: 11.30 (s, 1H, N-H),), 8.15 (d, 2H, Ar-H), 8.10 - 8.00 (m,

7H, Ar-H), 7.75 - 7.73 (m, 8H, Ar-H), 7.49 (d, 2H, Ar-H), 7.20 (d, 1H, H-3), 5.79 (d, 1H, H-2), 5.64 (d, 1H, H-1'), 5.39 (d, 1H, H-2'), 5.12 (d, 1H, H-3'), 4.14 (d, 1H, H-4'), 3.96 (m, 2H, H-5').

2.3.5 Synthesis of ZnMCPPc-ascorbic acid (ZnMCPPc-AA (7)) conjugate (Scheme 3.6A)

ZnMCPPc (**4**) (0.07g, 0.098 mmol) was stirred with 0.02 g (0.098 mmol) of DCC for 24 h in DMF to activate the carboxy group of the Pc substituent. After this time, 0.017g (0.098 mmol) of ascorbic acid (dissolved in 1 ml of distilled water) and 5 mg (0.04 mmol) of DMAP were added and the mixture further stirred for 48 h at room temperature according to modified literature method [117]. The solid product was precipitated out of solution using ethanol and repeatedly washed with ethanol to remove unreacted DCC and DMAP which were soluble in ethanol, it was further washed with de-ionized water to remove unreacted ascorbic acid. The solid product was purified by silica gel column chromatography using the solvent mixture of THF and hexane (95:5 v/v) as eluent.

ZnMCPPc-AA (**7**): Yield, 70 % (0.06g), UV-Vis (DMSO), λ_{max} (nm) (log ε): 675 (5.5), 602 (4.6), 330 (5.6). Anal. Calc. for $C_{45}H_{26}N_8O_8Zn$: C, 61.97; H, 3.00; N, 12.85. Found: C, 60.96; H, 3.12; N, 12.75 %. MALDI-TOF-MS (m/z): 872 amu, Found: 874 $[M+2H]^+$. IR [(ATR) ν_{max}/cm^{-1}]; 3341 - 2926 (O-H str.), 1711 and 1597 (C=O), 1393 (O-H bend) and 1088 (C-O-C str.). ^1H NMR (600 MHz, DMSO-d_6): δ/ppm: 9.09 - 8.88 (b, 5H, Ar-H), 8.21 - 8.14 (m, 8H, Ar-H), 7.76 - 7.53 (b, 6H, Ar-H), 4.70 (d, 1H, CH), 3.72 (m, 2H, CH), 3.41 (m, 1H, CH_2).

2.3.6 Synthesis of ZnTCPPc-ascorbic acid (ZnTCPPc-AA (9)) conjugate (Scheme 3.6B)

ZnTCPPc (**8**) (0.1g, 0.089 mmol) was stirred with 0.02 g (0.098 mmol) of DCC for 24 h in DMF to activate the carboxy groups of the Pc substituent. After this time, 0.062g (0.098 mmol) of

ascorbic acid and 5 mg (0.04 mmol) of DMAP were added and the mixture was further stirred for 48 h according to modified literature method [117]. The solid products was precipitated out of solution using ethanol, and repeatedly washed with ethanol to remove unreacted DCC and DMAP which were soluble in ethanol. The product was further washed with de-ionized water to remove unreacted ascorbic acid. The solid product was further purified by silica gel column chromatography using the solvent mixture of THF and hexane (95:5 v/v) as eluent.

ZnTCPPc-AA (**9**): Yield, 86 % (0.135 g), UV-Vis (DMSO), λ_{max} (nm) (log ε): 681 (5.6), 614 (5.1), 354 (6.0). Anal. Calc. for $C_{84}H_{56}N_8O_{32}Zn$: C, 57.49; H, 3.22; N, 6.39. Found: C, 57.46; H, 3.00; N, 5.10 %. MALDI-TOF-MS (m/z): 1754 amu, Found: 1756 $[M+2H]^+$. IR [(ATR) ν_{max}/cm^{-1}]; 3437 - 3093 (O-H str.), 1694 and 1600 (C=O), 1387 (O-H bend), 1091 and 1043 (C-O-C str.). ^{1}H NMR (600 MHz, DMSO- d_6): δ/ppm: 8.9 - 8.8 (d, 4H, Ar-H), 8.5 (m, 4H, Ar-H), 8.1 - 8.0 (d, 8H, Ar-H), 7.7 (m, 4H Ar-H), 7.5 - 7.3 (m, 8H, Ar-H), 4.72 - 4.70 (b, 4H, CH), 3.72 - 3.69 (b, 4H, CH), 3.41 - 3.40 (b, 8H, CH_2).

2.3.7 Synthesis of the ZnOCPc-bovine serum albumin (ZnOCPc-BSA (11)) conjugate (Scheme 3.4)

ZnOCPc (**10**) (20 mg, 0.02 mmol) in pH 9 buffer was stirred together with EDC (10 mg, 0.05 mmol) and NHS (5.8 mg, 0.05 mmol) for 2 h to activate the carboxy groups of ZnOCPc. Then BSA (20 mg) was added and the solution was further stirred at room temperature for 24 h, according to a modified literature procedure [53]. The solid product was precipitated out of solution using ethanol followed by centrifugation. The solid product was repeatedly washed with ethanol and further purified using size exclusion chromatography.

ZnOCPc-BSA (**11**): UV-Vis (buffer 9): λmax nm 687, IR [(ATR) ν_{max}/cm^{-1}]: 3362 - 2820 (N-H str.), 1560 (C=O amide and N-H bend).

2.4 Functionalization of single-walled carbon nanotubes (SWCNTs)

2.4.1 Functionalization of single-walled carbon nanotubes with carboxylic acid groups

SWCNTs were functionalized with carboxylic acid (represented as SWCNT-COOH), using established methods [118]. Briefly, the SWCNTs (60 mg) were suspended in a 3:1 mixture of concentrated HNO_3 and H_2SO_4. The solution was then stirred for 2 h at 70 ^oC. The resulting mixture was centrifuged and washed with Millipore water several times until a pH of 5 was attained. The SWCNT-COOH was subsequently dried in an oven at 110 ^oC for 12 h. SWCNT-COOH: IR [(ATR) $\nu max/cm^{-1}$]: 3296 - 3200 (O-H), 1751 (C=O). [Raman $\nu max/cm^{-1}$]: 2551(G*), 1592 (G), 1276 (D).

2.4.2 Covalent functionalization of SWCNT-COOH with folic acid (SWCNT-FA) (or ascorbic acid (SWCNT-AA)) (Scheme 3.7)

SWCNT-COOH (20 mg) in phosphate buffer pH 7 was stirred together with EDC (10 mg, 0.05 mmol) and NHS (5.8 mg, 0.05 mmol) for 2 h to activate the carboxy groups on the SWCNTs. Then, folic acid (20 mg, 0.045 mmol) (or 20 mg (0.034 mmol) of AA) was added and the solution was further stirred at room temperature for 24 h according to a modified method [119]. The solid product was precipitated out of solution using ethanol followed by centrifugation. SWCNT-FA: IR [(ATR) ν_{max}/cm^{-1}]: 3312 - 3001 (N-H str.), 1692 (C=O amide) and 1604 (N-H bend). [Raman ν_{max}/cm^{-1}]: 2554 (G*), 1592 (G), 1285 (D).

SWCNT-AA: IR[(ATR) ν_{max}/cm^{-1}]: 3480 - 3190 (O-H str.), 1740 (C=O), 1366 (O-H bend) and 1217 (C-O-C str.). [Raman ν_{max}/cm^{-1}]: 2548 (G*), 1589 (G), 1284 (D).

2.4.3 Covalent functionalization of SWCNT-COOH with amino substituted ZnPc derivatives (Scheme 3.8)

SWCNT-COOH was chemically modified with amino substituted ZnPcs complexes via diimide-activated amidation according to literature [119]. Briefly, 20 mg of SWCNT-COOH was stirred with 10 mg (0.048 mmol) of DCC for 24 h in DMF. After this time 20 mg (0.029 mmol) of ZnMAPPc (**12**) (or 10 mg (0.017 mmol) of ZnMAPc (**1**), or 20 mg (0.02mmol) of ZnTAPPc (**13**)) was added and the solution was further stirred at room temperature for 48 h. The solids were precipitated out using a solvent mixture of ethanol and hexane (1:1) and the solid products were obtained by centrifugation. Unreacted **1**, **12** and **13** and DCC were removed by repeated washing in ethanol. The resulting conjugates are ZnMAPc-SWCNT, linked (**19**) from **1**, ZnMAPPc-SWCNT, linked (**25**) from **12** and ZnTAPPc-SWCNT, linked (**27**) from **13**.

ZnMAPc-SWCNT, linked (**19**): UV-Vis (DMSO), λ_{max} (nm): 683. IR [(ATR) ν_{max}/cm^{-1}]; 3215 - 3061 (O-H str.), 1651 (C=O), 1602 (N-H bend), [Raman ν_{max}/cm^{-1}]: 2555 (G*), 1593 (G), 1268 (D).

ZnMAPPc-SWCNT, linked (**25**): UV-Vis (DMSO), λ_{max} (nm): 675. IR [(ATR) νmax/cm^{-1}]; 3205 - 3047 (N-H str.), 1656 (C=O amide), 1605 (N-H bend). [Raman νmax/cm^{-1}]: 2549 (G*), 1590 (G), 1283 (D).

ZnTAPPc-SWCNT, linked (**27**): UV-Vis (DMSO), λ_{max} (nm): 686. IR [(ATR) νmax/cm^{-1}]; 3316 - 3154 (N-H str.), 1650 (C=O amide), 1650 (N-H bend). [Raman νmax/cm^{-1}]: 2548 (G*), 1589 (G), 1283 (D).

2.4.4 Non-covalent functionalization of SWCNT-COOH with ZnPc derivatives, (Scheme 3.9)

ZnPc derivatives were adsorbed onto SWCNT-COOH according to literature methods for adsorption of other Pc [71] with slight modification as follows: 20 mg of SWCNT-COOH were ultrasonicated for 20 min in 5 ml of dry DMF to give a brown coloured suspension. 20 mg (0.029 mmol) of ZnMCPPc-uridine (**6**) (as an example) was added to the solution to give a green suspension and the resulting mixture was stirred for 5 days at room temperature to give a dark green suspension indicating the adsorption of complex **6** onto SWCNT-COOH. The reaction mixture was precipitated out of solution using the solvent mixture of ethanol and hexane (1:1) and the solid product (ZnMCPPc-uridine-SWCNT, adsorbed (**17**)) was obtained by centrifugation. Unadsorbed **6** was removed by repeated centrifugation and dispersion in ethanol. Similar procedure with varying stirring days was used to synthesize different ZnPc-SWCNT derivatives: ZnMAPc-FA-SWCNT, adsorbed (**14**), ZnMCPPc-SWCNT, adsorbed (**15**), ZnMCPPc-spermine-SWCNT, adsorbed **(16**), ZnMCPPc-AA-SWCNT, adsorbed (**18**), ZnMAPc-Py-SWCNT, adsorbed (**20**), ZnTCPPc-SWCNT, adsorbed (**21**), ZnTCPPc-AA-SWCNT, adsorbed (**22**), ZnOCPc-SWCNT, adsorbed (**23**), ZnOCPc-BSA-SWCNT, adsorbed (**24**), ZnMAPPc-SWCNT, adsorbed (**26**) and ZnTAPPc-SWCNT, adsorbed (**28**).

ZnMAPc-FA-SWCNT, adsorbed (**14**): UV-Vis (DMSO): λ_{max} nm 682, IR [(ATR) ν_{max}/cm^{-1}]; 3326 - 3200 (N-H str.), 1694 (C=O), 1601 (N-H bend). [Raman ν_{max}/cm^{-1}]: 2558 (G*), 1591 (G), 1267 (D).

ZnMCPPc-SWCNT, adsorbed (**15**): UV-Vis (DMSO), λ_{max} (nm): 677. IR [(ATR) ν_{max}/cm^{-1}]: 3429 - 3118 (O-H str.), 1598 (C=O), 1390 (O-H bend). 1010 (C-O-C str.). [Raman ν_{max}/cm^{-1}]: 2550 (G*), 1591 (G), 1280 (D).

ZnMCPPc-spermine-SWCNT, adsorbed (**16**): UV-Vis (DMSO): λ_{max} nm 675, IR [(ATR) ν_{max}/cm^{-1}]; 3362 - 3200 (N-H str.), 1646 (C=O), 1598 (N-H bend), 1082 and 1050 (C-O-C str.); [Raman ν_{max}/cm^{-1}]: 2547 (G*), 1589 (G), 1285 (D).

ZnMCPPc-uridine-SWCNT, adsorbed (**17**) : UV-Vis (DMSO): λ_{max} nm 674, IR [(ATR) ν_{max}/cm^{-1}]; 3397 - 3165 (O-H str.), 1597 (C=O), 1230 (OH bend), 1087 and 1045 (C-O-C); [Raman ν_{max}/cm^{-1}]: 2551 (G*), 1589 (G), 1284 (D).

ZnMCPPc-AA-SWCNT (**18**): UV-Vis (DMSO): λ_{max} (nm): 675. IR [(ATR) ν_{max}/cm^{-1}]; 3341 - 3037 (O-H str.), 1597 (C=O), 1382 (O-H bend) and 1014 (C-O-C str.). [Raman ν_{max}/cm^{-1}]: 2548 (G*), 1590 (G), 1281 (D).

ZnMAPc-Py-SWCNT (**20**): UV-Vis (DMSO): λ_{max} nm 682, IR [(ATR) ν_{max}/cm^{-1}]: 3183 - 2985 (C–C str.), 1643 - 1605 (–C=N). [Raman ν_{max}/cm^{-1}]: 2544 (G*), 1592 (G), 1277 (D).

ZnTCPPc-SWCNT, adsorbed (**21**): UV-Vis (DMSO), λ_{max} (nm): 682. IR [(ATR) ν_{max}/cm^{-1}]; 3377 - 3088 (O-H str.), 1664 and 1596 (C=O), 1384 (O-H bend). 1088 (C-O-C str.). [Raman ν_{max}/cm^{-1}]: 2550 (G*), 1589 (G), 1281 (D).

ZnTCPPc-AA-SWCNT (**22**): UV-Vis (DMSO) λ_{max} (nm): 683. IR [(ATR) ν_{max}/cm^{-1}]; 3412 - 3184 (O-H str.), 1635 and 1599 (C=O), 1391 (O-H bend). 1136 (C-O-C str.). [Raman ν_{max}/cm^{-1}]: 2549 (G*), 1590 (G), 1281 (D).

ZnOCPc-SWCNT, adsorbed (**23**): UV-Vis (buffer 9): λ_{max} (nm): 687, IR [(ATR) ν_{max}/cm^{-1}]; 3490 - 3158 (N-H str.), 1578 (C=O, N-H bend). [Raman ν_{max}/cm^{-1}]: 2549 (G*), 1591 (G), 1283 (D).

ZnOCPc-BSA-SWCNT (**24**): UV-Vis (buffer 9): λ_{max} (nm): 691, IR [(ATR) ν_{max}/cm^{-1}]; 3300 - 3118 (N-H str.), 1564 (C=O, N-H bend). [Raman ν_{max}/cm^{-1}]: 2554 (G*), 1592 (G), 1285 (D).

ZnMAPPc-SWCNT, adsorbed (**26**): UV-Vis (DMSO), λ_{max} (nm): 682. IR [(ATR) *v*max/cm^{-1}]; 3356 - 3194 (N-H str.), 1704 (C=O), 1570 (N H bend). [Raman *v*max/cm^{-1}]: 2548 (G*), 1589 (G), 1285 (D).

ZnTAPPc-SWCNT, adsorbed (**28**): UV-Vis (DMSO), λ_{max} (nm): 683. IR [(ATR) v_{max}/cm^{-1}]; 3357 - 3200 (O-H str.), 1709 (C=O), 1653 and 1605 (N-H bend), [Raman v_{max}/cm^{-1}]: 2548 (G*), 1591 (G), 1281 (D).

2.5 Cell studies

The list of ZnPcs or ZnPc-conjugates employed for cell studies are shown in Tables 1.2 and 1.3. The complexes are: ZnMAPc-FA (**3**)**,** ZnMCPPc (**4**), ZnMCPPc-spermine (**5**), ZnMCPPc-uridine (**6**), ZnMCPPc-AA (**7**), ZnMAPc-FA-SWCNT, adsorbed (**14**), ZnMCPPc-SWCNT, adsorbed (**15**), ZnMCPPc-spermine-SWCNT, adsorbed (**16**), ZnMCPPc-uridine-SWCNT, adsorbed (**17**) and ZnMCPPc-AA-SWCNT, adsorbed (**18**).

2.5.1 Cytotoxicity (dark toxicity) test

Cultures of human skin A375 melanoma or MCF-7 breast cancer cell lines were grown in Dulbecco's modified Eagle's medium (DMEM) containing L-glutamine and phenol red, supplemented with 10% heat-inactivated fetal calf serum (FCS) and 100 unit/ml-penicillin-100 µg/ml-streptomycin-amphotericin B. The cells were grown in T75 flask and incubated at 37 ^{o}C and 5% $CO_{2,}$ until a cell confluence of 80 - 100% was achieved. Following which the cells were rinsed with Dulbecco's modified phosphate buffer saline (DPBS) and lifted using trypsin. The cells were then counted using a hemocytometer by the addition of 50 µl of DPBS and cell cultured (from a known volume) and 100 µl trypan blue.

A375 melanoma cells were seeded and allowed to attach in 1 ml of supplemented DMEM containing phenol red at a density of 20,000 cells/well in a 24 well tissue culture plate and incubated at 37 ^{o}C in 5% CO_2 for 24 h. After this time, attached cells were rinsed with 2 ml DPBS, followed by addition of 1 ml fresh culture medium containing gradient concentrations of each complex. Control cells were given fresh medium without complex. Plates were re-incubated at 37 ^{o}C in 5% CO_2 in the dark for 24 h. Following this, the wells were then rinsed with 1 ml DPBS, the media were replaced with a fresh one and incubated overnight. Surviving cells were quantified 24 h after re-incubation with fresh culture media with the use of neutral red (NR) viability assay; a sensitive assay to evaluate toxicity in monolayer cultures as described in literature [120,121]. Only complexes **3** and **14** were tested on A375 melanoma cells.

Similar protocol as above was used for MCF-7 breast cancer cells, with slight modification, cells were seeded at a density of 10,000 cells/well (in 100 μl of supplemented media) in a 96 well tissue culture plate and the cell viability were read using WST-1 cell proliferation assay. The complexes tested on MCF-7 cancer cells are: **3**, **4**, **5**, **6**, **7**, **14** - **18**. Cell survival was expressed as percentage of non-treated controls (0 μM of the complex), each experiment was performed in triplicate.

2.5.2 Photodynamic therapy effect

Photodynamic therapy effects on A375 melanoma cancer cells were determined by incubating attached cells seeded as above with 10 μM of the complexes (**3** and **14**) in 35-mm glass dishes at a density of 2 x 10^4 cells per cm^2 in the culture medium (3 ml). The dishes were incubated at 37 ^{o}C in 5% CO_2 in the dark for 24 h, the dishes were then washed once with 2 ml DPBS and the medium was replaced with supplemented DMEM without phenol red. This was followed by

irradiation with 1 - 5 J/cm^2 laser doses. A 676 nm laser diode (from Thorlabs) with output power of 100 mW, expanded to a diameter of 35 mm to fill petri dish, resulting in a power density of 98 mW/cm^2 was used. The irradiation time was varied to result in irradiation doses between 1 and 5 J/cm^2.

For MCF-7 breast cancer cells, complexes **3**, **4**, **5**, **6**, **7**, **14 - 18** were tested. Photo-irradiation for the PDT effects of the complexes were performed after cells were seeded in a 96 well tissue culture plate at a density of 10,000 cells/well in a 100 µl of supplemented media and allowed to attach. Glass filtered light from a general electric quartz lamp (300 W) was expanded to cover the plate resulting in a power density of 93 mW/cm^2 for each well. A quartz lamp absorbs light from about 600 nm (following the use of a glass filter) and beyond 1000 nm, this allows the testing of the PDT and PTT effects of MPc and SWCNTs complexes respectively. SWCNTs absorb light near infrared region. A quartz lamp has been reported to be effective light source in the photo-irradiation of tumor cells [10,122-125]. The irradiation time was varied between 300 and 1200 s to result in irradiation doses between 28 - 112 J/cm^2. After irradiation, the media was replaced with a fresh one containing phenol red, and similar procedure was done on control dishes containing cells. Each experiment was performed in triplicate**.** Surviving cells were quantified after re-incubation with culture medium with the use of NR or WST-1 viability assay after 24 h for A375 melanoma cells or MCF-7 breast cancer cells respectively.

WST-1 and neutral red viability assay

Surviving cells for MCF-7 breast cancer cells or A375 melanoma cells were quantified 24 h after treatment with respective complexes with or without light using WST-1 assay (from Roche®) for MCF-7 breast cancer cells and neural red for A375 melanonma cells. WST-1 assay is a sensitive

assay to evaluate toxicity and cell proliferation in monolayer cultures (following the manufactures' instruction). The absorbance of the cells was read using a Synergy 2 multi-mode microplate reader (BioTek®) at an excitation wavelength of 450 nm.

The percentage cell viability was determined using the formula below:

$$\%\ \text{cell viability} = \frac{\text{Absorbance of sample}}{\text{Absorbance of control}} \times 100$$

where absorbance of sample are the cells containing the compound to be tested, while absorbance of control are the placebo cells.

Statistical analysis

Statistical significance (p value) was undertaken using Anova (analysis of variance) and a Student's t-test (analysis between two components) using error limits from at least three experimental data. Microsoft® excel sheet 2007 was used for the calculation. The analysis of variance for the *in vitro* cytotoxicity and photodynamic effects of the photosensitizers on either A375 melanoma cells or MCF-7 breast cancer cells were determined at the highest concentration and fluence respectively. A p-value < 0.05 was considered significant.

RESULTS AND DISCUSSIONS

3. **SYNTHESIS AND CHARACTERIZATION**
4. **PHOTOPHYSICAL AND PHOTOCHEMICAL PROPERTIES**
5. **CYTOTOXICITY AND PHOTODYNAMIC THERAPY ACTIVITY**

PUBLICATIONS

The results discussed in the following chapters have been presented in the articles listed below, that have been published or submitted for publication in peer-reviewed journals. These articles have not been referenced in this thesis:

1. **Racheal O. Ogbodu**, Edith Antunes, Tebello Nyokong. Physicochemical properties of zinc monoamino phthalocyanine conjugated to folic acid and single-walled carbon nanotubes. Polyhedron **60** (2013) 59.
2. **Racheal O. Ogbodu**, E.Antunes, T. Nyokong. Physicochemical properties of zinc phthalocyanine-pyrene conjugate adsorbed on single wall carbon nanotubes. Dalton Trans., **42** (2013) 10769.
3. **Racheal O. Ogbodu**, T. Nyokong. Effects of number of ring substituents on the physicochemical properties of zinc aminophenoxy phthalocyanine-single-walled carbon nanotube conjugate. J. Photochem. Photobiol. A: **274** (2014) 83.
4. **Racheal O. Ogbodu**, T. Nyokong. Effect of bovine serum albumin and single-walled carbon nanotube on the photophysical properties of zinc octacarboxy phthalocyanine. Spectrochim Acta A: **121** (2014) 81.
5. **Racheal O. Ogbodu**, Ivy Ndhundhuma, Aletta Karsten, Tebello Nyokong. Photodynamic therapy effect of zinc monoamino phthalocyanine-folic acid conjugate adsorbed on single-walled carbon nanotubes on melanoma cells. Spectrochim Acta A: **137** (2015) 1120.

6. **Racheal O. Ogbodu**, T. Nyokong. Enhanced triplet state parameters for zinc phenoxy carboxy phthalocyanine following conjugation to ascorbic acid and adsorption on single-walled carbon nanotubes. Polyhedron **90** (2015) 175.
7. **Racheal O. Ogbodu**, Janice L. Limson Earl Prinsloo and Tebello Nyokong Photophysical properties and photodynamic effect of zinc phthalocyanine-spermine-single-walled carbon nanotube conjugate against MCF-7 breast cancer cell line (in press).
8. **Racheal O. Ogbodu**, Edith K. Amuhaya, Philani Mashazi and Tebello Nyokong Photophysical Properties of Zinc Phthalocyanine-uridine single-walled carbon nanotube - conjugates. Inorg. Chim. Acta (submitted).
9. **Racheal O. Ogbodu**, Tebello Nyokong Effect of ascorbic acid on the photodynamic activities of zinc phthalocyanine-single-walled carbon nanotube conjugates on mcf-7 cancer cells. Spectrochim Acta A: (submitted).

CHAPTER THREE

3. SYNTHESIS AND CHARACTERIZATION

This chapter describes the detailed synthesis and spectroscopic characterization of all the complexes; ZnPc (or ZnPc-biomolecule conjugates) linked to (or adsorbed on) single-walled carbon nanotubes used in this work.

Pyrene is not a biomolecule, hence discussed separately.

3.1 Zinc phthalocyanine-pyrene (ZnMAPc-Py (2)) conjugate

Scheme 3.1 shows the synthetic route for the formation of ZnMAPc-Py (**2**) as a Schiff base reaction between ZnMAPc (**1**) and pyrene (Py). Fig. 3.1 (b) shows the FTIR spectrum of **2** with a –C=N bond stretch between 1690 - 1606 cm^{-1}, which is different from those of ZnMAPc or Py alone, indicating successful formation of the complex. The ^{1}H NMR spectrum of **2** were found at the expected region, with the imine proton at δ = 10.1 ppm and the aromatic protons for the Pc and pyrene units between δ = 9.5 - 7.8 ppm. Phthalocyanine aggregation at the concentrations used for the ^{1}H NMR measurements lead to broadening and overlap of the aromatic signals [126], hence the aromatic signal for the pyrene overlaps that of the Pc unit. The possibility of the existence of more than one isomer (i.e. cis and trans isomers) for the ZnMAPc-pyrene complex also complicated the interpretation of the ^{1}H NMR spectra. The mass spectra of **2** show a molecular ion at 807 amu instead of 805 the calculated mass. MPc complexes have been observed to degrade with molecular ion peaks $[M]^{+}$, $[M+nH]^{+}$ or $[M-nH]^{+}$ (n = 1-3) [127]. The elemental analysis also corresponds to 1:1 combination of **1** and pyrene.

The absorption spectrum of **2** in DMSO Fig. 3.2(a) shows the pyrene building block with signature peaks at 392 and 345 nm (attributed to the Py substituent Fig. 3.2(b)). Peaks for pyrene at 345 nm (as shown in Fig. 3.2(b)) have also been reported in the literature [128,129]. The Q-band for ZnMAPc-Py (**2**) was observed at 679 nm, Table 3.1. Complex **2** shows monomeric Q-band with slight red shift compared to **1**. The red shift of the Q-band of **2** (Fig. 3.2) compared to **1** is due to extended π conjugation as is typical of phthalocyanines [130]. The broadening of the Q-band might be due to aggregation. In phthalocyanine chemistry, splitting and broadening of the Q-band in most cases is explained as a result of coplanar association of Pc rings progressing

from monomers leading to aggregates. The most likely aggregates in Pc are the H aggregates (face to face). The formation of aggregate makes it difficult to study the photophysicochemical properties of Pc. However, from the excitation spectrum of **2** (Fig. 3.3b), there was no broadening of the Q-band and the photophysicochemical properties of **2** were studied in DMSO.

Typical absorption (a), excitation (b) and emission (c) spectra of ZnMAPc-Py (**2**) are shown in Fig. 3.3. The Q-band maxima of the absorption and excitation spectra were slightly different, most probably due to different equipment used. The broadening of the Q-band observed in the ground state absorption spectra was not observed in the excitation spectra.

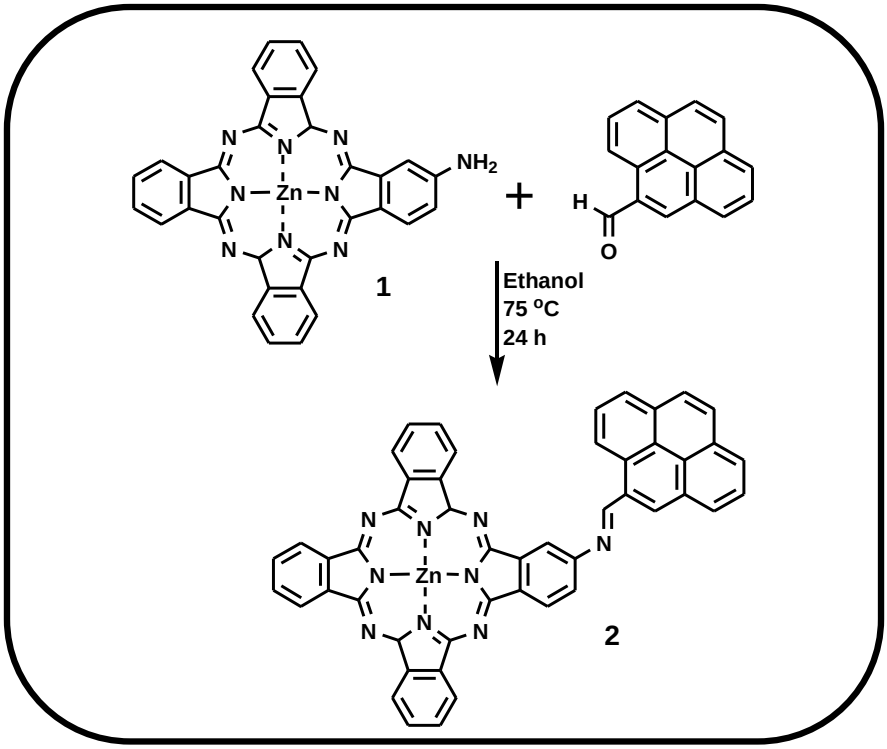

Scheme 3.1: Synthetic route for ZnMAPc-Py (**2**).

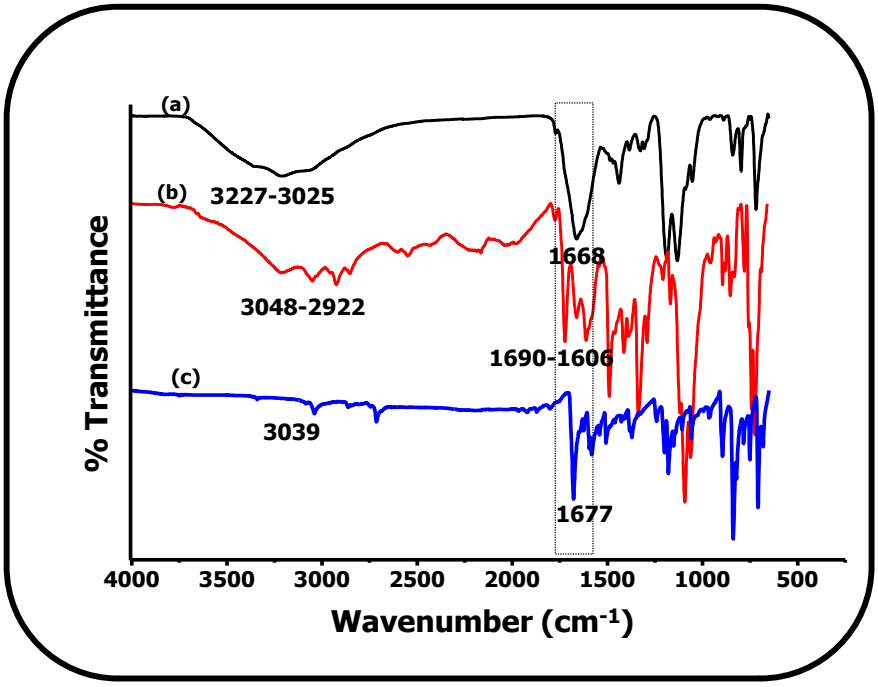

Fig. 3.1: FTIR spectra of ZnMAPc (**1**) (a), ZnMAPc-Py (**2**) (b) and Py (c).

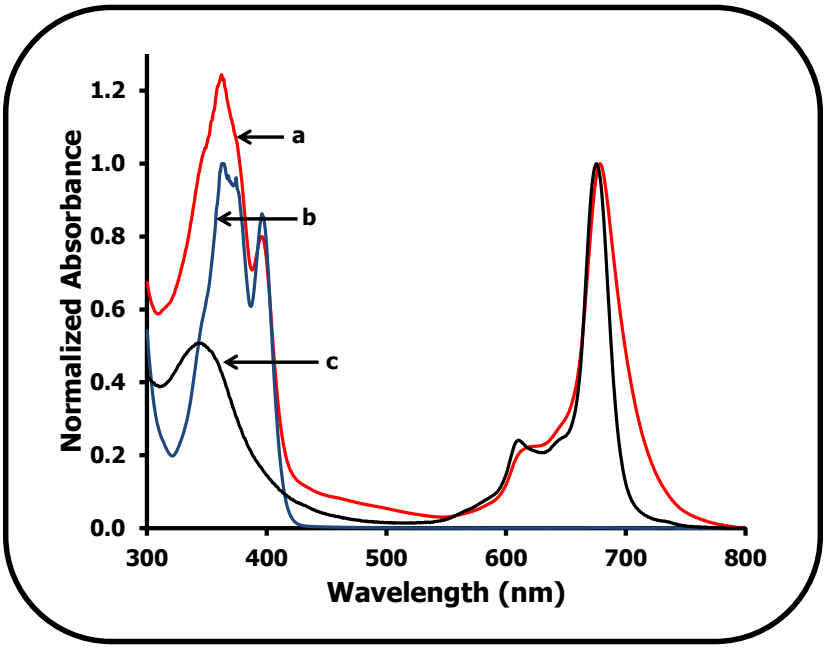

Fig. 3.2: Absorption spectra of ZnMAPc-Py (**2**) (a), Py (b) and ZnMAPc (**1**) (c) in DMSO.

The concentration of ZnMAPc-Py (**2**) is 9.5×10^{-6} M.

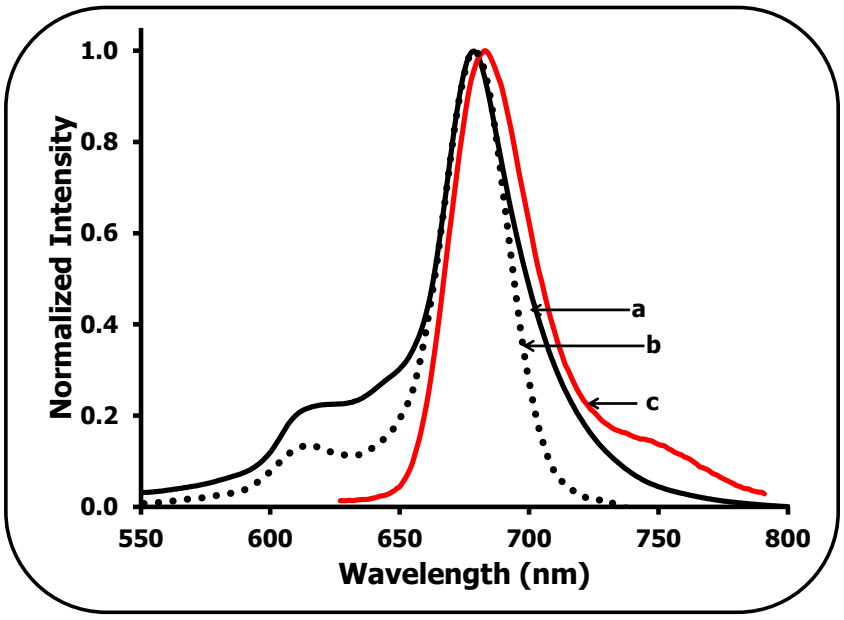

Fig. 3.3: Absorption (a), Excitation (b) and Emission (c) spectra of ZnMAPc-Py (**2**) in DMSO (excitation wavelength = 610 nm). The concentration of ZnMAPc-Py (**2**) is 6.3 × 10^{-7} M.

3.2 Metallophthalocyanine-biomolecule conjugates

The lists of MPcs and MPc-biomolecule conjugates reported in this work are listed in Table 3.1.

3.2.1 Amide bond conjugated metallophthalocyanine-biomolecule complexes

Complexes **3**, **5** and **11** were formed through amide bond linkage, a reaction between a carboxylic acid group and a primary amine.

3.2.1.1 ZnMAPc-folic acid (ZnMAPc-FA (3)) conjugate

ZnMAPc-FA (**3**) was formed by the activation of the carboxyl group of the folic acid (FA) using DCC as shown in Scheme 3.2. Folic acid possesses two carboxyl groups, termed α and γ, which can form covalent bonds through amide linkage with the amino group of ZnMAPc (**1**). It has been reported that the γ-carboxylic acid is more selectively activated due to its higher reactivity and it is most likely the one activated by DCC [131]. It has also been demonstrated that for porphyrin-FA conjugates, the covalent bond occurs mainly through the γ-carboxylic acid [132], thus it is assumed in this work that coordination is mainly through the γ-carboxylic acid. The mass spectrum of the complex ZnMAPc-FA shows a molecular ion at 1037 amu corresponding to a 1:1 ZnMAPc:FA combination. Fig. 3.4 (b) shows the FTIR spectrum of **3** which exhibits peaks at 1689 cm^{-1} (C=O amide), 1603 cm^{-1} (N-H bend) and between 3225 - 3071 cm^{-1} (N-H str.). Confirmation of the amide bond formation is complicated by the fact that FA alone has amide bonds and hence FTIR cannot conclusively confirm formation of the amide bond.

In the ^{1}H NMR spectrum of **3**, the benzene ring protons which are present between δ = 6.5 - 7.7 ppm in folic acid alone [61] were observed between δ = 7.0 - 7.2 ppm and these overlapped with the protons of **1**. It was difficult to obtain integration values due to overlapping peaks. Nonetheless, the shifts in the ^{1}H NMR spectra points to changes in the environment, indicating conjugation. The molecule was adequately confirmed using elemental analysis which also confirmed 1:1 combination.

As is typical of phthalocyanines, ZnMAPc is insoluble in water, but when chemically linked to folic acid, the conjugate becomes water soluble. No aggregation was observed for ZnMAPc-FA (**3**) in water (Fig. 3.5a) when the Q-band of **3** in water was compared to that of DMSO (Fig. 3.5b), except for a slight red shift of about 2 nm. The absorption spectra of ZnMAPc-FA (**3**) in

water (Fig. 3.5a) showed more intense B-band compared to ZnMAPc-FA (**3**) in DMSO (Fig. 3.5b) due to the add up of the signature peak of folic acid at this wavelength to the B-band of the Pc ring as a result of the complete solubility of folic acid in water.

Fig. 3.6 shows the absorption spectra of ZnMAPc-FA (**3**) (a), ZnMAPc (**1**) (b) and FA (c) in DMSO. The spectrum of **3** shows broadening of the Q-band. The broadening might be due to aggregation. Zinc tetraamino phthalocyanine (ZnTAPc) has been reported to have a very broad Q-band when alone or chemically linked to FA [61]. There was red shift in the Q-band maxima of **1** in the presence of FA and an enhancement in the B-band absorption (Fig. 3.6, Table 3.1). A blue shift in the Q-band has been observed when ZnTAPc was chemically linked to FA [61], while a red shift is observed in this work. A lack of significant change in spectra was observed when low symmetry phthalocyanines were studied in the presence of FA (mixed without a chemical bond) [133]. Amino groups result in red shifting of the Q-band maxima in MPc complexes [130], and blue shifting is often observed when these groups are engaged. Thus, the observed red shift is surprising.

The absorption (Fig 3.7a), emission (Fig 3.7b) and excitation (Fig 3.7c) spectra of ZnMAPc-FA (**3**) in DMSO are shown in Fig 3.7. The emission spectrum is a mirror image of the absorption and excitation spectra. The differences between excitation and absorption spectra are due to some slight aggregation in the latter. The photophysical and photochemical properties of **3** were studied in DMSO. However, it was difficult to obtain significant photophysical and photochemical information for **3** in water, although the conjugate was not aggregated in this solvent when compared to the absorption peak in DMSO (Fig. 3.5). The quenching of Pc photophysicochemical properties by water has been documented before [95].

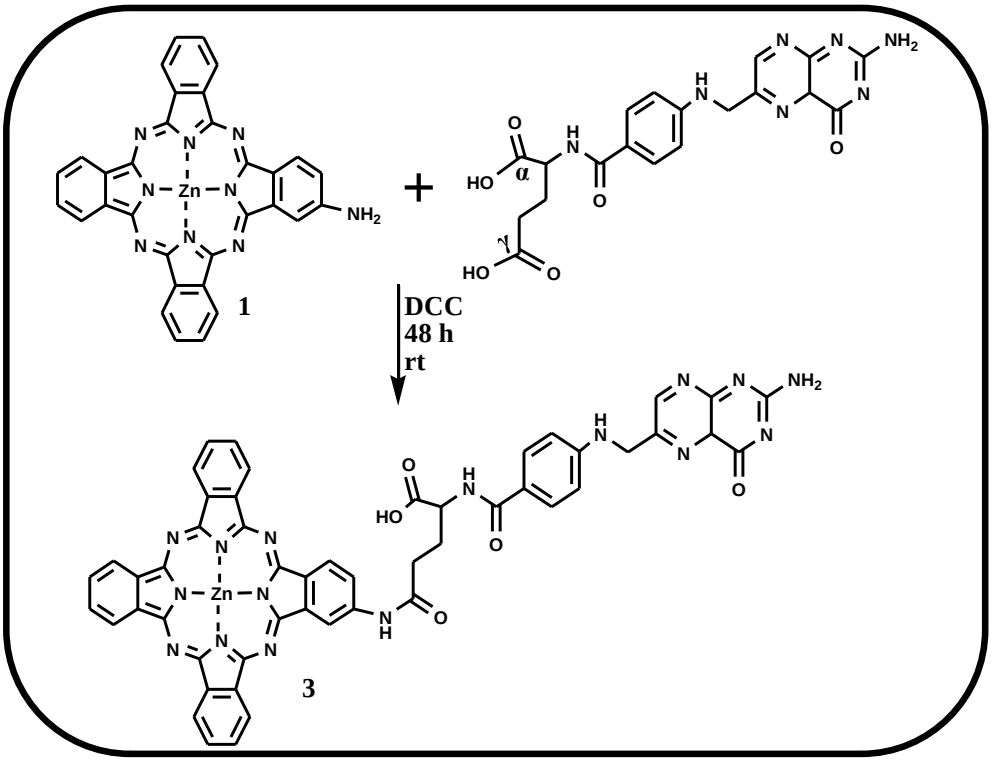

Scheme 3.2: Synthetic route for ZnMAPc-FA (**3**).

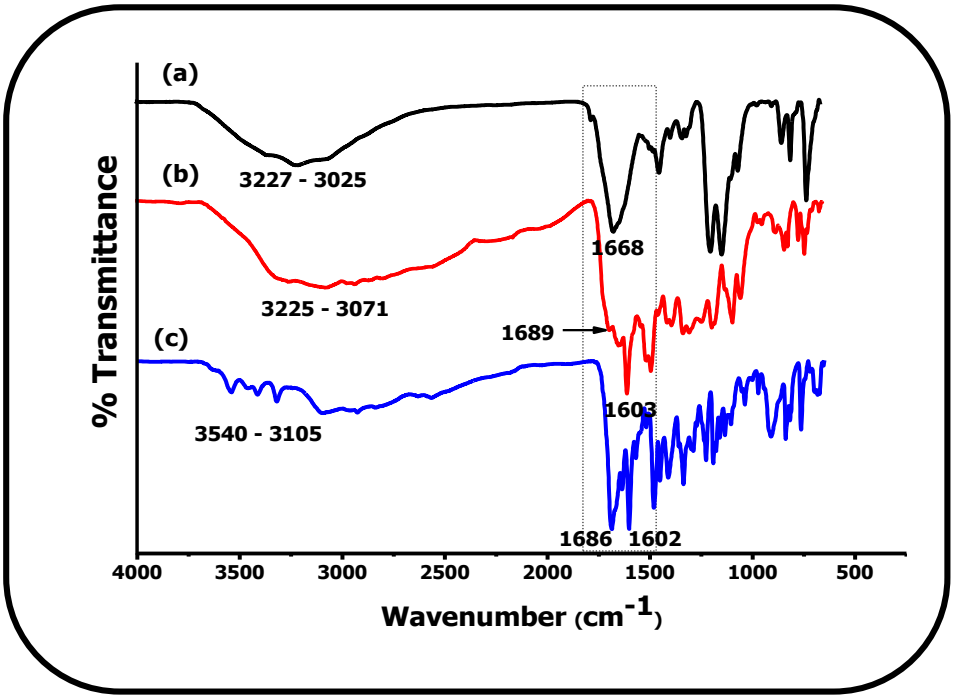

Fig. 3.4: FTIR spectra of ZnMAPc (**1**) (a), ZnMAPc-FA (**3**) (b) and FA (c).

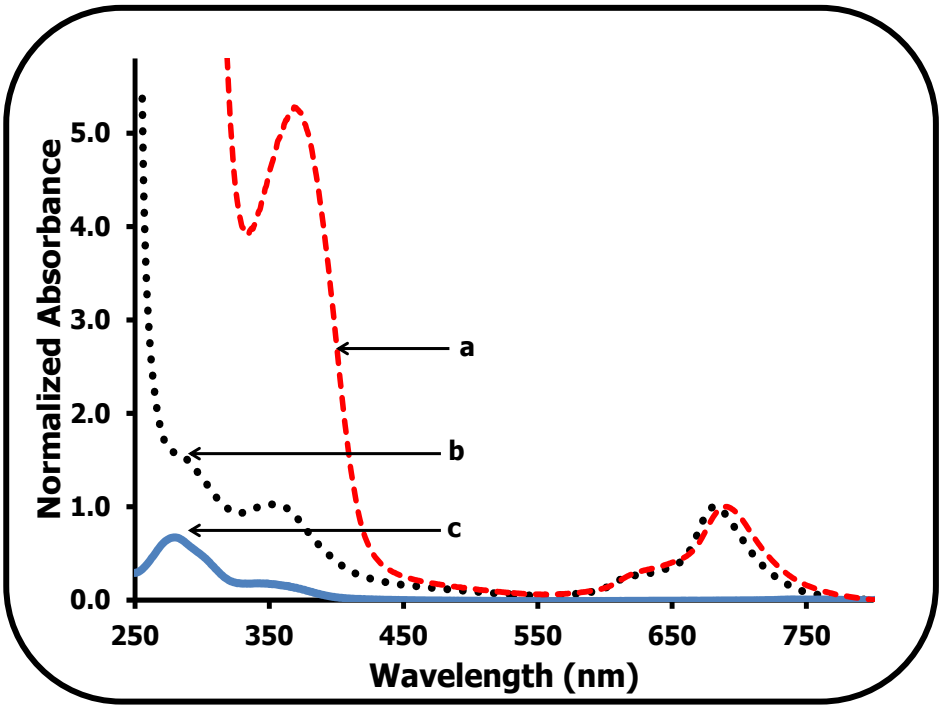

Fig. 3.5: Absorption spectra of ZnMAPc-FA (**3**) in water (a), ZnMAPc-FA (**3**) in DMSO (b) and FA in water (c). The concentration of ZnMAPc-FA (**3**) is 7.5×10^{-6} M.

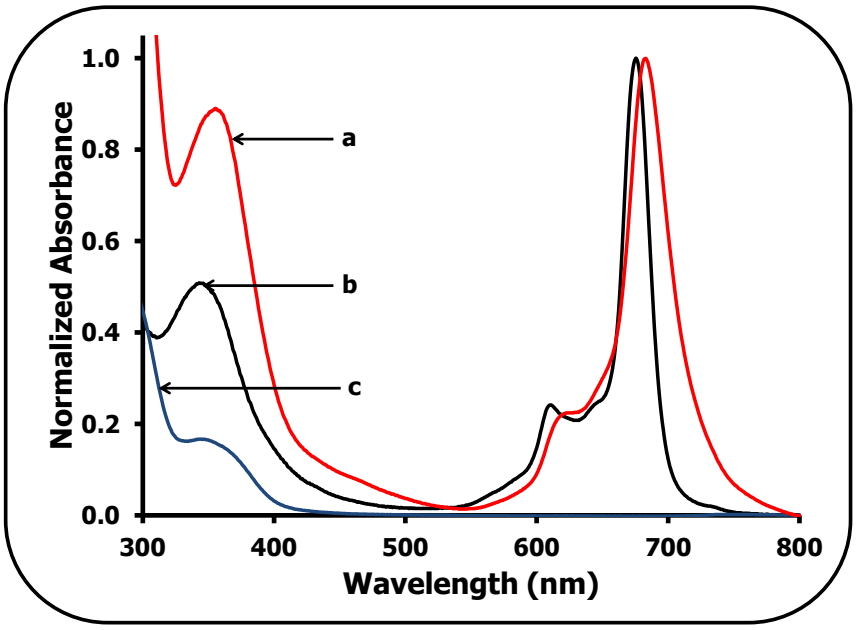

Fig. 3.6: Absorption spectra of ZnMAPc-FA (**3**) (a), ZnMAPc (**1**) (b) and FA (c) in DMSO. The concentration of ZnMAPc-FA (**3**) is 7.5×10^{-6} M.

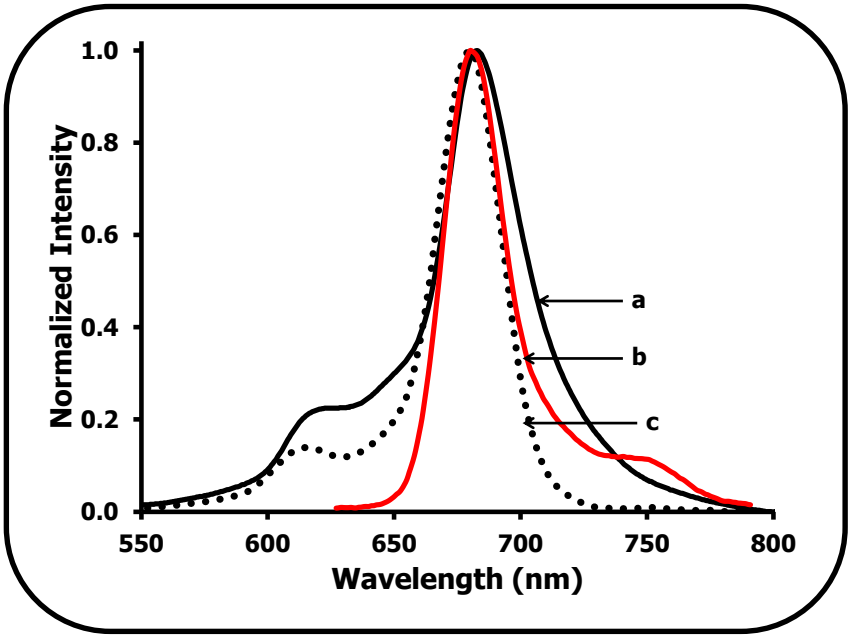

Fig. 3.7: Absorption (a), Emission (b) and Excitation (c) spectra of ZnMAPc-FA (**3**) in DMSO (excitation wavelength = 610 nm). The concentration of ZnMAPc-FA (**3**) is 5.0 × 10^{-7} M.

3.2.1.2 ZnMCPPc-spermine (5) conjugate

Conjugate **5** (ZnMCPPc-spermine) was synthesized by the formation of amide bond between ZnMCPPc (**4**) and spermine (Scheme 3.3). The carboxy group of ZnMCPPc (**4**) was first activated using DCC for 24 h followed by the addition of spermine. The respective protons for complex **5** as obtained from ^{1}H NMR were found at expected position (values are provided in section 2.3.3). The FTIR result confirms the formation of amide bond with N-H str. at 3412 - 3139 cm^{-1}, 1646 cm^{-1} (C=O, amide) and 1599 cm^{-1} (N-H bend) for **5** (Fig 3.8b). The C=O amide at 1646 cm^{-1} was not present either in **4** (Fig. 3.8a) or spermine (Fig. 3.8c) alone. Further prove of the formation of **5** was confirmed by elemental analysis and mass spectroscopy results (values

are provided in section 2.3.3), the data correspond to 1:1 combination of ZnMCPPc and spermine.

The ground state absorption spectrum of **5** was similar to **4**. Complex **4** and **5** exhibited monomeric Q-band with maximum at ~675 nm (Fig. 3.9), Table 3.1. There was no change in the Q-band maxima of **4** in the presence of spermine.

The Q-band of the absorption and excitation spectra were similar and mirror image of the emission spectrum (Table 3.1, figures not shown). There was no broadening due to aggregation in the Q-band of the absorption and excitation spectra.

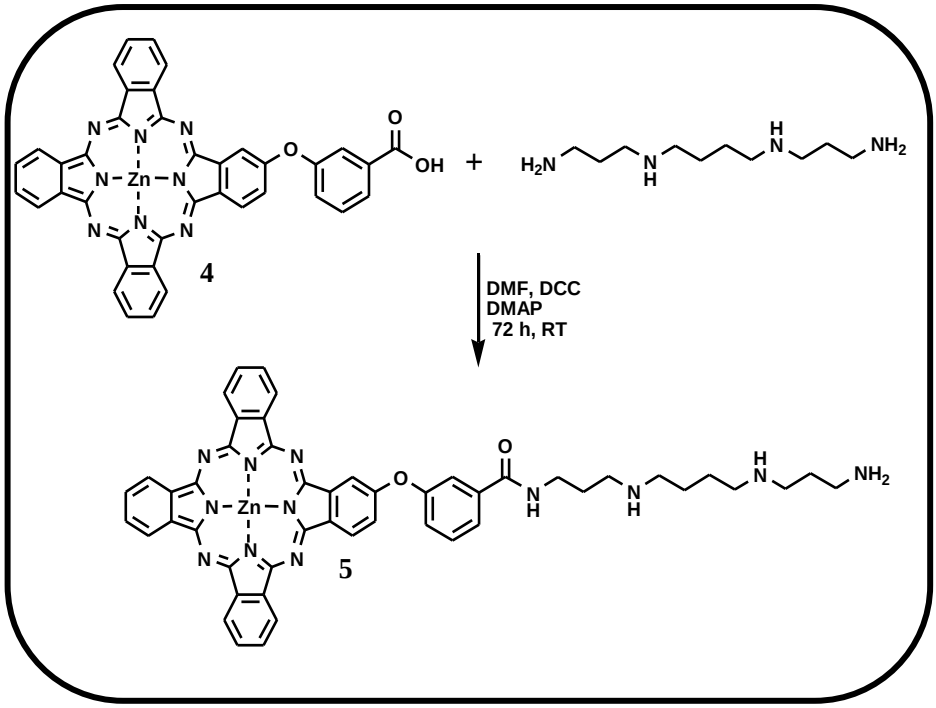

Scheme 3.3: Synthetic route for ZnMCPPc-spermine (**5**).

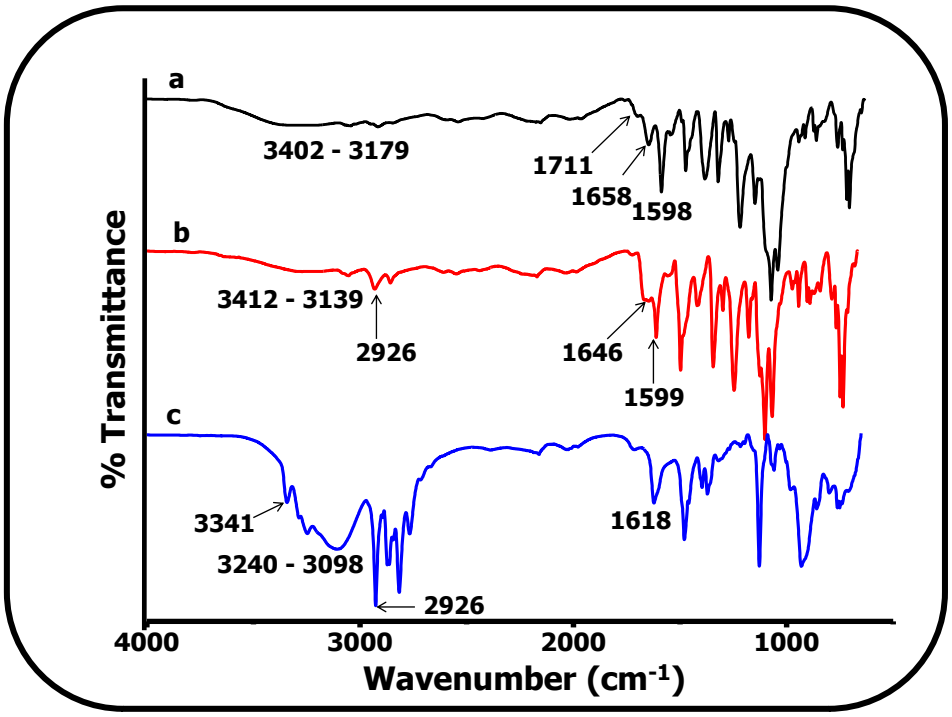

Fig. 3.8: FTIR spectra of ZnMCPPc (**4**) (a), ZnMCPPc-spermine (**5**) (b) and spermine (c).

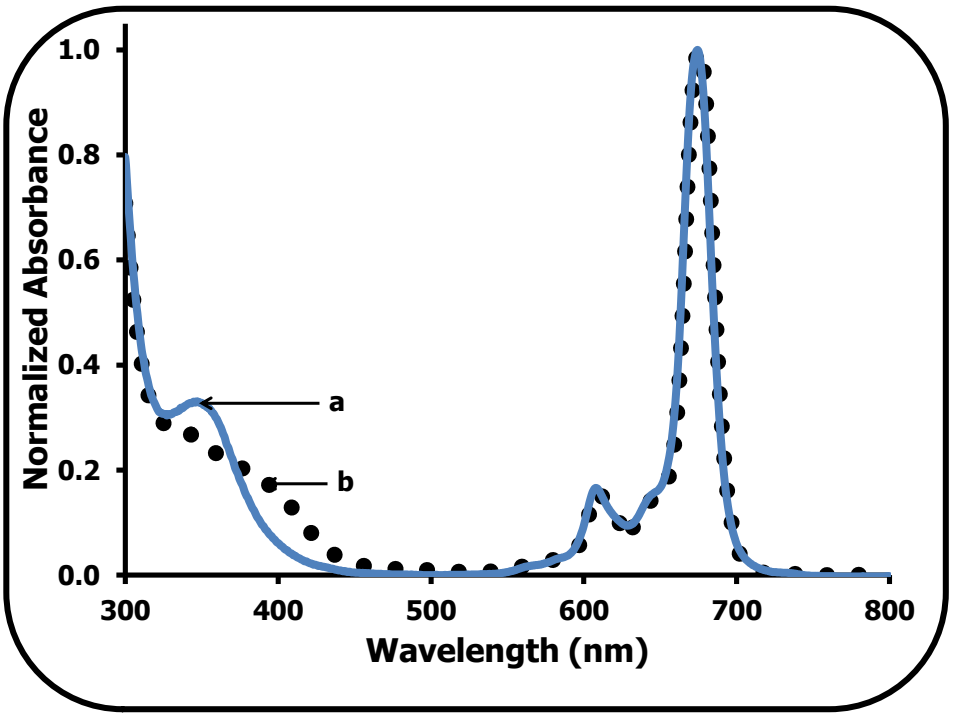

Fig. 3.9: Absorption spectra of ZnMCPPc-spermine (**5**) (a) and ZnMCPPc (**4**) (b) in DMSO. The concentration of ZnMAPc-spermine (**5**) is 4.7×10^{-6} M.

3.2.1.3 ZnOCPc- bovine serum albumin (ZnOCPc-BSA (11)) conjugate

ZnOCPc-BSA (**11**) was formed by conjugating ZnOCPc (**10**) to bovine serum albumin (BSA) through amide bond, the carboxyl groups on the ZnOCPc was activated using EDC and NHS (Scheme 3.4). The FTIR spectrum of conjugate **11** exhibits peaks between 3362 cm^{-1} and 2820 cm^{-1} (N-H str.), 1560 cm^{-1} (C=O amide and N-H bend), Fig. 3.10b. It was difficult to characterize this complex using FTIR because BSA alone has amide bonds. However, the appearance of the peaks in a new environment indicated successful formation of a new complex.

The absorption spectrum of **11** (Fig. 3.11a) shows characteristic monomeric Q-band maxima of MPc at 687 nm which was slightly blue shifted as compared to the Q-band maxima of 691 nm for **10**, Table 3.1. Such small changes may indicate changes in the Pc environment.

The absorption (Fig. 3.12a) and excitation (Fig. 3.12b) spectra were alike. There was no aggregation of ZnOCPc (**10**) in the presence of BSA in the excited or ground state.

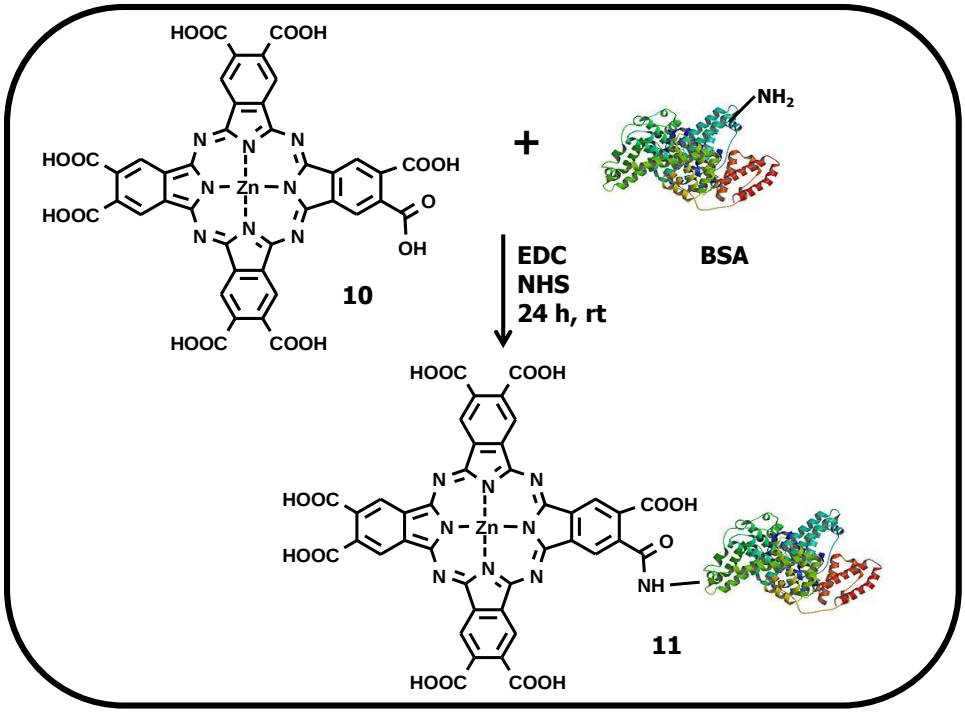

Scheme 3.4: Synthetic route for ZnOCPc-BSA (**11**).

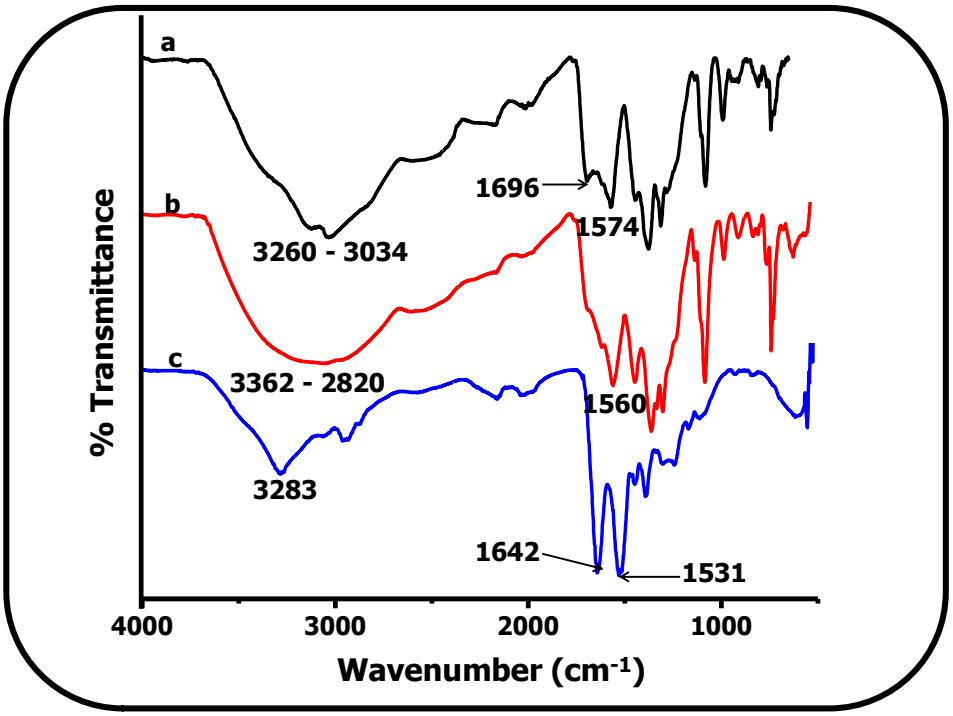

Fig. 3.10: FTIR spectra of ZnOCPc (**10**) (a), ZnOCPc-BSA (**11**) (b) and BSA (c).

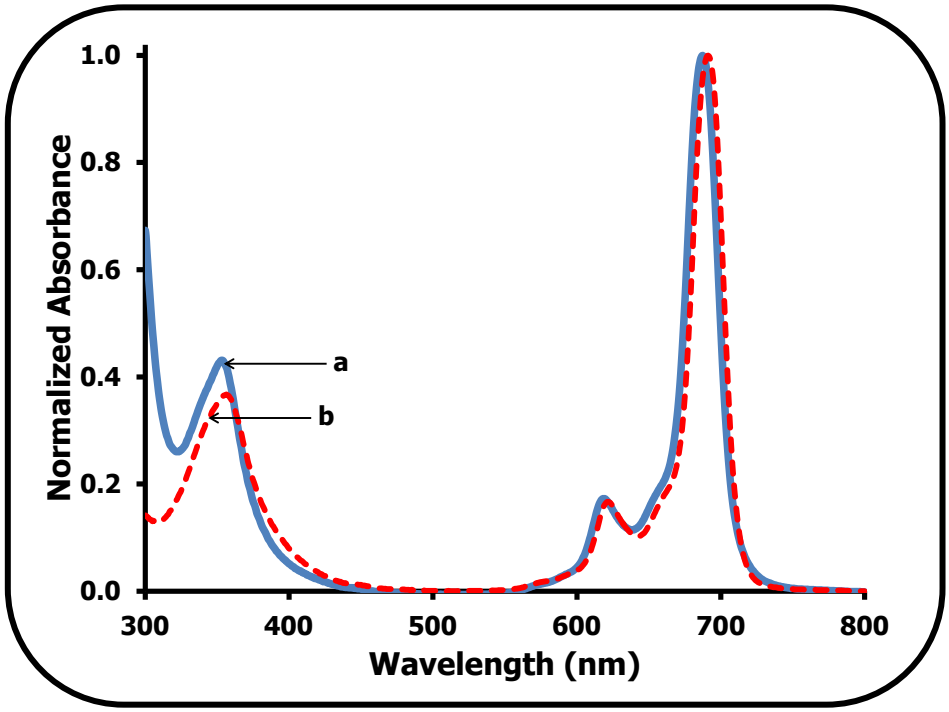

Fig. 3.11: Absorption spectra of ZnOCPc-BSA (**11**) (a) and ZnOCPc (**10**) (b) in pH 9 buffer. The concentration of ZnOCPc (**10**) is 7.5×10^{-6} M.

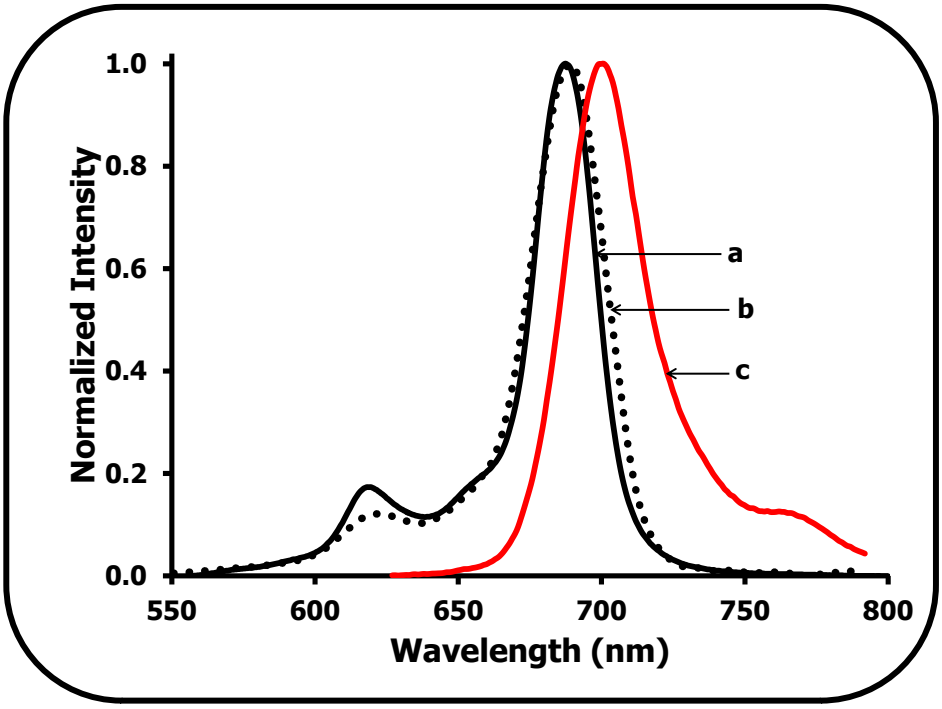

Fig. 3.12: Absorption (a), Excitation (b) and Emission (c) spectra of ZnOCPc-BSA (**11**) in pH 9 buffer. (Excitation wavelength = 610 nm). The concentration of ZnOCPc (**11**) is 5.0×10^{-7} M.

3.2.2 Ester bond conjugated metallophthalocyanine-biomolecule complexes

Complexes **6**, **7** and **9** were formed through ester bond linkage, a reaction between a carboxylic acid group and hydroxyl group.

3.2.2.1 ZnMCPPc-uridine (6) conjugate

Conjugate **6** (ZnMCPPc-uridine) was synthesised by first protecting uridine (Scheme 3.5). This was done to ensure that only one hydroxyl group was available for reaction. Uridine was treated with anhydrous acetone and H_2SO_4 to give the protected group (2',3'-O-isopropylideneuridine

[115]). An esterification reaction between (ZnMCPPc) **4** and 2',3'-O-isopropylideneuridine in the presence of DCC in order to activate the carboxyl group of **4**, afforded ZnMCPPc-2',3'-O-isopropylideneuridine, which was confirmed by FTIR, elemental analysis, ^{1}H NMR and mass spectroscopy. The de-protection of ZnMCPPc-2',3'-O-isopropylideneuridine was achieved by treating the conjugate with aqueous TFA to give ZnMCPPc-uridine (**6**), Scheme 3.5. There was a general shift in the ^{1}H NMR peaks of uridine to lower fields when compared to uridine alone due to de-shielding effect of the aromatic ring of the MPcs. The Aromatic protons of **6** were between δ = 8.15 and 7.49 ppm while the protons due to the presence of uridine were between δ = 5.79 - 3.96 ppm, instead of δ = 5.78 - 3.53 ppm in uridine alone.

The presence of ester bond in **6** was confirmed using FTIR. ZnMCPPc-2',3'-O-isopropylideneuridine exhibited an intense CH stretch at 2927 and 2851 cm^{-1}, C=O peak at 1713 and 1625 cm^{-1}, C-O-C stretch at 1088 and 1052 cm^{-1} (Fig. 3.13b). These peaks were at different wave-numbers compared to either **4** (Fig. 3.13d) or 2',3'-O-isopropylideneuridine (Fig. 3.13a). On the formation of ZnMCPPc-uridine (**6**), there was decrease in the intensities of the CH stretches of ZnMCPPc-2',3'-O-isopropylideneuridine (Fig. 3.13b), shift in the broad O-H peaks between 3412 - 3053 cm^{-1} for **4** (Fig. 3.13d) to 3058 - 2918 cm^{-1} (Fig. 3.13c) for **6** and the appearance of the C=O peaks at different wave-numbers of 1687 and 1596 cm^{-1} (Fig. 3.13c) in **6**. The elemental analysis and mass spectra data also confirm the successful formation of ZnMCPPc-uridine (**6**) conjugate in 1:1 combination.

The UV-VIS absorption spectrum of the conjugate in DMSO showed negligible change in the Q-band maxima of **4** in the presence of uridine. And there was no change in the Q-band of the absorption and excitation spectra which were mirror image of the emission spectrum, Table 3.1.

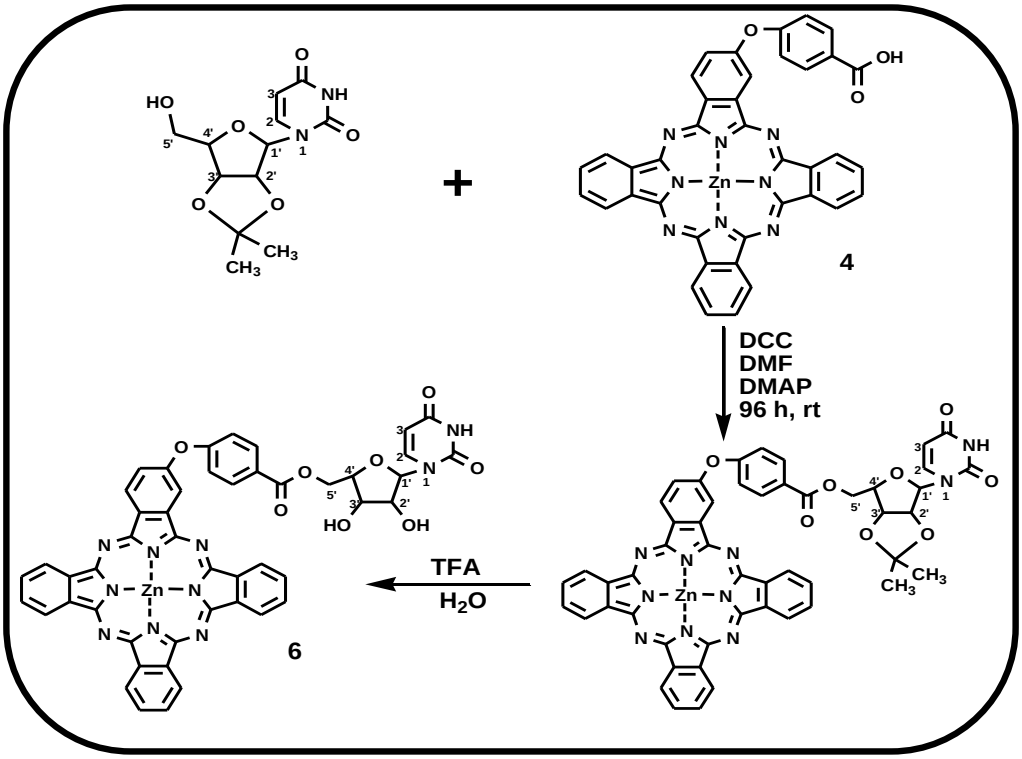

Scheme 3.5: Synthetic route for ZnMCPPc-uridine (**6**).

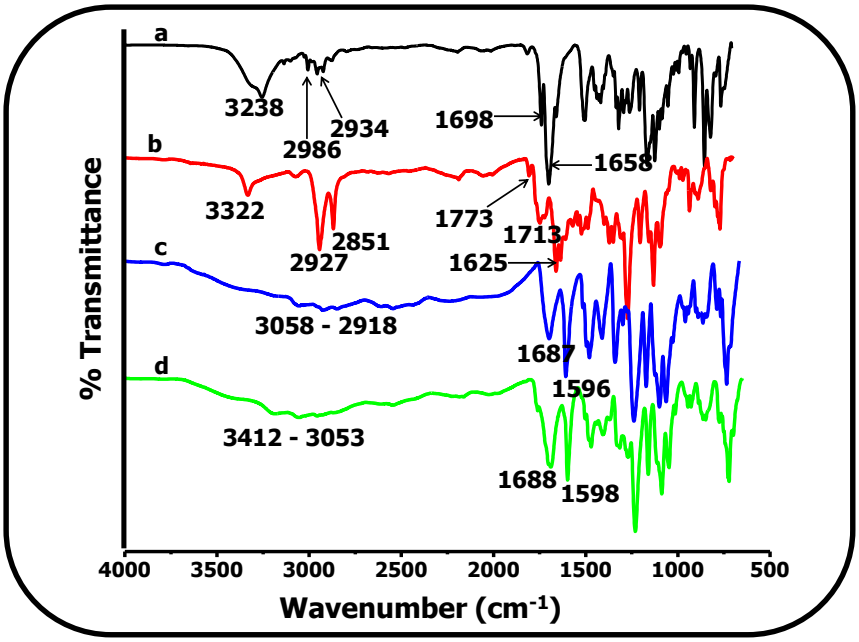

Fig 3.13: FTIR spectra of 2',3'-O-isopropylideneuridine (a), ZnMCPPc-2',3'-O-isopropylideneuridine, (b), ZnMCPPc-uridine (**6**) (c) and ZnMCPPc (**4**) (d).

3.2.2.2 ZnMCPPc-AA (7) and ZnTCPPc-AA (9) conjugate

The synthetic route used for the formation of ZnMCPPc-AA (**7**) is shown in Scheme 3.6A. The activation of the carboxyl group on the ZnMCPPc was done using DCC. Similar procedure was used in the formation of ZnTCPPc-AA (**9**) conjugate, Scheme 3.6B. ZnMCPPc-AA (**7**) was confirmed pure by ^{1}H NMR with both the substituent and ring protons observed in their respective regions. In the ^{1}H NMR spectrum of **7** the aromatic Pc protons appear between 9.09 and 7.53 ppm (integrating for 19H). The aliphatic protons from the CH of the ascorbic acid unit of **7** were observed at 4.70 ppm (1H, CH), 3.72 ppm (1H, CH) and 3.41 ppm (2H, CH_2) integrating for a total of 4 protons. In the mass spectrum of **7**, the presence of molecular ion peaks at amu 874 $[M+2H]^+$ confirmed the proposed structures. As stated above, MPc complexes have been observed to degrade with molecular ion peaks $[M]^+$, $[M+nH]^+$ or $[M-nH]^+$ (n = 1-3) [127]. The ^{1}H NMR of **9** shows a broader spectrum with the 28 aromatic proton signals between δ = 8.9 - 7.3 ppm and the proton from the CH of the ascorbic acid units were between δ = 4.70 - 3.40 ppm. The elemental analysis and the mass spectra data also confirm mono-substituted conjugate for **7** and a tetra-substituted conjugate for **9**.

The FTIR spectrum of complex **7** is shown in Fig. 3.14, it exhibits broad O-H stretch between 3341 and 2926 cm^{-1} (Fig. 3.14b). The C=O peak shifted from 1713 cm^{-1} (Fig. 3.14 a) for **4**, 1752 and 1651 cm^{-1} (Fig. 3.14c) for ascorbic acid (AA) to 1711 and 1597 cm^{-1} (Fig. 3.14b) for **7** as a result of conjugation. O-H bend at 1393 cm^{-1}, C-O-C stretches at 1088 cm^{-1} and 1051 cm^{-1} were also observed in **7**. Similar shift was observed for **9**, Fig. 3.15b shows the FTIR spectrum of complex **9** which exhibits broad O-H stretch between 3437 and 3093 cm^{-1}, which are at longer wave-numbers compared to the O-H stretch of complex **8** between 3372 and 2840 cm^{-1} Fig. 3.15a, as a result of the presence of ascorbic acid in the latter. The C=O peak shifted from 1711

cm^{-1} (Fig. 3.15a) (**8**) and 1752 cm^{-1} (Fig. 3.15c) (ascorbic acid) to 1694 cm^{-1} and 1600 cm^{-1} (Fig. 3.15b) for **9** as a result of conjugation. A new peak for O-H bend at 1387 cm^{-1} and C-O-C stretches at 1091 cm^{-1} and 1043 cm^{-1} (Fig. 3.15b) were also observed in **9**.

There was no change in the Q-band maxima of **4** in the presence of ascorbic acid (complex **7**). Similar negligible change in the Q-band maxima was observed on conjugating AA to **8** to give ZnTCPPc-AA (**9**), Table 3.1. On comparing the absorption spectra of **7** (Fig. 3.16A (b)) and **9** (Fig. 3.16A (a)), about 7 nm red shift was observed in the Q-band maxima of **9** (from **8**) compared to that of **7** (from **4**) and there was slight broadening of the Q-band of **9**. The broadening observed in **9** is due to aggregation. Similar red shift of the Q-band was observed in the absorption spectra of **8** and **4** (Fig. 3.16B). The red shift observed in **8** is due to the presence of more electron withdrawing groups (four carboxy groups) as compared to **4** with one carboxy group. Red or blue shifts in the Q-band maxima of phthalocynines are as a result of the presence of either electron-withdrawing (carboxyl, floro, sulphonyl) or electron-donating (amino, alkoxy and alkyl) groups [20]. Electron-withdrawing substituent causes red shift of the Q-band maxima, while electron-donating substituent causes blue shift. Thus, the Q-band of complexes **8** and **9** were red shifted as compared to **4** and **7**.

The absorption and excitation spectra of either **7** or **9** were similar, Table 3.1 (figures not shown).

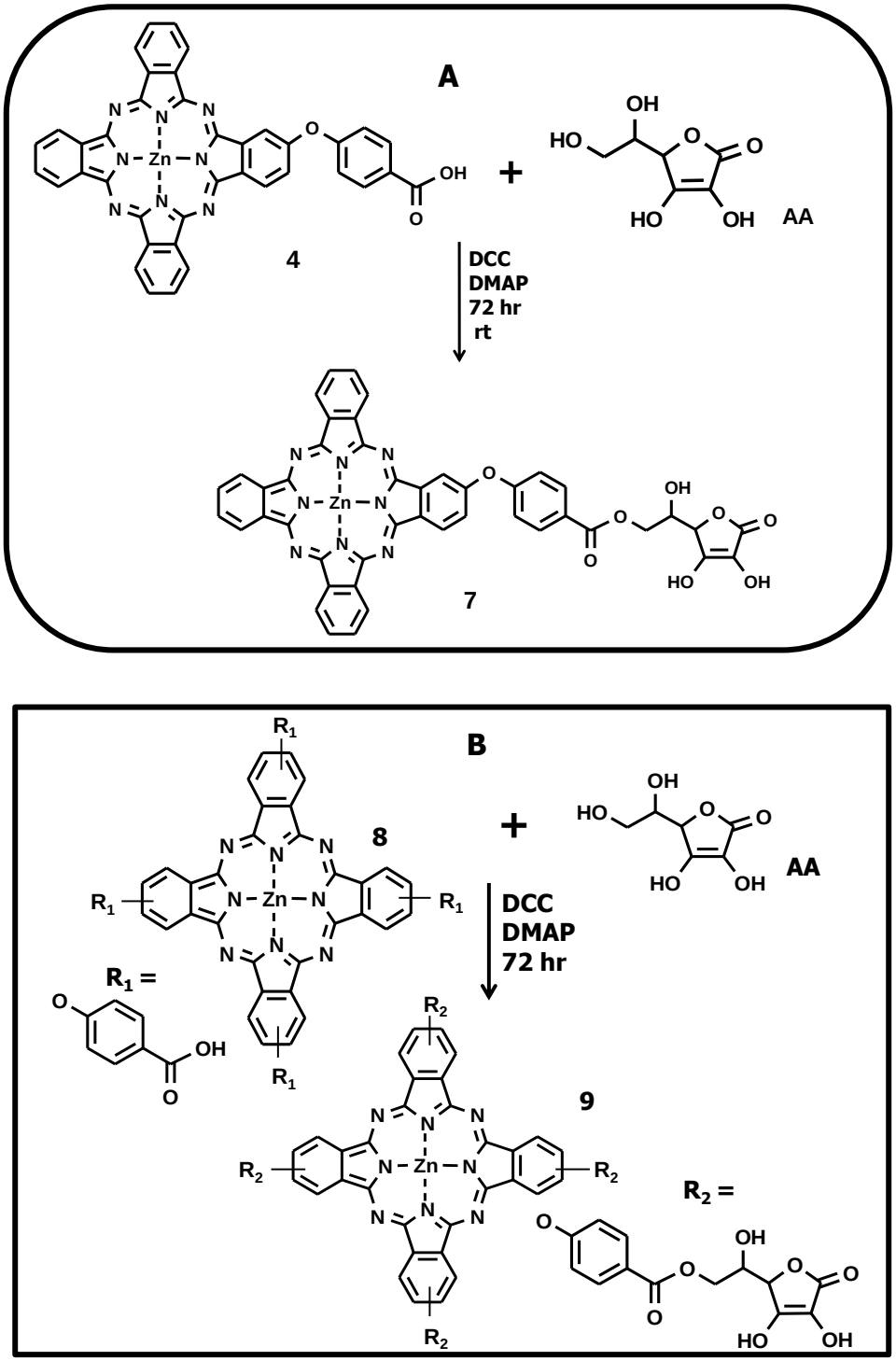

Scheme 3.6: Synthetic routes for ZnMCPPc-AA (**7**) (A) and ZnTCPPc-AA (**9**) (B).

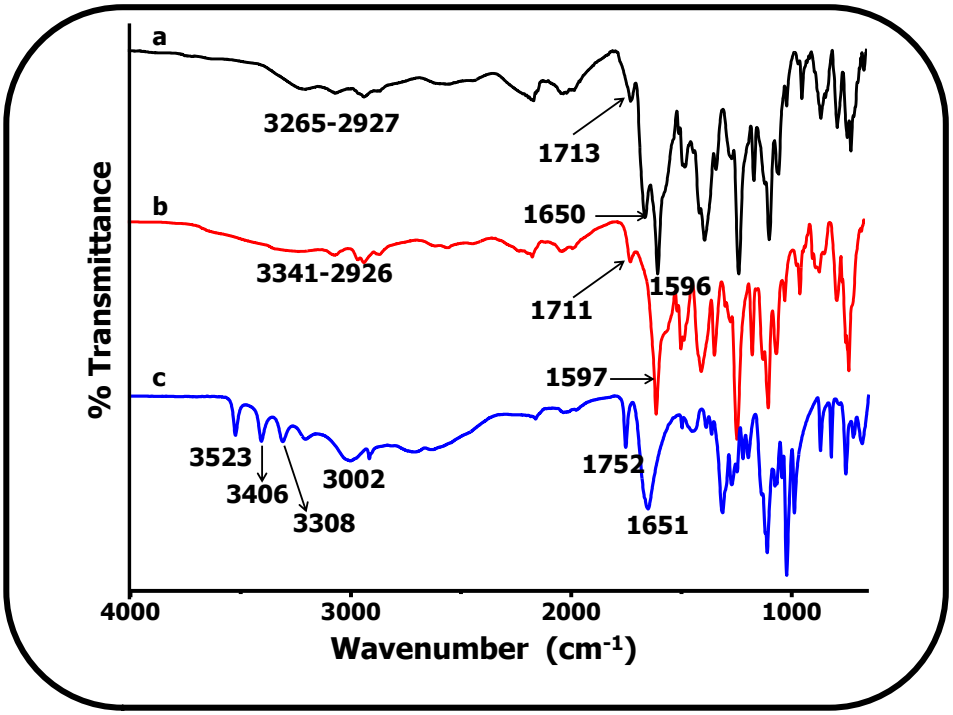

Fig. 3.14: FTIR spectra of ZnMCPPc (**4**) (a), ZnMCPPc-AA (**7**) (b) and ascorbic acid (c).

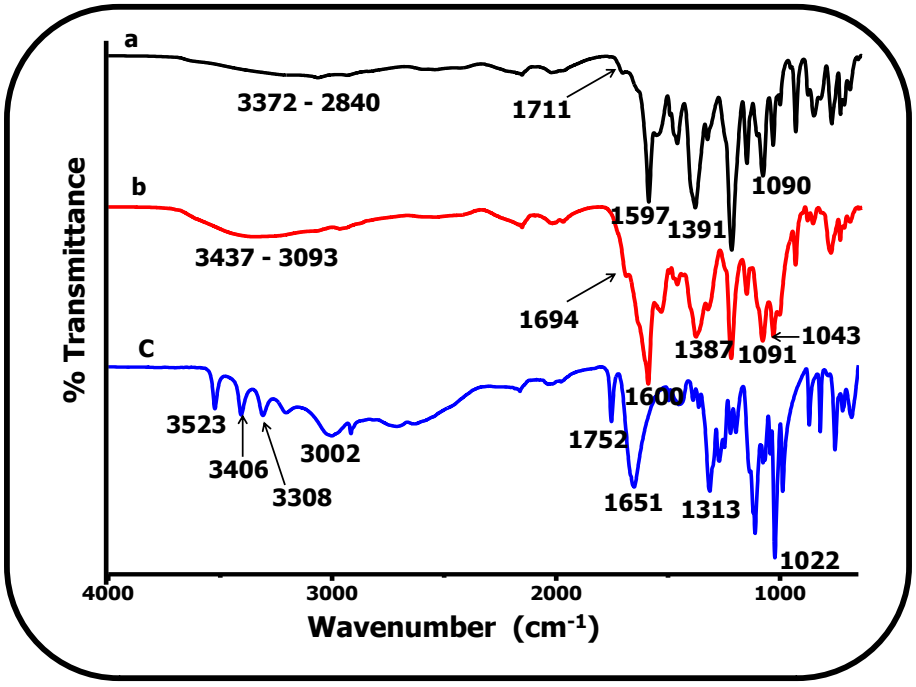

Fig. 3.15: FTIR spectra of ZnTCPPc (**8**) (a), ZnTCPPc-AA (**9**) (b) and ascorbic acid (c).

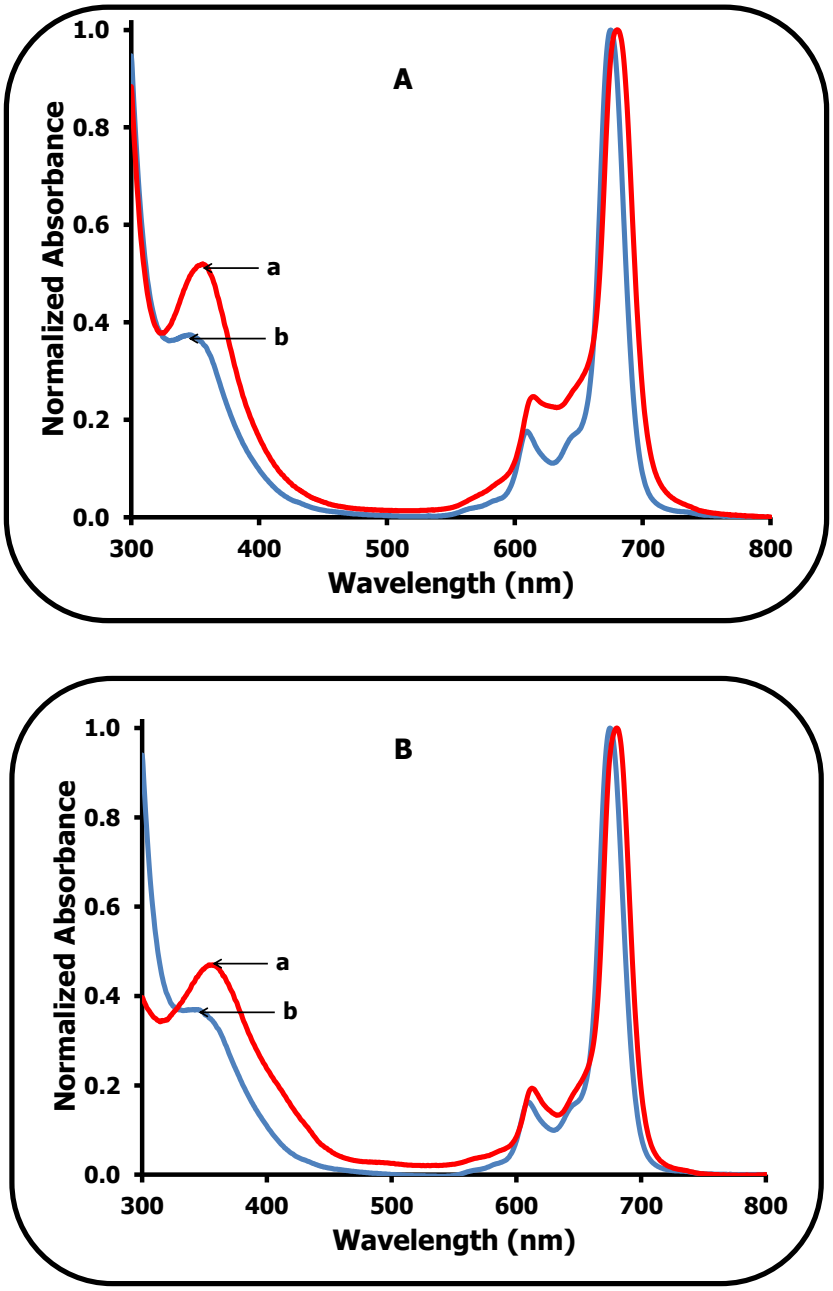

Fig. 3.16: Absorption spectra of (A); ZnTCPPc-AA (**9**) (a) and ZnMCPPc-AA (**7**) (b) and (B); ZnTCPPc (**8**) (a) and ZnMCPPc (**4**) (b) in DMSO. The concentration of ZnTCPPc-AA (**9**) = 3.8×10^{-6} M, ZnMCPPc-AA (**7**) = 4.7×10^{-6} M, ZnTCPPc (**8**) = 7.5×10^{-6} M and ZnMCPPc (**4**) is 4.7×10^{-6} M.

Table 3.1: Spectra properties of ZnPc (or ZnPc-biomolecule) complexes

ZnPcs (or ZnPc-biomolecule conjugates)	**Solvent**	**Q-band $^{a}\lambda_{max}$ /nm**	**Emission $^{b}\lambda_{Em}$ /nm**	**Excitation $^{c}\lambda_{Exc}$ /nm**	**Log ε at Q-band maxima**
ZnMAPc (**1**)	DMSO	676	683	676	5.2
ZnMAPc-Py (**2**)	DMSO	679	683	677	5.2
ZnMAPc-FA (**3**)	DMSO	683	688	682	5.3
ZnMCPPc (**4**)	DMSO	675	685	675	5.5
ZnMCPPc-spermine (**5**)	DMSO	675	682	675	5.5
ZnMCPPc-uridine (**6**)	DMSO	674	683	674	5.5
ZnMCPPc-AA (**7**)	DMSO	675	686	676	5.5
ZnTCPPc (**8**)	DMSO	680	691	681	5.3
ZnTCPPc-AA (**9**)	DMSO	681	692	683	5.6
ZnOCPc (**10**)	Buffer 9	691	700	690	5.3
ZnOCPc-BSA (**11**)	Buffer 9	687	700	689	5.3
ZnMAPPc (**12**)	DMSO	675	684	675	5.1
ZnTAPPc (**13**)	DMSO	686	695	687	5.3

$^{a}\lambda_{max}$ = absorption maxima, $^{b}\lambda_{Em}$ = emission maxima, $^{c}\lambda_{Exc}$ = excitation maxima

3.3 Characterization of SWCNT-COOH complexes functionalized with ZnPcs or biomolecules

3.3.1 Covalently linked SWCNT-COOH conjugates

SWCNT-COOH was covalently linked to folic acid (FA), ascorbic acid (AA), ZnMAPc (**1**), ZnMAPPc (**12**) or ZnTAPPc (**13**) by activating the carboxy groups of SWCNT-COOH. Amide bonds for FA, ZnMAPc (**1**), ZnMAPPc (**12**) or ZnTAPPc (**13**) and ester bond for AA.

3.3.1.1 SWCNT-folic acid (SWCNT-FA) (or SWCNT-COOH-ascorbic acid (SWCNT-AA)) conjugate

The formation of SWCNT-FA is shown in Scheme 3.7A. The carboxy groups of SWCNT-COOH were activated using EDC and NHS in pH 7 buffer, followed by the addition of folic acid. The FTIR spectrum of SWCNT-FA exhibits peaks between 3312 cm^{-1} and 3001 cm^{-1} (N-H str.), 1692 cm^{-1} (C=O amide) and 1604 cm^{-1} (N-H bend), (figure not shown). These peaks were not found in either folic acid or SWCNT-COOH alone. This indicates successful conjugation of folic acid to SWCNT-COOH. Confirmation of the amide bond is complicated by the fact that FA alone has amide bonds.

SWCNT-AA was formed via an ester bond linkage between SWCNT-COOH and ascorbic acid, Scheme 3.7B. The carboxy groups of SWCNT-COOH were activated using EDC and NHS, followed by the addition of ascorbic acid. The modification of SWCNT-COOH with ascorbic acid via ester bond resulted in changes of the FTIR spectra of the complexes (figure not shown). SWCNT-AA exhibited an O-H str. between 3480 and 3190 cm^{-1}, which overlaps with the O-H

str. of SWCNT-COOH and AA. A new C=O peak at 1740 cm^{-1} which is not found in either SWCNT-COOH or AA alone was also observed.

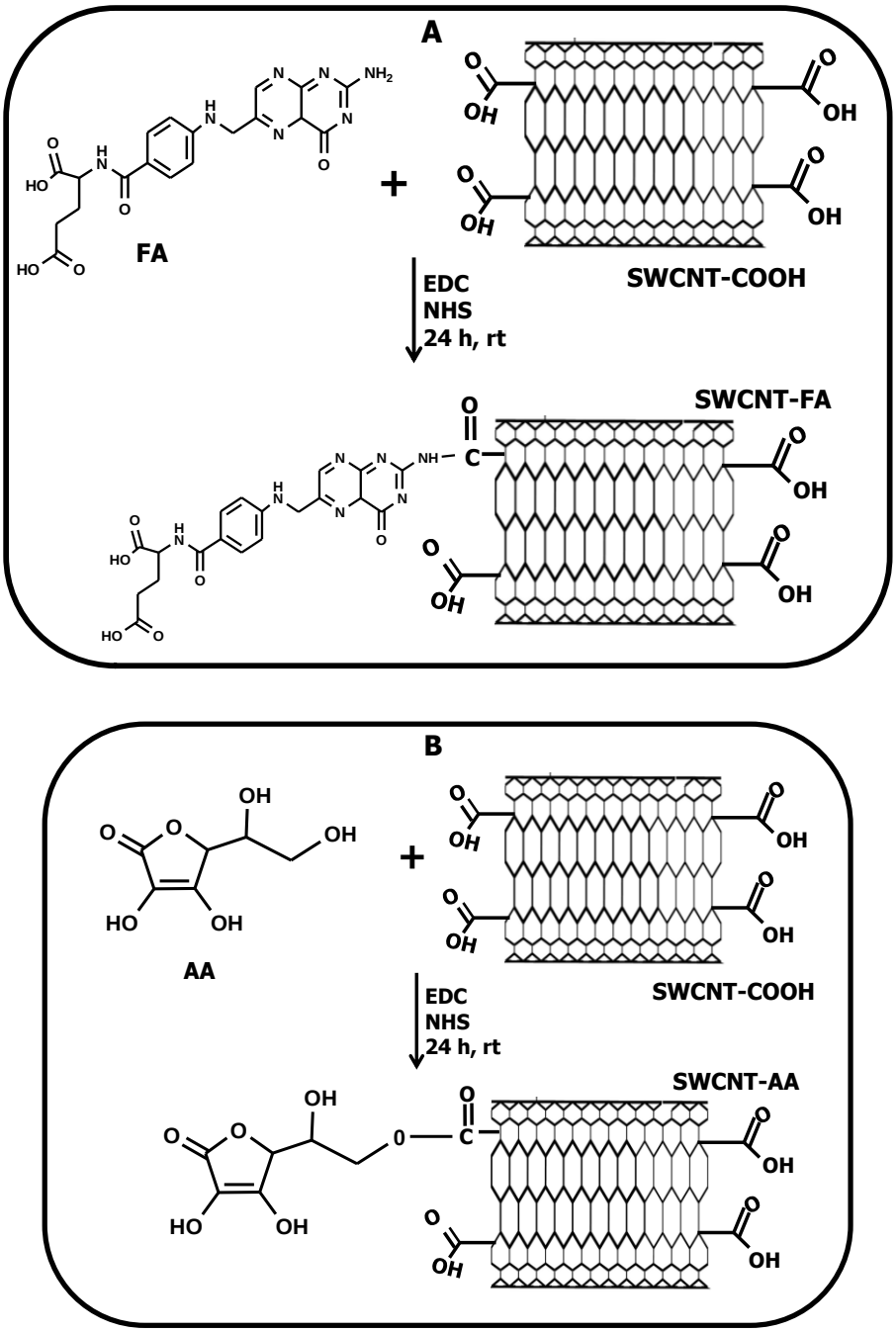

Scheme 3.7: Synthetic routes for SWCNT-FA (A) and SWCNT-AA (B).

3.3.1.2 Covalently linked SWCNT-COOH with amino substituted ZnPc derivatives

SWCNT-COOH was covalently linked to ZnMAPc (**1**), ZnMAPPc (**12**) and ZnTAPPc (**13**) due to the presence of amino group on the Pcs which can form an amide bond linkage with the carboxy group of SWCNT-COOH. The conjugates obtained are ZnMAPc-SWCNT, linked (**19**), ZnMAPPc-SWCNT, linked (**25**) and ZnTAPPc-SWCNT, linked (**27**).

Scheme 3.8 shows a typical synthetic route employed for the formation of ZnPc-SWCNT, linked conjugates using ZnMAPPc-SWCNT (linked) (**25**) as an example. The carboxyl group of SWCNT-COOH was activated using DCC, ZnMAPPc (**12**) was then added and the mixture was stirred at room temperature for 48 h to form ZnMAPPc-SWCNT (linked) (**25**). Similar procedure was used in the formation of **19** and **27**. The FTIR spectrum of **25** (Fig. 3.17b) shows peaks between 3209 - 3047 cm^{-1} (N-H str.), 1656 cm^{-1} (C=O amide), 1605 cm^{-1} (N-H bend), these are at different wave-numbers when compared to **12** or SWCNT-COOH alone. Similar shifts in FTIR peaks indicating the formation of amide bond between the ZnPc moiety and SWCNT-COOH was observed for **19** and **27** (values are provided in section 2.4.3).

The absorption spectra of complexes **25** and **27** (figure not shown) resulted in negligible changes in the Q-band maxima as compared to the precursor Pc, Table 3.2. While a red shift was observed in the absorption spectra of **19** (ZnMAPc-SWCNT) as compared to the precursor Pc (Fig. 3.18). Red or blue shift in the absorption spectra of Pc in the presence of SWCNTs depend largely on the orientation of the Pc with the SWCNTs. Complex **19** was synthesized from ZnMAPc (**1**) which contains an amino group while **25** and **27** were synthesized from **12** (mono amino phenoxy) and **13** (tetra amino phenoxy) respectively. This suggests that the spacer (phenoxy group) acted as a bridge, between the Pc rings and the amino groups in **25** and **27**. Thus, it reduces π electron contribution from the SWCNTs. It is possible that in **19**, the Pc ring is

closer to the SWCNTs, resulting in red shifting of the Q-band maxima due to closer π-π interactions.

The absorption, emission and excitation spectra of ZnMAPc-SWCNT, linked (**19**) are shown in Fig. 3.19. The absorption and excitation spectra are similar, except for slight broadening of the former due to aggregation.

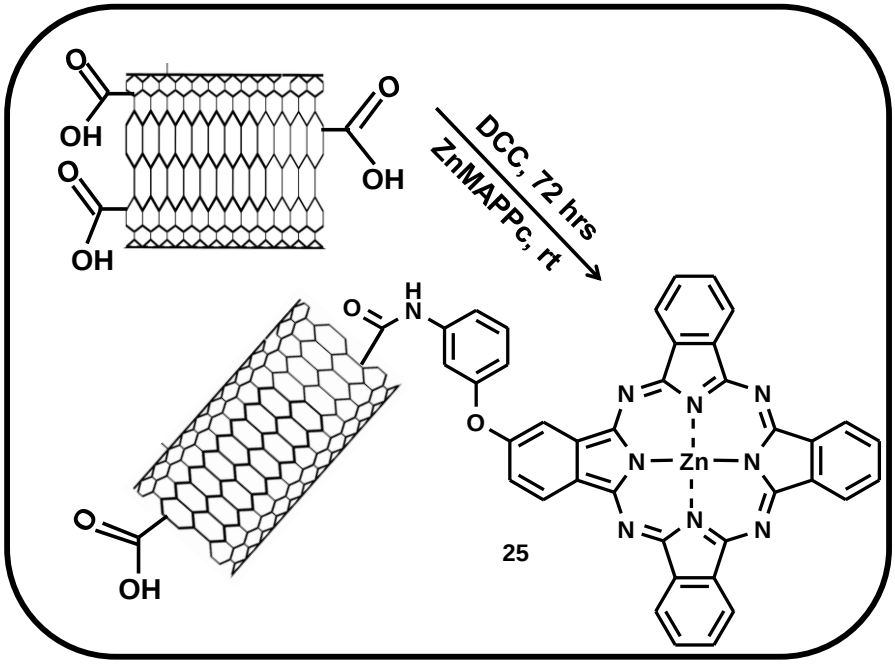

Scheme 3.8: Synthetic route for ZnMAPPc-SWCNT (linked) (**25**).

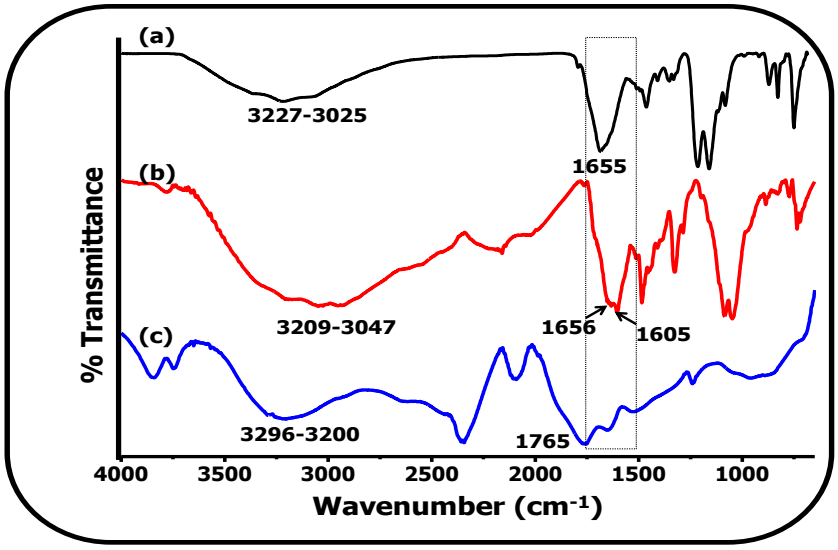

Fig. 3.17: FTIR spectra of ZnMAPPc (**12**) (a), ZnMAPPc-SWCNT (linked) (**25**) (b) and SWCNT-COOH (c).

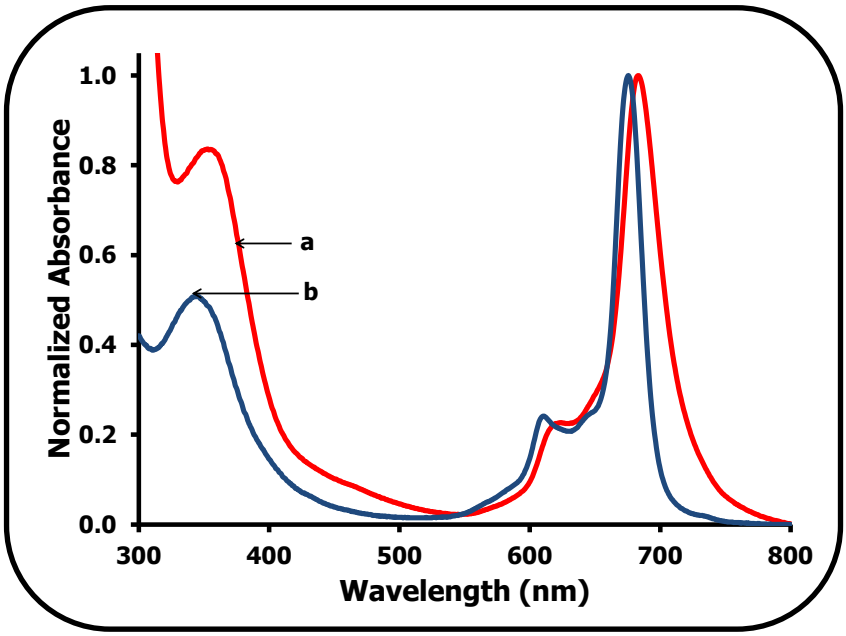

Fig. 3.18: Absorption spectra of ZnMAPc-SWCNT, linked (**19**) (a) and ZnMAPc (**1**) (b) in DMSO. The concentration of ZnMAPc is 1.2×10^{-5} M.

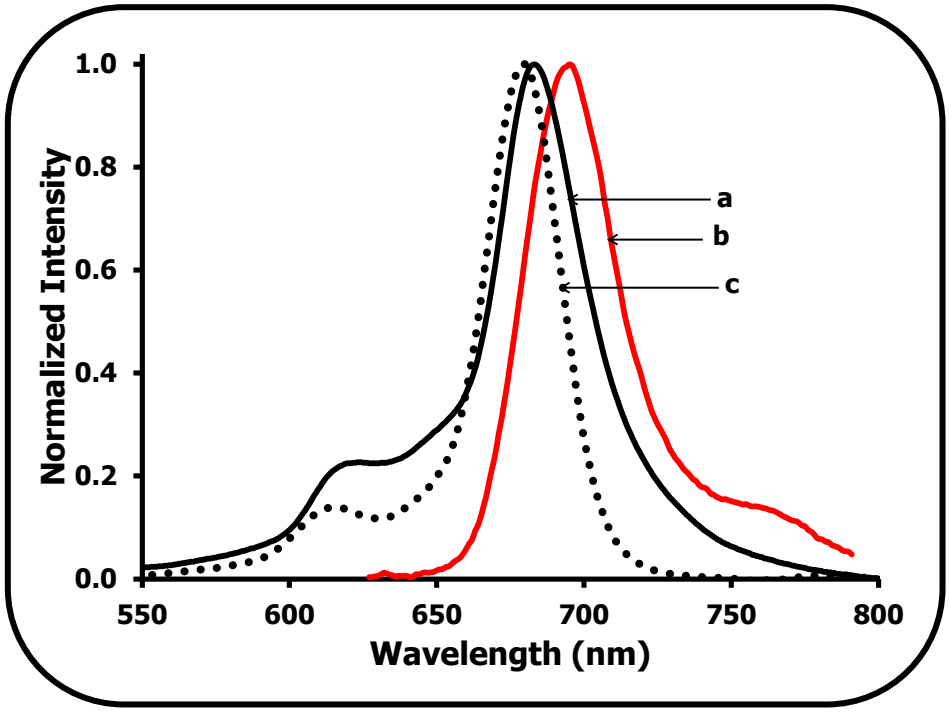

Fig. 3.19: Absorption (a), Emission (b) and Excitation (c) spectra ZnMAPc-SWCNT, linked (**19**) in DMSO. The concentration of ZnMAPc is 1.6×10^{-6} M.

3.3.2 Non-covalently linked SWCNT-COOH with ZnPc derivatives

A typical synthetic route for non-covalent linkage (adsorption) of ZnPcs (or ZnPc-biomolecule conjugates) on SWCNT-COOH is shown in Scheme 3.9 (using ZnMCPPc-uridine-SWCNT, adsorbed (**17**) as an example). The reaction proceeded through π-π stacking interactions between ZnMCPPc-uridine (**6**) and SWCNT-COOH. There was colour change from blue to dark-blue upon adsorption, and the presence of SWCNTs was confirmed using combination of analytical methods, such as, FTIR, x-ray diffractometry (XRD), transmission electron microscopy (TEM), UV-Vis spectrophotometry and Raman spectroscopy.

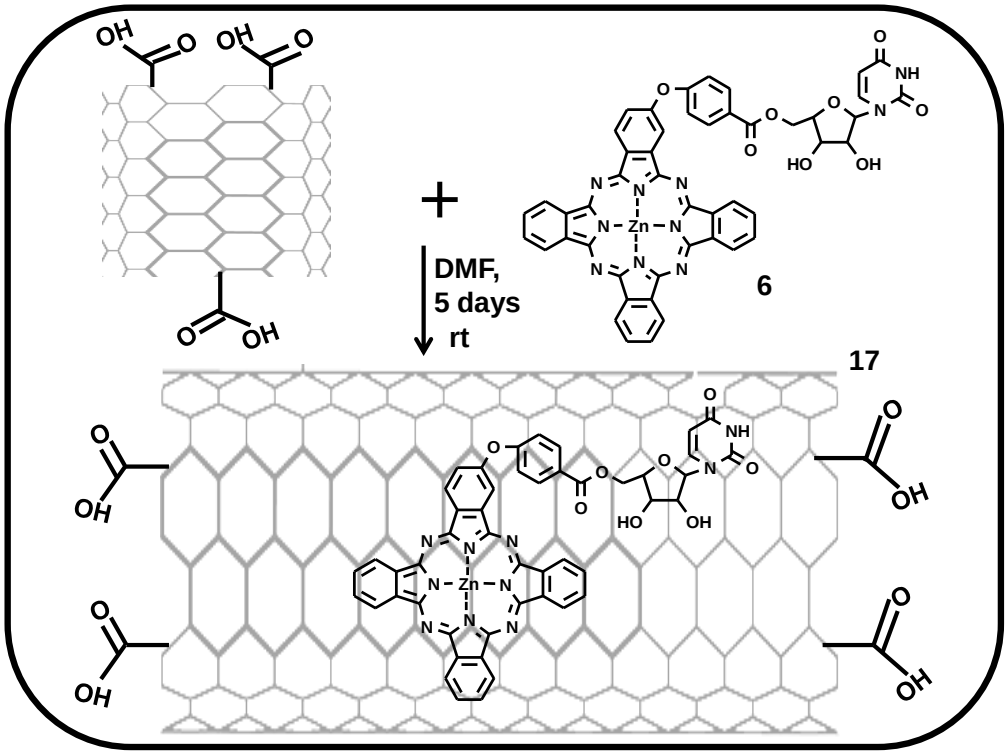

Scheme 3.9: Synthetic route for ZnMCPPc-uridine-SWCNT (adsorbed) (**17**).

3.3.2.1 Fourier transform infrared spectroscopy (FTIR)

FTIR was employed in characterizing all the adsorbed complexes. The FTIR spectrum of **17** is shown in Fig 3.20 as an exmple. Complex **17** (Fig 3.20) exhibited both the characteristics peaks of **6** and SWCNT-COOH, it shows an O-H broad between 3397 - 3165 cm^{-1} similar to the O-H broad at 3296 - 3200 cm^{-1} for SWCNT-COOH. The C=O peak for **17** was observed at 1597 cm^{-1}. Similar shifts and broadness of peaks were observed for all the adsorbed complexes.

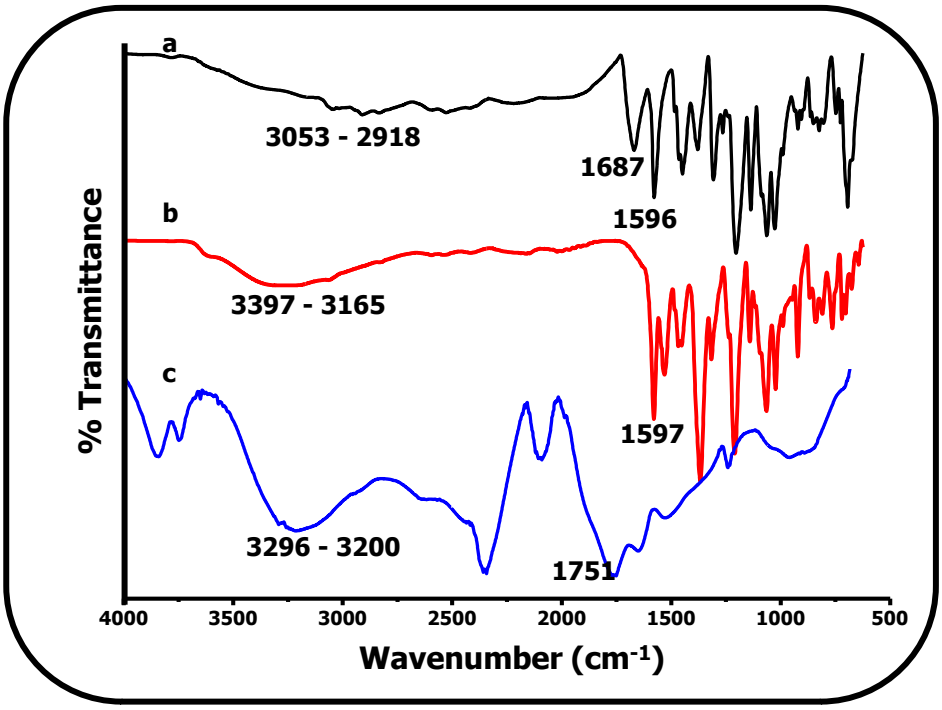

Fig. 3.20: FTIR spectra of ZnMCPPc-uridine (**6**) (a), ZnMCPPc-uridine-SWCNT (adsorbed) (**17**) (b) and SWCNT-COOH (c).

3.3.2.2 UV-Vis absorption and emission spectra

The absorption spectrum of ZnMCPPc-uridine-SWCNT, adsorbed (**17**) is shown in Fig. 3.21 as an example for adsorbed Pc-SWCNT conjugates. Except for few conjugates (complexes, **20** and **24**), negligible changes were observed in the Q-band maxima for most adsorbed complexes as compared to the ZnPcs (or ZnPc-biomolecule conjugates) alone, Table 3.2. An increase in the intensity of the B-band and broadening of the Q-band were observed for most adsorbed complexes, due to the absorption of SWCNTs (as seen in Fig. 3.21 for **17**). Several reports have shown that when Pcs or porphyrins are adsorbed onto carbon nanotubes (CNTs), there is no shift in the absorption bands of the former [72,134], only broadening of the peaks was observed. Broadening of the spectra were observed in this work for most of the adsorbed complexes, in

accordance with literature [72] for π-π interaction of Pc and CNTs. Table 3.2 shows the Q-band maxima for all the complexes in the presence (or absence, values in brackets) of SWCNTs (linked or adsorbed).

Complexes **20** and **24** show red shifted Q-band when compared to the precursor Pc. The red shift might be due to the contribution of the π electron of the SWCNTs depending on the orientation of the Pc. Complex **20** (ZnMAPc-Py-SWCNT) contains pyrene which extended the π conjugation of the Pc ring resulting in a stronger aromatic system, this might have resulted in a stronger π-π interaction with the SWCNTs. While **24** (ZnOCPc-BSA-SWCNT) has BSA, a protein containing multiple sequence of amino acids, this might have also interacted with SWCNTs resulting in red shift of the Q-band.

Typical absorption (a), emission (b) and excitation (c) spectra of ZnPc-SWCNT conjugate using ZnMAPc-Py-SWCNT (adsorbed) (**20**) as an example are shown in Fig. 3.22. The shapes of the absorption and excitation spectra were similar except for the broadening of the former due to some slight aggregation. The excitation spectrum showed a monomeric Q-band without broadening and it is blue shifted by about 2 nm (Fig. 3.22, Table 3.2) compared to the absorption spectrum of **20**, but such a shift is not significant considering different equipment used for obtaining the absorption and excitation spectra. The emission spectrum is a mirror image of the excitation and absorption spectra.

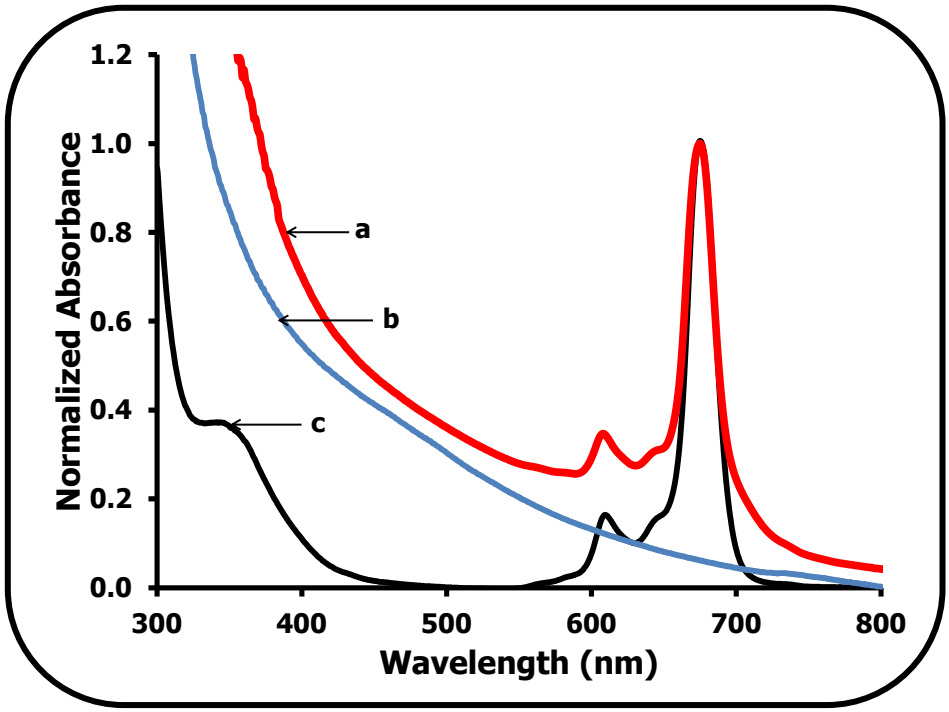

Fig. 3.21: Absorption spectra of ZnMCPPc-uridine-SWCNT, adsorbed (**17**) (a), SWCNT-COOH (b) and ZnMCPPc-uridine (**6**) (c) in DMSO. The concentration of ZnMCPPc-uridine is 1.2×10^{-5} M.

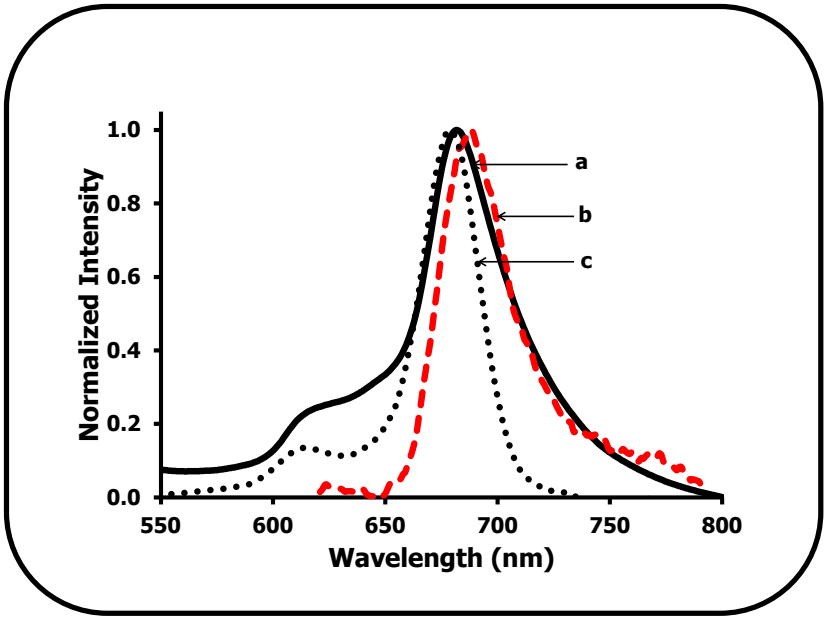

Fig. 3.22: Absorption (a), Emission (b) and Excitation (c) spectra of ZnMAPc-Py-SWCNT (adsorbed) (**20**) in DMSO. Excitation wavelength is 610 nm. The concentration of ZnMAPc-Py is 6.3×10^{-7} M.

Table 3.2: Spectra properties of ZnPc derivatives (or ZnPc-biomolecule conjugates) linked to (or adsorbed on) SWCNTs

ZnPc (or ZnPc-biomolecule) SWCNTs conjugate	**Solvent**	**Q band** [a] λ_{max} **/nm**	**Emission** [b] λ_{Em} **/nm**	**Excitation** [c] λ_{Exc} **/nm**
ZnMAPc-FA-SWCNT (ad) (**14**)	DMSO	682 (683)	689	680
ZnMCPPc-SWCNT (ad) (**15**)	DMSO	676 (675)	692	684
ZnMCPPc-spermine-SWCNT (ad) (**16**)	DMSO	675 (674)	685	674
ZnMCPPc-uridine-SWCNT (ad) (**17**)	DMSO	674 (674)	684	675
ZnMCPPc-AA-SWCNT (ad) (**18**)	DMSO	675 (675)	688	676
ZnMAPc-SWCNT (linked) (**19**)	DMSO	683 (676)	695	682
ZnMAPc-Py-SWCNT (ad) (**20**)	DMSO	683 (679)	688	680
ZnTCPPc-SWCNT (ad) (**21**)	DMSO	682 (680)	692	687
ZnTCPPc-AA-SWCNT (ad) (**22**)	DMSO	683 (681)	690	684
ZnOCPc-SWCNT (ad) (**23**)	Buffer 9	690 (691)	699	689
ZnOCPc-BSA-SWCNT (ad) (**24**)	Buffer 9	691(687)	702	690
ZnMAPPc-SWCNT (linked) (**25**)	DMSO	675 (676)	683	677
ZnMAPPc-SWCNT (ad) (**26**)	DMSO	675 (676)	683	676
ZnTAPPc-SWCNT (linked) (**27**)	DMSO	686 (686)	695	688
ZnTAPPc-SWCNT (ad) (**28**)	DMSO	686 (686)	693	685

[a] λ_{max} = absorption maxima, [b] λ_{Em} = emission maxima, [c] λ_{Exc} = excitation maxima. ad = adsorbed

Values in bracket are in the absence of SWCNTs.

3.3.2.3 Raman spectroscopy

Raman spectroscopy was employed to characterize all the ZnPcs (or ZnPc-biomolecule conjugates) linked to (or adsorbed on) SWCNT-COOH (or SWCNTs). The extent of functionalization of a material can be determined using Raman spectroscopy. SWCNTs are known to exhibit characteristics Raman peaks which are centred at 2500 cm^{-1} (G*), 1590 cm^{-1} (G-band (tangential mode) sp^2) [135,136] and 1270 cm^{-1} (D-band (disorder, breathing mode) sp^3), these peaks were observed in all the complexes containing SWCNTs (linked or adsorbed). The D:G ratio is generally considered as a good parameter for measuring the extent of functionalization of carbon nanotubes. The intensity of the D-band is expected to be enhanced on functionalization [119,137], resulting in an increase in the D:G ratio. This is because the G-band is not affected by defects, whereas the D-band is enhanced by the presence of defects due to conversion of sp^2 to sp^3. This is often observed on direct chemical linking of materials to SWCNTs. Increases in the G-band or D-band intensity on functionalization depends on the type of functionalization (covalent or non-covalent) among other factors. The higher frequency tangential displacement G-band near ~ 1590 cm^{-1} and the second order G*-band near 2500 cm^{-1} are sensitive to the charge exchanged between nanotubes and the guest moiety [138]. Negligible changes in the D-band intensity were generally observed on non-covalent functionalization of SWCNTs with ZnPc derivatives.

On functionalization of SWCNT-COOH with ZnMAPc (**1**) via amide bond linkage, the D:G ratio of 0.13 for SWCNT-COOH increases to 0.21 for **19** (ZnMAPc-SWCNT, linked) (Fig. 3.23a). Negligible changes were observed on linking ZnMAPPc (**12**) and ZnTAPPc (**13**) to SWCNT-COOH to form **25** (ZnMAPPc-SWCNT, linked) and **27**

(ZnTAPPc-SWCNT, linked) respectively. The D:G ratio of 0.13 for SWCNT-COOH slightly decreased to 0.12 for **25** and remained as 0.13 for **27**. The increase observed in **19** might be due to closer interaction of the Pc ring with the SWCNTs.

A decrease in the D:G ratio may be observed on non-covalent functionalization (adsorption) of SWCNTs with MPc (or MPc-biomolecule conjugate), since the interacting compounds are not chemically linked, increases are not expected. A typical example is shown for conjugate **17** (Fig. 3.24). An increase in the intensity of the G-band was observed on adsorption of ZnPcs (or ZnPc-biomolecule conjugates) on SWCNTs as typified in Fig. 3.24a for **17**. Calculations reveal that the D:G ratio of 0.13 for SWCNT-COOH (Fig. 3.24b) decreases to 0.06 upon adsorption of **6** onto SWCNTs to give **17**, this type of decrease was observed for all the adsorbed complexes. The decrease in the D:G ratio is due to increase in the G-band intensity. Increases in the G-band are associated with removal of some amorphous carbon from the nanotubes [139].

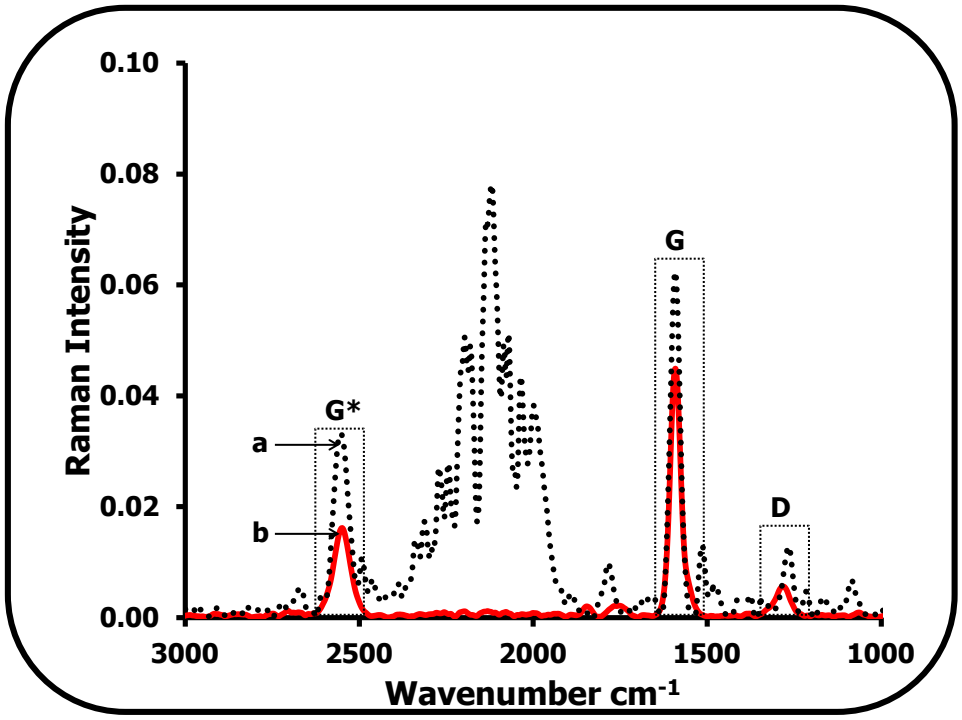

Fig. 3.23: Raman spectra of ZnMAPc-SWCNT (linked) (**19**) (a) and SWCNT-COOH (b). G* is the non-dispersive phonon mode, G is the tangential vibrational mode (sp^2) and D is the breathing mode; disorder band (sp^3).

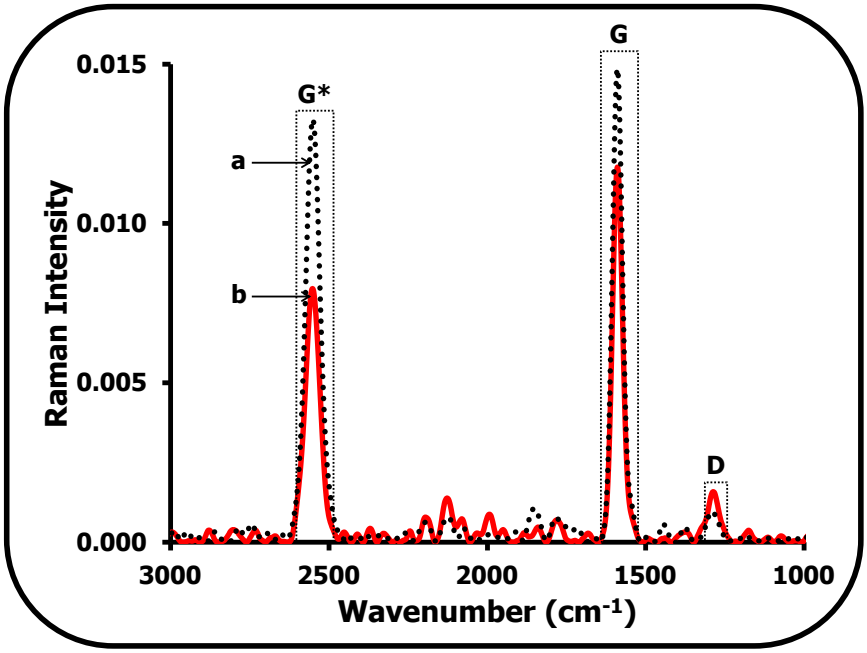

Fig. 3.24: Raman spectra of ZnMCPPc-uridine-SWCNT (adsorbed) (**17**) (a) and SWCNT-COOH (b). G* is the non-dispersive phonon mode, G is the tangential vibrational mode (sp^2) and D is the breathing mode; disorder band (sp^3).

3.3.2.4 X-ray diffractometry (XRD) characterization

X-ray diffractometry is a spectroscopic technique used for the elucidation of structural information of a material with relation to the broadness or sharpness of the XRD peak, which are indicative of the amorphous or crystalline nature of the material respectively [140]. Typical XRD patterns are shown in Fig. 3.25 for SWCNT-COOH, **5** and **16** as examples. SWCNT-COOH (Fig. 3.25a) show characteristic XRD pattern with two main peaks at 2θ values of 25.2° and 43.5° with d-spacing at 3.5 and 2.1 respectively, corresponding to the (002) [141,142] and (111) [143] reflections of carbon. Conjugate **5**

(Fig. 3.25c) showed a broad peak between 2θ = 19.2° and 26.2° with d-spacing at an average of 3.4, this peak is consistent with the broad phthalocyanine peak [144]. Conjugate **16** (Fig. 3.25b) exhibited peaks for SWCNTs and phthalocyanine, showing a broad peak between 2θ = 19.7° (for **5**) and 26.2° (for SWCNT-COOH) with a corresponding d-spacing of 4.5 and 3.4, respectively. The new peak at 44.6° with d-spacing at 2.0 is consistent with that of SWCNT-COOH. The changes observed in the XRD pattern of SWCNTs in the presence of ZnPcs (or ZnPc-biomolecule conjugates) indicate successful formation of a nanohybrid. Similar XRD patterns were observed for all the complexes.

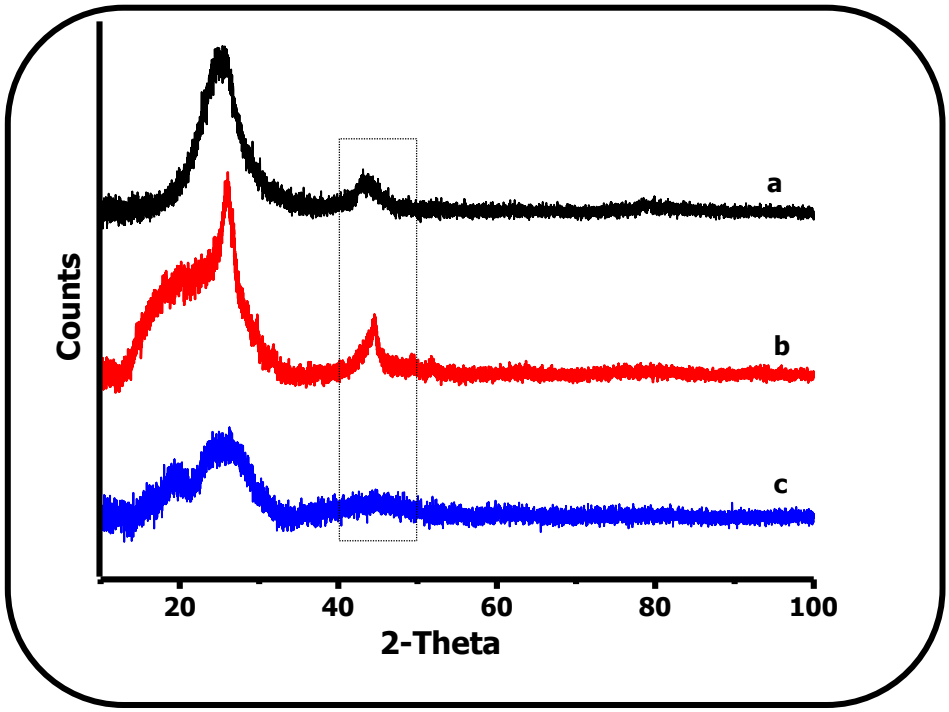

Fig. 3.25: XRD patterns of SWCNT-COOH (a), ZnMCPPc-spermine-SWCNT (adsorbed) (**16**) (b) and ZnMCPPc-spermine (**5**) (c).

3.3.2.5 Thermogravimetric analysis (TGA)

Thermogravimetric analysis was used to determine the thermal decay profiles of the complexes which points to different structural materials. The thermal decomposition profiles were obtained under a steady flow of N_2, at a heating rate of 10 $^oC\ min^{-1}$. Typical TGA profiles of **4**, **7**, **15** and **18** as examples (Fig. 3.26) show different thermal decay profiles of the complexes. The initial mass loss experienced (at ~100 ^oC) for each complex may be attributed to solvent losses (e.g. H_2O) or decomposition of functional groups [72,135]. The thermal decomposition profile of ZnMCPPc (**4**) (Fig. 3.26e) and ZnMCPPc-AA (**7**) (Fig. 3.26d) showed a weight loss of 43% at 500 ºC, which improved to 19% and 32% on adsorption onto SWCNTs for ZnMCPPc-SWCNT (**15**) (Fig. 3.26a) and ZnMCPPc-AA-SWCNT (**18**) (Fig. 3.26b) respectively. SWCNT-COOH showed a weight loss of 33% at 500 ^oC. Thus, functionalization of SWCNTs with ZnPc (or ZnPc-biomolecule conjugates) improved the thermal stability of the individual components. The TGA profile of SWCNTs on functionalization depends on the initial purity of the SWCNTs used (different batches of SWCNTs was used in the course of the program, which resulted in variations of its thermal stability on functionalization). Improvement of the thermal stability of SWCNTs on functionalization with ZnPc (or ZnPc-biomolecule conjugates) was observed for most complexes.

The percentage composition of ZnPcs, ZnPc-biomolecule conjugates or SWCNTs in the nanohybrids were calculated from the TGA profiles of the complexes according to literature method [145]. Using complexes **15** and **18** as examples, the weight percentage of ZnMCPPc (**4**) and ZnMCPPc-AA (**7**) attached to SWCNTs to form **15** and **18** respectively, were calculated to be about 24% and 11% respectively. This corresponds to one ZnMCPPc unit per 188 carbons of SWCNTs for **15** and one ZnMCPPc-AA unit per 588 carbons of SWCNTs for **18**. Thus,

ZnMCPPc-SWCNT (**15**) composes of ZnMCPPc (24%) and SWCNTs (76%), while ZnMCPPc-AA-SWCNT (**18**) consists of ZnMCPPc-AA (11%) and SWCNTs (89%), Table 3.3.

The percentage compositions for other complexes containing SWCNTs are listed in Table 3.3. It was difficult to conclude on a trend in the percentage composition of the complexes (**14 - 28**), because it depends on a number of factors: the thermal stability of each component of the complex, the molecular weight of the precursor ZnPc (or ZnPc-biomolecule conjugate) among others. The percentage composition of ZnOCPc-BSA-SWCNT, adsorbed (**24**) was not determined due to the inability to determine the molecular weight of ZnOCPc-BSA. BSA is a protein containing multiple sequences of amino acid.

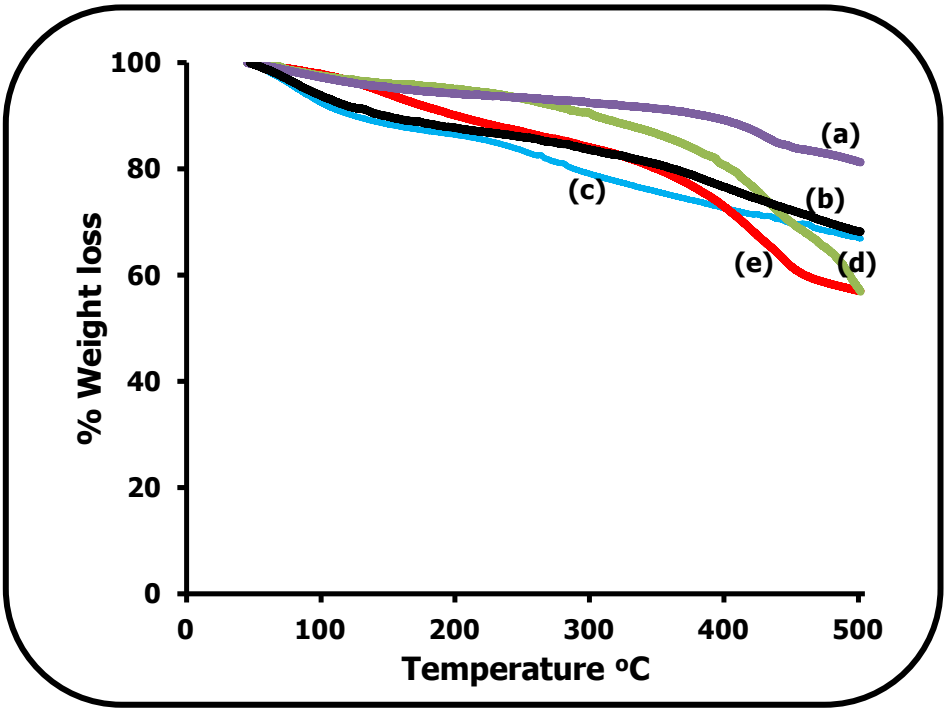

Fig. 3.26: TGA profiles of ZnMCPPc-SWCNT, adsorbed (**15**) (a), ZnMCPPc-AA-SWCNT, adsorbed (**18**) (b), SWCNT-COOH (c), ZnMCPPc-AA (**7**) (d) and ZnMCPPc (**4**) (e) recorded at 10 ^{o}C /min under N_2 atmosphere.

Table 3.3: % Composition of ZnPcs, ZnPc-biomolecule conjugates or SWCNTs in ZnPc-SWCNT (or ZnPc-biomolecule-SWCNT) nanohybrid

ZnPc (or ZnPc-biomolecule) SWCNTs conjugate	**% composition of ZnPc (or ZnPc-biomolecule)**	**% composition of SWCNTs**	**One unit of ZnPc (or ZnPc-biomolecule) per (X) carbons in SWCNTs X =**
ZnMAPc-FA-SWCNT (ad) (**14**)	5	95	1574
ZnMCPPc-SWCNT (ad) (**15**)	24	76	188
ZnMCPPc-spermine-SWCNT (ad) (**16**)	42	58	107
ZnMCPPc-uridine-SWCNT (ad) (**17**)	44	56	99
ZnMCPPc-AA-SWCNT (ad) (**18**)	11	89	588
ZnMAPc-SWCNT (linked) (**19**)	**5**	95	1000
ZnMAPc-Py-SWCNT (ad) (**20**)	16	84	352
ZnTCPPc-SWCNT (ad) (**21**)	10	90	766
ZnTCPPc-AA-SWCNT (ad) (**22**)	12	88	1071
ZnOCPc-SWCNT (ad) (**23**)	30	70	180
ZnOCPc-BSA-SWCNT (ad) (**24**)	ND	ND	ND

ad = adsorbed, ND = not determined.

Table 3.3 contd.

ZnPc (or ZnPc-biomolecule) SWCNTs conjugate	**% composition of ZnPc (or ZnPc-biomolecule)**	**% composition of SWCNTs**	**One unit of ZnPc (or ZnPc-biomolecule) per (X) carbons in SWCNTs X =**
ZnMAPPc-SWCNT (linked) (**25**)	6	94	894
ZnMAPPc-SWCNT (ad) (**26**)	8	92	656
ZnTAPPc-SWCNT (linked) (**27**)	10	90	754
ZnTAPPc-SWCNT (ad) (**28**)	10	90	754

ad = adsorbed

3.3.2.6 Transmission electron microscopy (TEM)

Transmission electron microscopy (TEM) provides information on the internal surface structure which gives access to morphological fine structural details of a material. TEM was employed to characterize all the complexes containing SWCNTs used in this work. Typical TEM images for SWCNT-COOH (A), ZnMAPc-SWCNT (linked) (**19**) (B) and ZnMAPc-Py-SWCNT (adsorbed) (**20**) (C) dispersed through ultrasonication in DMF are shown in Fig. 3.27 as example. The TEM images obtained for SWCNT-COOH, **19** and **20** were clearly different.

The bead-like structure along the length of the SWCNT-COOH in **19** (Fig 3.27B) shows that there is a strong interaction between the ZnMAPc and SWCNT-COOH, which indicate successful chemical linkage of the two complexes, while the particle-like compounds dispersed

on the SWCNTs shows the presence of ZnMAPc-Py (**2**) on the surface of SWCNTs in **20** (Fig. 3.27C). Similar TEM images were observed for all the complexes containing SWCNTs.

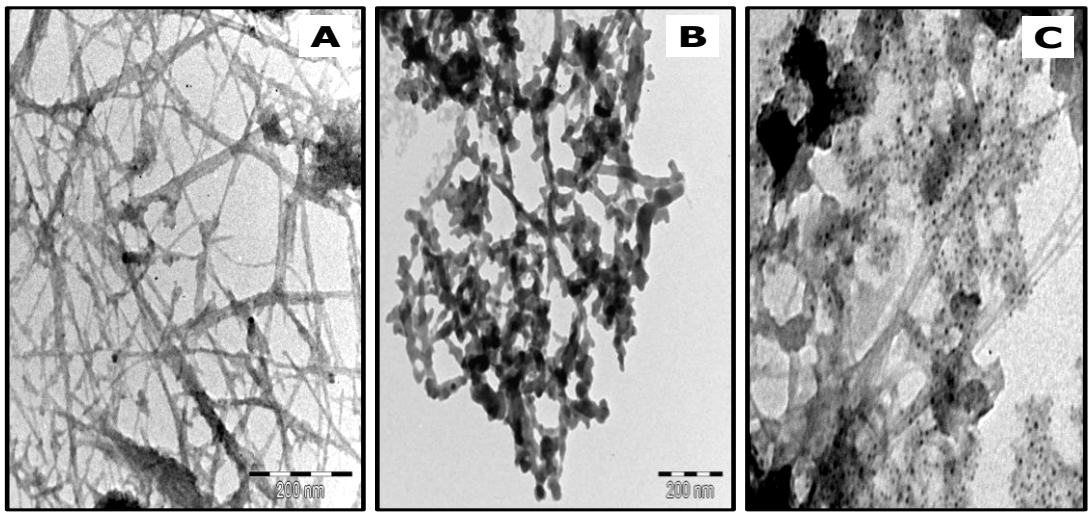

Fig. 3.27: TEM images of SWCNT-COOH (A), ZnMAPc-SWCNT (linked) (**19**) (B) and ZnMAPc-Py-SWCNT (adsorbed) (**20**) (C).

3.4 General conclusion

The synthesis and spectroscopic characterizations of ZnPcs derivatives in the presence of either biomolecules or SWCNTs were successfully presented. The conjugates were characterized using ^{1}H NMR, FTIR, elemental analysis and mass spectroscopy to confirm the respective mono- or tetra- substituted conjugates. The presence of SWCNTs in complexes **14 - 28** were confirmed using combination of spectroscopic techniques: FTIR, XRD, TEM and Raman spectroscopy. The characteristic signatures of carbon at (002) and (111) were observed for the complexes containing SWCNTs has obtained by XRD. The TEM images of all the complexes (**14 - 28**) showed a long tube-like substance suggesting the presence of SWCNTs in these complexes.

Characteristics Raman peaks of SWCNTs which are centered at 2500 cm^{-1} (G*), 1590 cm^{-1} (G-band (tangential mode) sp^2) and 1270 cm^{-1} (D-band (disorder, breathing mode) sp^3) were observed in all the complexes containing SWCNTs (linked or adsorbed).

All the studied complexes **1 - 28** showed monomeric Q-band. Complexes **2** and **3** showed broadening in the Q-band of the ground state absorption spectra indicating aggregation. However, on excitation this broadening was not observed. The absorption and excitation spectra of all the studied complexes coincide and were mirror images of the emission spectra.

CHAPTER FOUR

4. PHOTOPHYSICAL AND PHOTOCHEMICAL PROPERTIES

This chapter explains the photophysical and photochemical properties; fluorescence quantum yields and life-times, fluorescence resonance energy transfer, photo-induced electron transfer, triplet quantum yields and life-times, singlet oxygen quantum yields of zinc phthalocyanine derivatives when covalently linked to pyrene, folic acid, spermine, uridine, ascorbic acid or bovine serum albumin and the interaction of the complexes with single-walled carbon nanotubes.

4.1 Fluorescence life-times (τ_F) and quantum yields (Φ_F) of ZnPc derivatives (or ZnPc-biomolecule conjugates) linked to (or adsorbed on) SWCNTs

The fluorescence quantum yields (Φ_F) were determined by comparative method, by comparing the fluorescence intensity of the complexes to that of ZnPc standard when both were excited at 610 nm. The Φ_F values were calculated according to Equation 1.1, shown as Equation 4.1.

$$\Phi_F = \Phi_F^{std} . \frac{F . A_{std} . n^2}{F_{std} . A . n_{std}^2} \qquad 4.1$$

Unsubstituted ZnPc in DMSO was employed as standard (Φ_F^{std} = 0.2 [95]).

4.1.1 Fluorescence life-times (τ_F) and quantum yields (Φ_F) in the absence of SWCNTs

The fluorescence quantum yield (Φ_F) values of complexes **2**, **3** and **11** were higher than that of the precursor ZnPcs, this is due to intrinsic fluorescence property of the substituent in this complexes. Pyrene contained in **2** have been reported to exhibit high fluorescence quantum yields and life-times (0.65 and 410 ns, respectively, in ethanol at 293 K) [73,74,146], folic acid in **3** have been reported to enhance the fluorescence quantum yields of porphyrin and Pcs [61,132] and the increase in the Φ_F value for **11** could be as a result of the fact that BSA contains two tryptophan residues with intrinsic fluorescence [147]. The substituents present in complexes **5**, **6**, **7** and **9** are non-fluorescing, hence negligible changes were observed in their Φ_F values as compared to the precursor ZnPcs.

The fluorescence life-time (τ_F) of a complex defines the time the molecule spends in the excited state before returning to the ground state through fluorescence and it is directly related to the fluorescence quantum yield. The τ_F of all the complexes were determined using a time correlated

single photon count (TCSPC) method, following excitation at the emission maxima. A typical fluorescence decay profile for **6** as an example is shown in Fig. 4.1. A mono-exponential decay profile indicating one life-time was obtained for some of the complexes (**1** – **10** and **12**), while others showed bi-exponential decay profile indicating two life-times (complexes, **11** and **13**) (Table 4.1). The presence of two life-times could be explained in terms of quenched and unquenched fluorescence life-times due to the formation of aggregates. Complex **11** (ZnOCPc-BSA) contains BSA a large biomolecule, this might have quenched the fluorescence of the Pc ring while **13** contain four amino groups which have been reported to quench excited state properties [101,148].

There was decrease in the τ_F value of 3.40 ns for ZnMAPc (**1**) on chemical conjugation to pyrene (ZnMAPc-Py (**2**)) or folic acid (ZnMAPc-FA (**3**)) with τ_F values of 2.99 ns and 2.79 ns respectively, this suggests that the substituents quenched the excited state. The decreases in the τ_F values for **2** and **3** do not correspond to the increases observed in the Φ_F values; increases in the Φ_F values are expected to result in increases in τ_F values. Negligible changes were observed for complexes **5**, **6**, **7** and **9** (Table 4.1).

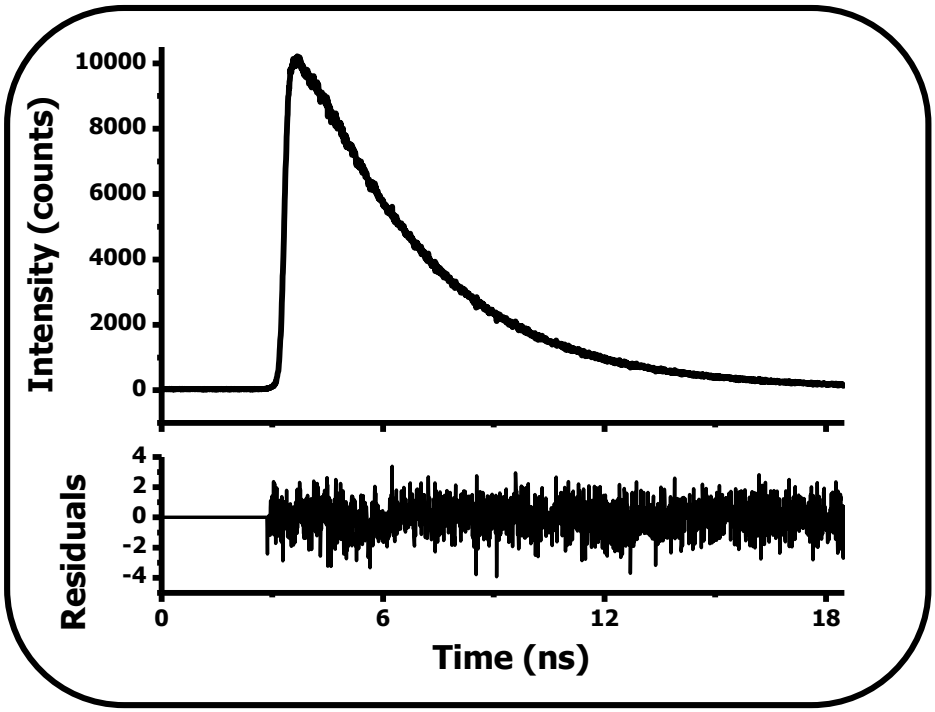

Fig. 4.1: Fluorescence decay curve of ZnMCPPc-uridine (**6**).

Table 4.1: Fluorescence data of ZnPc derivatives (or ZnPc-biomolecule conjugates)

ZnPc complexes	Solvent	Φ_F ±0.02	τ_F (ns)[a] ±0.01
ZnMAPc (**1**)	DMSO	0.16	3.40 (1.0)
ZnMAPc-Py (**2**)	DMSO	0.20	2.99 (1.0)
ZnMAPc-FA (**3**)	DMSO	0.21	2.79 (1.0)
ZnMCPPc (**4**)	DMSO	0.18	3.00 (1.0)
ZnMCPPc-spermine (**5**)	DMSO	0.18	2.86 (1.0)
ZnMCPPc-uridine (**6**)	DMSO	0.21	3.04 (1.0)
ZnMCPPc-AA (**7**)	DMSO	0.18	3.10 (1.0)
ZnTCPPc (**8**)	DMSO	0.10	3.00 (1.0)
ZnTCPPc-AA (**9**)	DMSO	0.22	2.82 (1.0)
ZnOCPc (**10**)	Buffer 9	0.15	2.90 (1.0)
ZnOCPc-BSA (**11**)	Buffer 9	0.20	2.99 (0.98), 0.35 (0.02) [b][2.94]
ZnMAPPc (**12**)	DMSO	0.12	3.2 (1.0)
ZnTAPPc (**13**)	DMSO	0.06	2.79 (0.90), 0.49 (0.04) [b][2.70]

[a] = Amplitude in round brackets, [b] = average τ_F values in square brackets.

4.1.2 Fluorescence life-times (τ_F) and quantum yields (Φ_F) in the presence of SWCNTs

The presence of SWCNTs often results in the quenching of the fluorescence properties, due to the ability of SWCNTs to deactivate photo-excited phthalocyanine through photo-induced electron transfer (PET) [119]. The adsorption of ZnMAPc derivatives on SWCNTs resulted in sharp decrease of the Φ_F values, which were observed for ZnMAPc-FA-SWCNT (adsorbed) (**14**) (Φ_F = 0.02) and ZnMAPc-Py-SWCNT (adsorbed) (**20**) (Φ_F = 0.05), Table 4.2. While negligible change was observed in the Φ_F value of ZnMAPc (**1**) (Φ_F = 0.16) on linkage to SWCNT-COOH to give ZnMAPc-SWCNT (linked) (**19**) (Φ_F = 0.17). Slight decrease or negligible changes were observed in the Φ_F values of complexes containing ZnMCPPc derivatives (or ZnMCPPc-biomolecule conjugates) on adsorption onto SWCNTs (complexes, **15** - **18**). The Φ_F values of **22** (ZnTCPPc-AA-SWCNT) and **21** (ZnTCPPc-SWCNT) decreases sharply when compared to **9** and **8** respectively, indicating that more quenching occurred in these complexes. The Φ_F values for complexes **23**, **26** - **28** remained relatively the same or slightly decrease on either linkage or adsorption of the precursor ZnPcs on SWCNTs, Table 4.2. The Φ_F values of **24** (ZnOCPc-BSA-SWCNT) and **25** (ZnMAPPc-SWCNT, linked) decreases compared to the precursor Pcs, the decrease in **24** might be due to BSA also interacting with SWCNTs.

The τ_F values of complexes **14** - **28** containing SWCNTs (either linked or adsorbed) slightly decreased (or remained relatively the same for some complexes) when compared to the precursor Pcs. All the complexes containing ZnMCPPc (**15** - **18**) exhibited mono-exponential decay curves, indicating one life-time, the rest of the complexes showed bi-exponential curves (Table 4.2). Comparing the τ_F average value of a complex (containing SWCNTs) to the τ_F value of the

precursor ZnPc (or ZnPc-biomolecule conjugate) the fluorescence life-time was indeed quenched as shown in Table 4.2.

The two life-times observed for some ZnPc-SWCNT conjugates were due to the presence of SWCNTs which are 2D materials, and the two sides (with different orientation) interact differently with Pc, resulting in quenched and unquenched photo-excited singlet state. Indeed, SWCNTs quenches the photo-excited singlet state of Pc as seen from the steady state decay profile, Fig. 4.2 (using the fluorescence decay curve of **22** as an example).

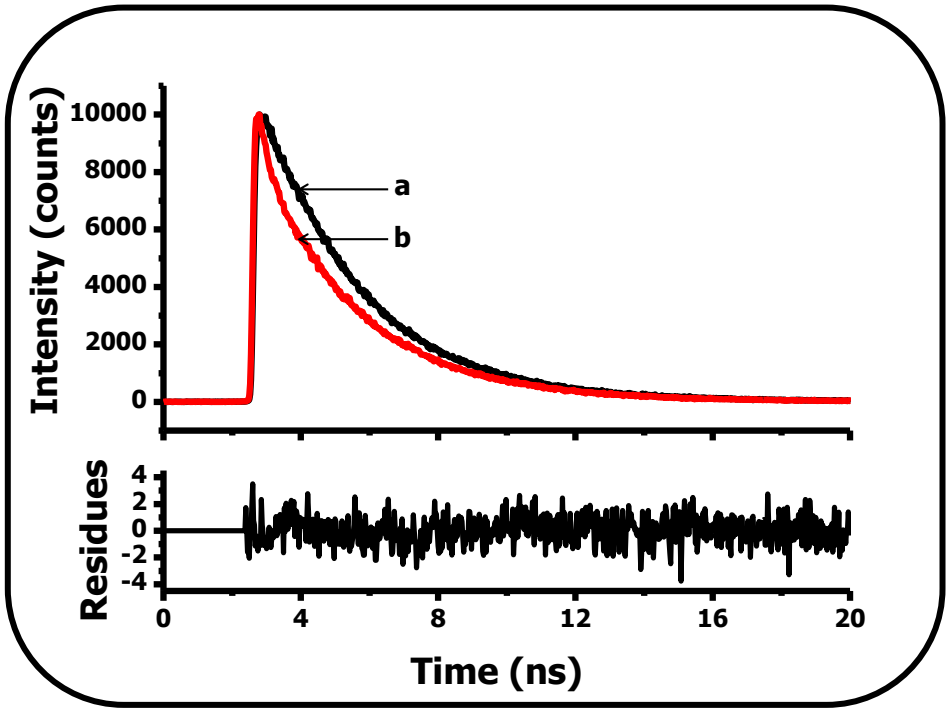

Fig 4.2: Fluorescence decay curves of ZnTCPPc-AA (**9**) (a) and ZnTCPPc-AA-SWCNT, adsorbed (**22**) (b) in DMSO. Excitation wavelength = 690 nm for **9** and 692 nm for **22**. The concentration of ZnTCPPc-AA is 3.2 x10^{-7} M.

Table 4.2: Fluorescence data of ZnPc derivatives (or ZnPc-biomolecule conjugates) linked to (or adsorbed on) SWCNTs

[a] ZnPc complexes	Solvent	Φ_F [b] ±0.02	τ_F (ns), [b, c] ±0.01	$\tau_{F\ (average)}$ (ns)
ZnMAPc-FA-SWCNT (ad) (**14**) [from **3**]	DMSO	0.02 [0.21]	2.74 (0.95), 0.62 (0.05) [3.40]	2.70
ZnMCPPc-SWCNT (ad) (**15**) [from **4**]	DMSO	0.12 [0.18]	3.00 (1.0) [3.00]	-
ZnMCPPc-spermine-SWCNT (ad) (**16**) [from **5**]	DMSO	0.17 [0.18]	2.99 (1.0) [3.00]	-
ZnMCPPc-uridine-SWCNT (ad) (**17**) [from **6**]	DMSO	0.19 [0.21]	3.11 (1.0) [3.00]	-
ZnMCPPc-AA-SWCNT (ad) (**18**) [from **7**]	DMSO	0.13 [0.18]	3.10 (1.0) [3.10]	-
ZnMAPc-SWCNT (linked) (**19**) [from **1**]	DMSO	0.17 [0.16]	2.73 (0.94), 1.06 (0.06) [3.40]	2.63
ZnMAPc-Py-SWCNT (ad) (**20**) [from **2**]	DMSO	0.05 [0.20]	2.94 (0.84), 1.07 (0.16) [2.99]	2.80
ZnTCPPc-SWCNT (ad) (**21**) [from **8**]	DMSO	0.02 [0.10]	2.91 (0.98), 0.3 (0.02) [3.00]	2.86
ZnTCPPc-AA-SWCNT (ad) (**22**) [from **9**]	DMSO	0.03 [0.22]	2.81 (0.95), 0.27 (0.05) [2.99]	2.68

[a] = ad = adsorbed, [b] = values in square brackets are in the absence of SWCNTs, [c] = Amplitude in round brackets for τ_F.

Table 4.2: contd.

[a] ZnPc complexes	Solvent	Φ_F [b] ±0.02	τ_F (ns), [b, c] ±0.01	$\tau_{F\ (average)}$ (ns)
ZnOCPc-SWCNT (ad) (**23**) [from **10**]	Buffer 9	0.15 [0.15]	2.99 (0.98), 0.35 (0.02) [2.90]	2.95
ZnOCPc-BSA-SWCNT (ad) (**24**) [from **11**]	Buffer 9	0.10 [0.20]	2.98 (0.97), 0.38 (0.03) [2.99 (0.98), 0.35 (0.02)]	2.93 [2.94]
ZnMAPPc-SWCNT (linked) (**25**) [from **12**]	DMSO	0.07 [0.12]	2.89 (0.96), 0.59 (0.04) [3.2]	2.80
ZnMAPPc-SWCNT (ad) (**26**) [from **12**]	DMSO	0.10 [0.12]	3.0 (0.96), 0.47 (0.04) [3.2]	2.91
ZnTAPPc-SWCNT (linked) (**27**) [from **13**]	DMSO	0.05 [0.06]	2.79 (0.97), 0.36 (0.03) [2.79 (0.96), 0.49 (0.04)]	2.72 [2.70]
ZnTAPPc-SWCNT (ad) (**28**) [from 1**3**]	DMSO	0.06 [0.06]	2.78 (0.93), 0.48 (0.06) [2.79 (0.96), 0.49 (0.04)]	2.70 [2.70]

[a] = ad = adsorbed, [b] = values in square brackets are in the absence of SWCNTs, [c] = Amplitude in round brackets for τ_F.

4.2 Energy transfer study

The interactions of different substituents on the ZnPc complexes used in this work, resulted in either enhancement or quenching of its fluorescence properties, which were either through fluorescence resonance energy transfer (FRET) or photo-induced energy transfer (PET). The

former often results in the enhancement of the fluorescence properties of MPc molecule while the later results in quenching.

FRET involves non-radiative energy transfer from a photo-excited donor fluorophore, after the absorption of a higher energy photon, to an acceptor fluorophore of a different species which is in close proximity. FRET results from dipole-dipole interactions and is extremely dependent on the center-to-center separation distance between the donor and the acceptor (r), the degree of spectra overlap of the donor's fluorescence emission spectrum and the acceptor's absorption spectrum [99,146] as shown in Fig. 4.3A.

The linking of pyrene to ZnMAPc (**1**) to form **2** resulted in FRET. Practically, a stimulated increase in the acceptor's photo-emission was observed, while a consequential quenching in the donor photo-emission on excitation at 400 nm; where absorption by **1** alone is minima and absorption by pyrene is substantial (Fig 4.3B).

The presence of SWCNTs in either ZnPcs or ZnPc-biomolecule conjugates resulted in quenching of the fluorescence properties through PET for most of the complexes. Typical example of the quenching of the fluorescence properties of a photo-excited phthalocyanine singlet state for some of the complexes containing SWCNTs is evident in the decrease of the emission spectra on adsorption of ZnPcs (or ZnPc-biomolecule conjugates) on SWCNTs, using complex **9** and its adsorbed conjugate on SWCNTs **22** as examples (Fig 4.4).

The quenching factor (Q_F), photo-induced energy transfer rate constant (Ket) and electron transfer efficiency (PET Eff.) were calculated from the fluorescence quantum yields and life-times of the donor in the absence and presence of the acceptor according to Equation 1.2 - 1.4, shown as Equation 4.2 - 4.4.

$$Q_F = \frac{\Phi_{F(D)}}{\Phi_{F(A)}} \qquad 4.2$$

$$\text{Ket} = \left(\tau_{F\,(A)}\right)^{-1} - \left(\tau_{F\,(D)}\right) - 1 = \frac{\left(\frac{\Phi_{F\,(D)}}{\Phi_{F\,(A)}}\right) - 1}{\tau_{F\,(D)}} \qquad 4.3$$

$$\text{PET Eff.} = \left(1 - \left(\frac{\Phi_{F\,(A)}}{\Phi_{F\,(D)}}\right)\right) \qquad 4.4$$

The quenching factor (Q_F) for the fluorescence emission of pyrene on conjugation to ZnMAPc is 3.3, this value increased to 4.0 on adsorption of **2** onto SWCNTs (to give complex **20**), suggestion more quenching in the presence of the latter. The Q_F, Ket and PET Eff. values for **2** and all the complexes containing SWCNTs are in Table 4.3, these values depend on the nature of the substituents on the ZnPcs and the interaction of ZnPc complex with the SWCNTs.

The photo-induced energy transfer rate constant (Ket) values are in the order of 10^7 - 10^9. The quenching rate of the complexes containing SWCNTs are in these order: **14** > **22** > **21** > **20** > **18** > **24** > **25** > **15** > **26** = **27** > **16** > **17**, Table 4.3. There were no changes in the fluorescence quantum yields of complexes **19**, **23** and **28**, as compared to the precursor ZnPc derivatives. Thus, PET was not observed. Generally, the Q_F, Ket and PET values are related, decrease in one results in the corresponding decrease in the other, and these trends were observed in the studied complexes (**14** - **28**). The highest Ket value was observed for **14** (ZnMAPc-FA-SWCNT, adsorbed) suggesting more energy transfer from ZnMAPc-FA to SWCNTs, with Q_F = 10.5, PET. = 90% and Ket = 3.4×10^9. The least was observed for **17** (ZnMCPPc-uridine-SWCNT, adsorbed) indicating less energy transfer from the precursor ZnPc-uridine conjugate to SWCNTs.

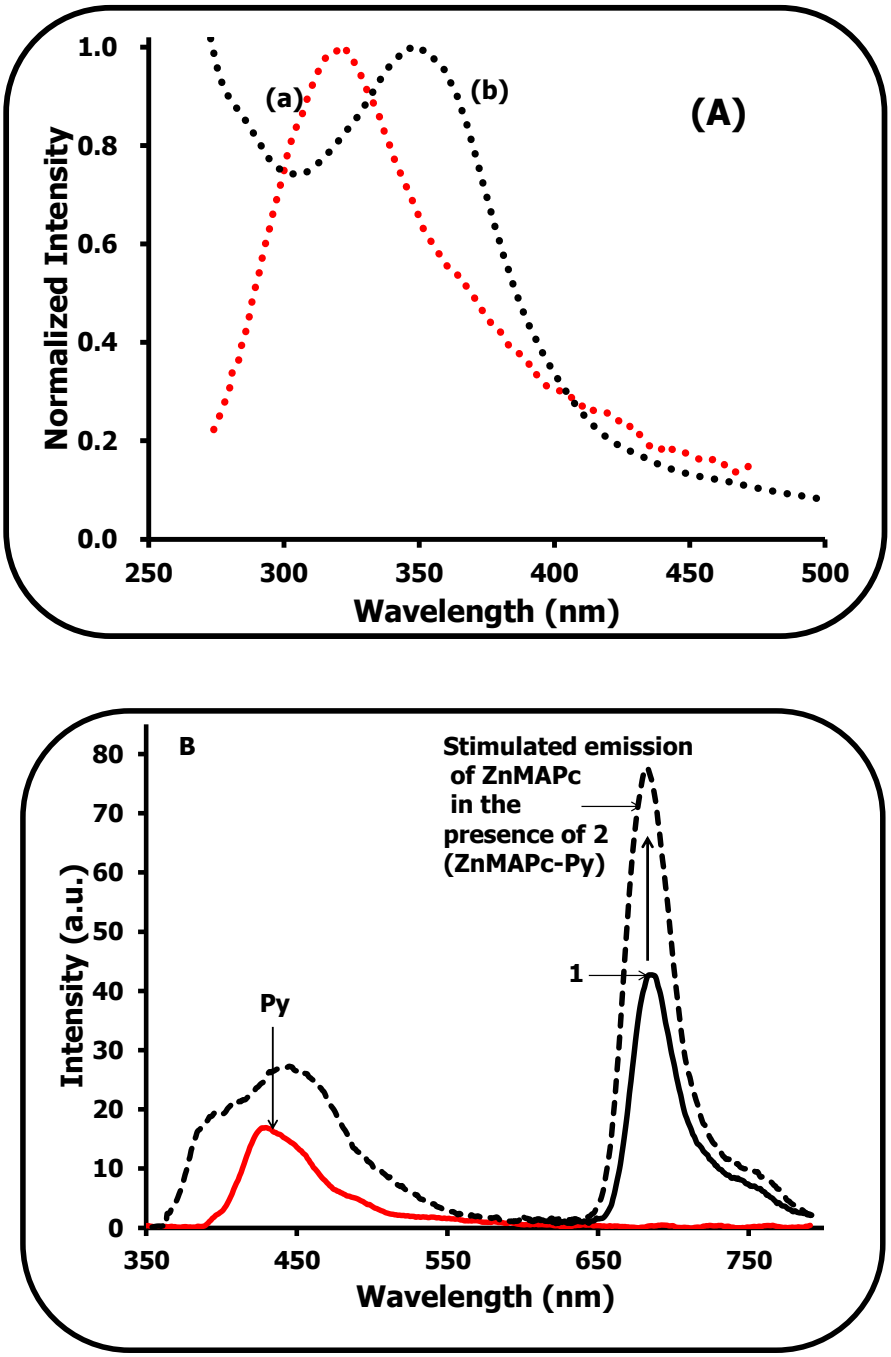

Fig. 4.3: (A); Emission spectra of Py (a) and absorption spectra of ZnMAPc **1** (b) and (B); emission spectra of Pyrene (Py), ZnMAPc-Py (**2**) and ZnMAPc (**1**) in DMSO. Excitation wavelength = 400 nm. The concentration of ZnMAPc-Py (**2**) and ZnMAPc (**1**) = 1.3×10^{-6} M.

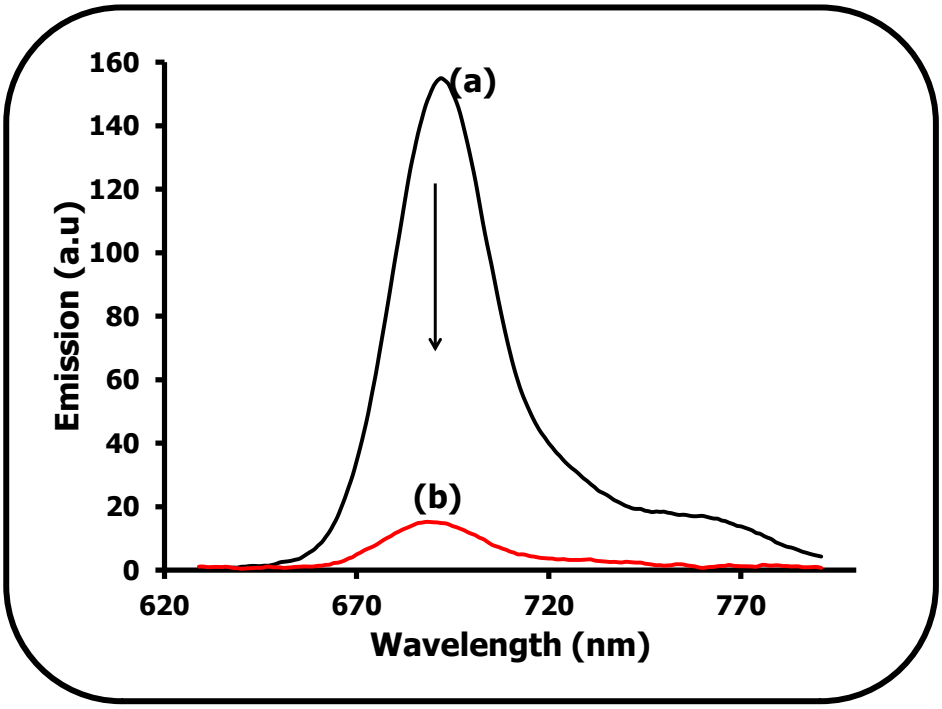

Fig. 4.4: Emission spectra of ZnTCPPc-AA (**9**) (a) and ZnTCPPc-AA-SWCNT (adsorbed) (**22**) (b) in DMSO. Excitation wavelength = 600 nm. The concentration of ZnTCPPc-AA is 5.0×10^{-7} M

Table 4.3: Photo-induced energy transfer rate constant (Ket), electron transfer efficiency (PET Eff.) and quenching factor (Q_F) for ZnPcs (or ZnPc-SWCNT) conjugates

ZnPc complexes	Solvent	Q_F	ket s^{-1}	PET Eff. (%)
ZnMAPc-Py (**2**)	DMSO	3.3	5.6×10^8	69
ZnMAPc-FA-SWCNT (ad) (**14**)	DMSO	10.5	3.4×10^9	90
ZnMCPPc-SWCNT (ad) (**15**)	DMSO	1.5	1.7×10^8	33
ZnMCPPc-spermine-SWCNT (ad) (**16**)	DMSO	1.1	4.4×10^7	11
ZnMCPPc-uridine-SWCNT (ad) (**17**)	DMSO	1.1	3.5×10^7	9.5
ZnMCPPc-AA-SWCNT (ad) (**18**)	DMSO	1.4	4.8×10^8	60
ZnMAPc-SWCNT (linked) (**19**)	DMSO	0.9	a	a
ZnMAPc-Py-SWCNT (ad) (**20**)	DMSO	4.0	1.0×10^9	75
ZnTCPPc-SWCNT (ad) (**21**)	DMSO	5	1.3×10^9	80
ZnTCPPc-AA-SWCNT (ad) (**22**)	DMSO	7	2.2×10^9	86
ZnOCPc-SWCNT (ad) (**23**)	Buffer 9	a	a	a
ZnOCPc-BSA-SWCNT (ad) (**24**)	Buffer 9	2	3.3×10^8	50
ZnMAPPc-SWCNT (linked) (**25**)	DMSO	1.7	2.2×10^8	42
ZnMAPPc-SWCNT (ad) (**26**)	DMSO	1.2	6.3×10^7	17
ZnTAPPc-SWCNT (linked) (**27**)	DMSO	1.2	7.2×10^7	17
ZnTAPPc-SWCNT (ad) (**28**)	DMSO	a	a	a

ad = adsorbed, [a] = No change in fluorescence quantum yield between donor and acceptor

4.3 Triplet quantum yields (Φ_T) and life-times (τ_T) of ZnPc derivatives (or ZnPc-biomolecule conjugate) linked to (or adsorbed on) SWCNTs

The triplet state of the studied complexes were generated and studied using laser flash photolysis technique, following introduction of intense pulses of light from a laser source into an MPc molecule, this generated a time-evolved electronic absorption from the $T_1 - T_n$ state, from which the time spent (τ_T) and the population (Φ_T) of the triplet state can be calculated. The Φ_T values for all the complexes were calculated using Equation 1.5, shown as Equation 4.5.

$$\Phi_T = \Phi_T^{std} . \frac{\Delta A_T . \varepsilon_T^{std}}{\Delta A_T^{std} . \varepsilon_T} \qquad 4.5$$

Unsubstituted ZnPc in DMSO was employed as standard (Φ_T^{std} = 0.65 [103]).

4.3.1 Triplet quantum yields (Φ_T) and life-times (τ_T) in the absence of SWCNTs

The triplet state of a complex depends on its ability to undergo intersystem crossing (ISC). ISC involves forbidden $T_1 \rightarrow S_0$ transition to the triplet state; ISC can be achieved either through spin-orbit charge transfer intersystem crossing (SOCT-ISC) or radical-pair intersystem crossing (RP-ISC) mechanisms. The SOCT-ISC mechanism requires the donor and acceptor orbitals to be nearly perpendicular and it largely depends on the donor-bridge-acceptor charge separation. It has been shown that complexes that are connected with a phenyl bridge exhibit fast intersystem crossing rates which often result in increase in the triplet quantum yield (Φ_T) and life-time (τ_T) [149]. Similarly, complexes that can generate free radicals also result in high Φ_T and τ_T values [149,150]. Triplet decay profiles, which obeyed first order kinetics were observed for all the complexes, a typical triplet decay profile is shown in Fig. 4.5.

There was increase in the Φ_T values for all the ZnPc-biomolecule conjugates when compared to the precursor ZnPcs with the exception of **11** (ZnOCPc-BSA) where there was a decrease. The Φ_T values depend on a number of factors. Increase in Φ_T value for **2** as compared to ZnMAPc (**1**) was due to the presence of pyrene which increases the π conjugation of **1**, and π conjugation has been reported to enhance intersystem crossing [75]. Complex **2** containing pyrene showed higher Φ_T value as compared to **3** (ZnMAPc-FA) from the same precursor Pc (ZnMAPc (**1**)), this shows the advantage of extending π conjugation of Pc ring. The increase in Φ_T values for **5**, **6**, **7** and **9** is due to the presence of the phenyl bridge connecting the ZnMCPPc moiety to the respective biomolecules: spermine in **5**, uridine in **6** and ascorbic acid in **7** and **9**. The phenyl bridge encourages SOCT-ISC mechanism explained above.

The triplet state properties of MPcs are generally quenched by water [95], hence a very weak signal was observed for complex **11** in pH 9 buffer. A decrease was observed in the Φ_T value of ZnOCPc-BSA (**11**) as compared to ZnOCPc (**10**), this might be due to quenching by BSA; a large biomolecule.

ZnMAPPc (**12**) containing one amino group showed better Φ_T values than ZnTAPPc (**13**) containing four amino groups; this could be related to the reported quenching of excited states by amino groups [101,148].

The triplet life-time (τ_T) value of 229 μs for ZnMAPc (**1**) decreases to 193 and 200 μs for **2** and **3** respectively on linking of pyrene or folic acid to **1**, (Table 4.4). The decreases in τ_T values correspond to the increases in Φ_T values. The shortening in triplet life-time with increase in triplet quantum yield is an established phenomenon [151].

The triplet life-time (τ_T) of ZnMCPPc (**4**) increases on conjugation to spermine (ZnMCPPc-spermine (**5**)), uridine (ZnMCPPc-uridine (**6**)) and ascorbic acid (ZnMCPPc-AA (**7**)), similar

increase in τ_T value was observed on conjugating ZnTCPPc to AA (ZnTCPPc-AA (**9**)), Table 4.4. The increases in τ_T values are not expected to accompany increases in Φ_T values [151]. However, increases in τ_T values of complexes **5**, **6**, **7**, and **9** may suggest the protection of the Pc from the environment by the biomolecule.

The triplet life-time of ZnOCPc-BSA (**11**) is longer than ZnOCPc (**10**), Table 4.3. The increase in τ_T value corresponds to the decrease in Φ_T value. It was reported that porphyrin binding to BSA reduces the quenching constants of the porphyrin triplet states by molecular oxygen due to shielding [152]. Thus, the increase in the triplet life-time for ZnOCPc in the presence of BSA could be due to shielding by BSA. The photophysical and photochemical properties of complexes **10** and **11** were studied in aqueous media (pH 9 buffer), therefore, low triplet life-times obtained is due to the reported [95] quenching of the triplet state of ZnPc derivatives in water.

There was increase in the τ_T value of ZnMAPPc (**12**) on increasing the amino group on the Pc ring to form tetra-substituted complex (ZnTAPPc, **13**). Again, the increases in the τ_T values correspond to decreases in Φ_T values observed in these complexes (Table 4.4).

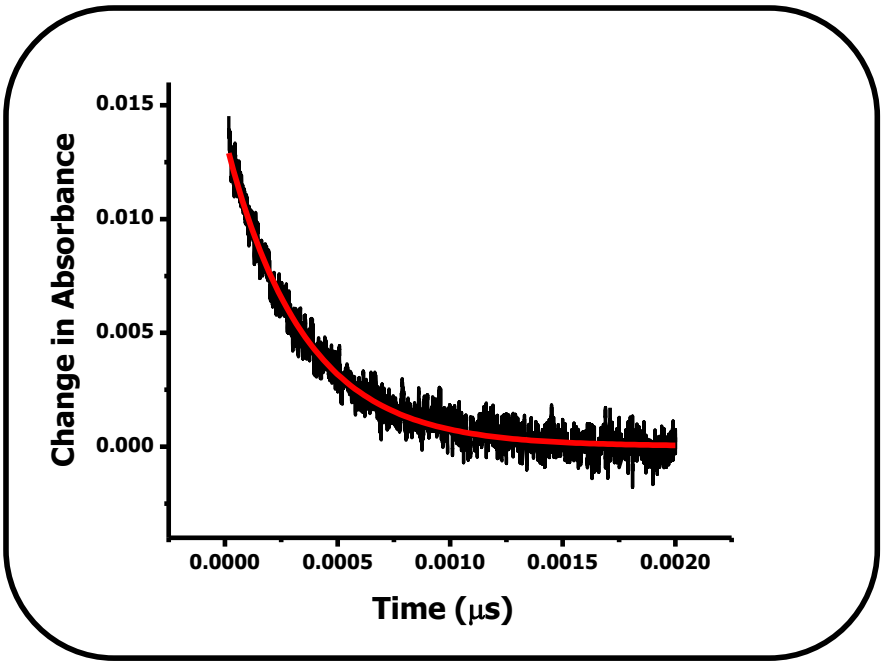

Fig. 4.5: Mono-exponential triplet decay curve of ZnMAPc-Py (**2**) in DMSO.

Table 4.4: Triplet life-times and triplet quantum yields for ZnPc derivatives (or ZnPc-biomolecule conjugates)

ZnPc complexes	Solvent	τ_T (μs)	Φ_T ±0.02
ZnMAPc (**1**)	DMSO	229	0.48
ZnMAPc-Py (**2**)	DMSO	193	0.78
ZnMAPc-FA (**3**)	DMSO	200	0.53
ZnMCPPc (**4**)	DMSO	202	0.35
ZnMCPPc-spermine (**5**)	DMSO	303	0.84
ZnMCPPc-uridine (**6**)	DMSO	447	0.62
ZnMCPPc-AA (**7**)	DMSO	344	0.65
ZnTCPPc (**8**)	DMSO	238	0.49
ZnTCPPc-AA (**9**)	DMSO	344	0.67
ZnOCPc (**10**)	Buffer 9	10	0.34
ZnOCPc-BSA (**11**)	Buffer 9	24	0.27
ZnMAPPc (**12**)	DMSO	220	0.70
ZnTAPPc (**13**)	DMSO	315	0.54

4.3.2 Triplet quantum yields (Φ_T) and life-times (τ_T) in the presence of SWCNTs

The ability of SWCNTs to accept electron from photo-excited electron donor such as Pc often results in the quenching of the photo-excited state of the later, however this depends on different factors. In the present study both decreases and increases in triplet quantum yield (Φ_T) values were observed in the presence of SWCNTs. In general, there were decreases in the Φ_T values of the ZnPc-biomolecule-SWCNT conjugates (complexes, **14**, **16**, **17**, **18**, **22** and **24**) when compared to the corresponding precursor ZnPc-biomolecule conjugate alone, Table 4.5. Similar decreases in the Φ_T values were observed for complexes **20**, **23**, **25 - 28** on formation of either linked or adsorbed ZnPc-SWCNT conjugates. Pcs are highly aromatic in nature and they interact strongly with CNTs by π-π stacking. Charge transfer processes which lead to the formation of excited-state radical ion pair in a Pc-carbon nanotube system (where the Pc acts as the electron donor and the carbon nanotubes as the electron acceptor) are known [153,154], this results in quenching of the excited state of the Pc as observed for complexes **14**, **16**, **17**, **18**, **20**, **22 - 28** (Table 4.5).

The Φ_T values of complexes; **15**, **19** and **21** (Table 4.5) increased compared to the precursor ZnPcs (complexes, **15**, **19** and **21** and their precursor Pcs were not linked to biomolecules). The formation of a radical ion pair that encourages RP-ISC to triplet state is dependent on the length of the spacer separating the Pc and the carbon nanostructure [154]. A short linker produces highly short-lived radical ion pair, such that the charge recombination process is extremely fast [154] and quenching of the excited state by CNTs is not observed. The absence of charge transfer process in Pc-fullerene dyad has been reported in the literature [155]. This suggests that the charge recombination process is extremely fast in these complexes (**15**, **19** and **21**) since they were not conjugated to biomolecule.

Complexes **15**, **19**, **21, 25 - 28** do not contain biomolecules. These complexes interact differently with SWCNTs. The differences between complexes **25 - 28** (where there are quenching of the triplet quantum yields by SWCNTs) and **15**, **19** and **21** (where there are enhancements in triplet quantum yields in the presence of SWCNTs) is that complexes **25 - 28** contain amino phenoxyl substitutents which are known to quench photo-excited state properties [101,148].

The τ_T values of the nanohybrid of ZnPc derivatives (or ZnPc-biomolecule conjugates) with SWCNTs generally increases for most complexes, except for complexes **16**, **17**, **19**, **21**, **22** and **24**, where decreases were observed (Table 4.5). The increases in the τ_T values correspond to the decreases in the Φ_T values.

Table 4.5: Triplet life-times and triplet quantum yields for ZnPc derivatives (or ZnPc-biomolecule conjugates) linked to (or adsorbed on) SWCNTs

ZnPc complexes	Solvent	τ_T (μs)	Φ_T ±0.02
ZnMAPc-FA-SWCNT (ad) (**14**) [from **3**]	DMSO	492 (200)	0.32 (0.58)
ZnMCPPc-SWCNT (ad) (**15**) [from **4**]	DMSO	329 (202)	0.47 (0.35)
ZnMCPPc-spermine-SWCNT (ad) (**16**) [from **5**]	DMSO	292 (303)	0.76 (0.84)
ZnMCPPc-uridine-SWCNT (ad) (**17**) [from **6**]	DMSO	344 (447)	0.50 (0.62)
ZnMCPPc-AA-SWCNT (ad) (**18**) [from **7**]	DMSO	355 (344)	0.52 (0.65)
ZnMAPc-SWCNT (linked) (**19**) [from **1**]	DMSO	213 (200)	0.53 (0.48)
ZnMAPc-Py-SWCNT (ad) (**20**) [from **2**]	DMSO	261 (193)	0.64 (0.78)
ZnTCPPc-SWCNT (ad) (**21**) [from **8**]	DMSO	243 (283)	0.54 (0.49)
ZnTCPPc-AA-SWCNT (ad) (**22**) [from **9**]	DMSO	254 (374)	0.59 (0.82)
ZnOCPc-SWCNT (ad) (**23**) [from **10**]	Buffer 9	14 (10)	0.21 (0.34)
ZnOCPc-BSA-SWCNT (ad) (**24**) [from **11**]	Buffer 9	14 (24)	0.19 (0.27)
ZnMAPPc-SWCNT (linked) (**25**) [from **12**]	DMSO	314 (220)	0.59 (0.70)
ZnMAPPc-SWCNT (ad) (**26**) [from **12**]	DMSO	239 (220)	0.38 (0.70)
ZnTAPPc-SWCNT (linked) (**27**) [from **13**]	DMSO	364 (315)	0.48 (0.54)
ZnTAPPc-SWCNT (ad) (**28**) [from **13**]	DMSO	432 (315)	0.44 (0.54)

ad = adsorbed, values in bracket are in the absence of SWCNTs

4.4 Singlet oxygen quantum yields (Φ_Δ) of ZnPc derivatives (or ZnPc-biomolecule conjugates) linked to (or adsorbed on) SWCNTs

Singlet oxygen ($^1O_2$), the major cytotoxic species responsible for cancer cells death in PDT were determined through either chemical method using DPBF as singlet oxygen quencher (Fig. 4.6) or through the detection of singlet oxygen characteristics phosphorescence at 1270 nm using sodium azide as singlet oxygen quencher (Fig. 4.7). The two methods, have been compared [104] and both give similar results, hence there is no differentiation of data from the two methods, Tables 4.6 and 4.7. The Φ_Δ values were calculated using a relative method. The Φ_Δ values depend on the nature of the substituents on the MPcs, the triplet quantum yields and life-times.

The Φ_Δ value for the chemical method was calculated according to Equation 1.7, shown as Equation 4.6.

$$\Phi_\Delta = \Phi_\Delta^{std} . \frac{R . I_{abs}^{std}}{R^{std} . I_{abs}} \qquad 4.6$$

The Φ_Δ value using singlet oxygen characteristics phosphorescence signal at 1270 nm was calculated using Equation 1.9, shown as Equation 4.7.

$$\Phi_\Delta = \Phi_\Delta^{std} . \frac{A . OD^{std}}{A^{std} . OD} \qquad 4.7$$

Unsubstituted ZnPc in DMSO was employed as standard (Φ_Δ^{std} = 0.67 [75]).

4.4.1 Singlet oxygen quantum yields (Φ_Δ) in the absence of SWCNTs

The conjugated biomolecules increases the singlet oxygen quantum yield of the ZnPc derivatives. The presence of folic acid in **3**, spermine in **5**, uridine in **6**, BSA in **11**, ascorbic acid in **7** and **9** resulted in enhanced singlet oxygen quantum yield values as compared to the precursor ZnPcs (Table 4.6). The increases in the Φ_Δ values for complexes **5**, **6**, **7**, **9** are due to the presence of the phenyl bridge connecting the ZnMCPPc moiety to the respective biomolecules that encourages SOCT-ISC mechanism explained above. The enhanced Φ_Δ value in **6** could also be due to the ability of uridine (a nucleoside) to generate singlet oxygen at excited state [156], complex **11** contained BSA which have multiple sequences of amino acid including tryptophan and tyrosine that have the ability to form free radicals such as hydrogen peroxide which may form singlet oxygen [157,158]. This also explains why the singlet oxygen quantum yields were higher than the triplet quantum yields for complex **11** and **24** (Table 4.7). The increases in the Φ_Δ values in all the complexes also correspond to the increases in Φ_T values except for **11** as explained above (Table 4.6). The Φ_Δ value for ZnMAPc (**1**) also increases on conjugation to pyrene to form ZnMAPc-Py (**2**) due to extended π conjugation resulting in increase in Φ_T value and a corresponding increase in Φ_Δ value. The efficiency of energy transfer ($S_\Delta = \frac{\Phi_\Delta}{\Phi_T}$) between triplet state and molecular oxygen were high in the presence of biomolecules as compared to the precursor Pcs alone (Table 4.6).

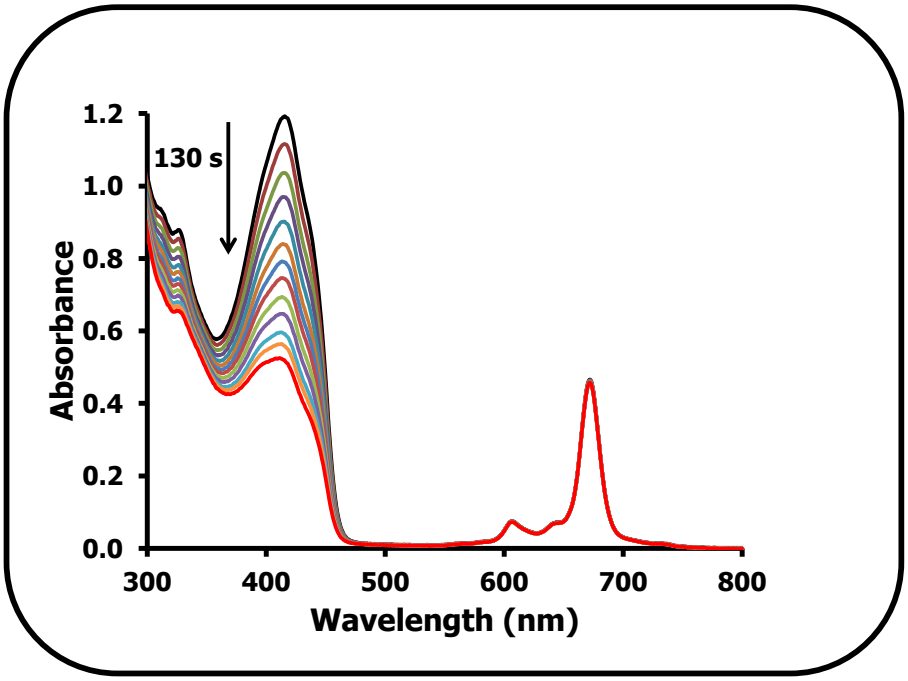

Fig. 4.6: A typical spectra for the determination of singlet oxygen quantum yield. The spectra show the degradation of DPBF in the presence of ZnMAPPc (**12**) in DMSO. The concentration of ZnMAPPc is 7.9×10^{-6} M.

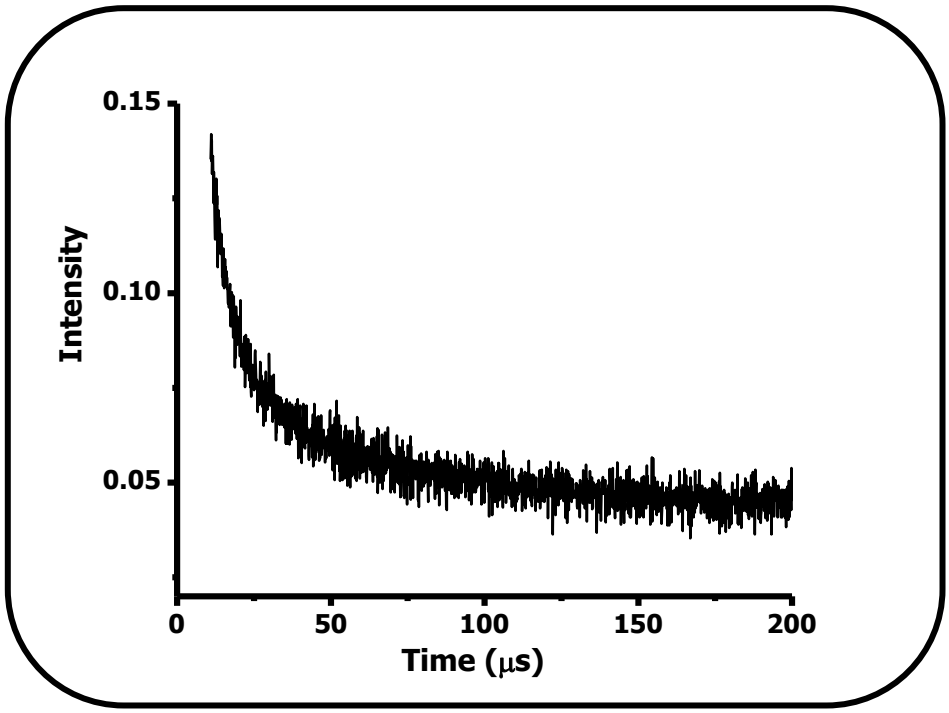

Fig. 4.7: Representative singlet oxygen phosphorescence decay profile of ZnTCPPc-AA (**9**) in DMSO solution. The concentration of ZnTCPPc-AA is 4.7 $x10^{-6}$ M.

Table 4.6: Singlet oxygen quantum yields and triplet quantum yields for ZnPc derivatives (or ZnPc-biomolecule conjugates)

ZnPc complexes	Solvent	Φ_T ±0.02	Φ_Δ ±0.02	S_Δ
ZnMAPc (**1**)	DMSO	0.48	0.43	0.90
ZnMAPc-Py (**2**)	DMSO	0.78	0.53	0.68
ZnMAPc-FA (**3**)	DMSO	0.53	0.48	0.91
ZnMCPPc (**4**)	DMSO	0.35	0.20	0.57
ZnMCPPc-spermine (**5**)	DMSO	0.84	0.83	0.99
ZnMCPPc-uridine (**6**)	DMSO	0.62	0.49	0.79
ZnMCPPc-AA (**7**)	DMSO	0.67	0.65	0.97
ZnTCPPc (**8**)	DMSO	0.49	0.17	0.34
ZnTCPPc-AA (**9**)	DMSO	0.82	0.80	0.98
ZnOCPc (**10**)	Buffer 9	0.34	0.21	0.62
ZnOCPc-BSA (**11**)	Buffer 9	0.27	0.44	-
ZnMAPPc (**12**)	DMSO	0.70	0.52	0.74
ZnTAPPc (**13**)	DMSO	0.54	0.38	0.70

4.4.2 Singlet oxygen quantum yields (Φ_Δ) in the presence of SWCNTs

The presence of SWCNTs in the ZnPc-biomoleule-SWCNT conjugates resulted in decrease in the Φ_T values and corresponding decrease in Φ_Δ values were observed (Table 4.7) as compared to the precursor ZnPc-biomolecule (Table 4.7). Complexes **25 - 28** also show similar decreases in the Φ_Δ values for the mono- and tetra- aminophenoxyl complexes on linkage and adsorption to SWCNTs. Decreases in Φ_Δ values for these complexes correspond to decreases in the Φ_T values. However, increase was observed in the Φ_Δ values of **15**, **19** and **21**. The increases in the Φ_Δ values for **15**, **19** and **21** correspond to the increases observed in the Φ_T values as discussed above.

Table 4.7: Singlet oxygen quantum yields and triplet quantum yields for ZnPc derivatives (or ZnPc-biomolecule conjugates) linked to (or adsorbed on) SWCNTs

ZnPc complexes	Solvent	Φ_T ±0.02	Φ_Δ ±0.02	S_Δ
ZnMAPc-FA-SWCNT (ad) (**14**) [from **3**]	DMSO	0.32 (0.53)	0.18 (0.48)	0.56 (0.91)
ZnMCPPc-SWCNT (ad) (**15**) [from **4**]	DMSO	0.53 (0.35)	0.47 (0.20)	0.89 (0.57)
ZnMCPPc-spermine-SWCNT (ad) (**16**) [from **5**]	DMSO	0.76 (0.84)	0.62 (0.83)	0.82 (0.99)
ZnMCPPc-uridine-SWCNT (ad) (**17**) [from **6**]	DMSO	0.50 (0.62)	0.44 (0.49)	0.88 (0.79)

ad = adsorbed, Values in bracket are in the absence of SWCNTs.

Table 4.7: contd.

ZnPc complexes	Solvent	Φ_T ±0.02	Φ_Δ ±0.02	S_Δ
ZnMCPPc-AA-SWCNT (ad) (**18**) [from **7**]	DMSO	0.59 (0.67)	0.52 (0.65)	0.88 (0.98)
ZnMAPc-SWCNT (linked) (**19**) [from **1**]	DMSO	0.53 (0.48)	0.52 (0.43)	0.98 (0.90)
ZnMAPc-Py-SWCNT (ad) (**20**) [from **2**]	DMSO	0.64 (0.78)	0.29 (0.53)	0.45 (0.66)
ZnTCPPc-SWCNT (ad) (**21**) [from **8**]	DMSO	0.54 (0.49)	0.53 (0.17)	0.98 (0.34)
ZnTCPPc-AA-SWCNT (ad) (**22**) [from **9**]	DMSO	0.59 (0.82)	0.58 (0.80)	0.98 (0.98)
ZnOCPc-SWCNT (ad) (**23**) [from **10**]	Buffer 9	0.21 (0.34)	0.16 (0.21)	0.76 (0.62)
ZnOCPc-BSA-SWCNT (ad) (**24**) [from **11**]	Buffer 9	0.19 (0.27)	0.41 (0.44)	-
ZnMAPPc-SWCNT (linked) (**25**) [from **12**]	DMSO	0.59 (0.70)	0.45 (0.52)	0.76 (0.64)
ZnMAPPc-SWCNT (ad) (**26**) [from **12**]	DMSO	0.38 (0.70)	0.23 (0.52)	0.60 (0.64)
ZnTAPPc-SWCNT (linked) (**27**) [from **13**]	DMSO	0.48 (0.54)	0.34 (0.38)	0.71 (0.75)
ZnTAPPc-SWCNT (ad) (**28**) [from **13**]	DMSO	0.44 (0.54)	0.22 (0.38)	0.50 (0.75)

ad = adsorbed, Values in bracket are in the absence of SWCNTs.

4.5 General conclusion

The photophysical and photochemical properties of ZnPcs (or ZnPc-biomolecule conjugates) linked to (or adsorbed on) SWCNTs were studied. Different substituents attached to the Pc affected the photophysical and photochemical properties. The characteristic intrinsic fluorescence properties of pyrene, folic acid or BSA resulted in increase of the fluorescence quantum yields (Φ_F) of the conjugates. The presence of spermine, uridine and ascorbic acid resulted in negligible changes in the fluorescence properties of the conjugates. There were decreases in the Φ_F values on adsorption of ZnPc-biomolecule conjugates onto SWCNTs (and on going from **2** to **20**), while negligible changes were observed in the Φ_F values of other complexes. A mono-exponential fluorescence decay curve was obtained for most ZnPc derivatives or ZnPc-biomolecule conjugates (complexes, **1** - **10** and **12**) except **11** and **13**. Bi-exponential fluorescence decay curves were obtained for the conjugates containing SWCNTs, except for mono-substituted carboxy phenoxy ZnPc derivatives (complexes, **15** - **18**).

There were increases in the triplet quantum yield (Φ_T) values in the presence of either pyrene or biomolecules in the ZnPc conjugates due to extended π conjugation of Pc ring by pyrene and the presence of the phenyl bridge connecting the ZnMCPPc moiety to the respective biomolecules that encourages SOCT-ISC mechanism for complexes **5**, **6**, **7** and **9**. However, decrease was observed in the Φ_T value for ZnOCPc-BSA (**11**), whose photophysical properties were studied in pH 9 buffer due to quenching of triplet state properties by water. Triplet life-times (τ_T) increases in complexes **5**, **6**, **7** and **9** compared to the precursor ZnPcs. While the τ_T values for ZnMAPc-Py (**2**) and ZnMAPc-FA (**3**) decreases. Both τ_T and Φ_T values increases for all the biomolecule conjugates. Increases in τ_T values correspond to decreases in Φ_T values for mono- and tetra-aminophenoxy complexes. The Φ_T values for the ZnPc-biomolecule-SWCNT conjugates

(complexes, **14**, **16**, **17**, **18**, **22 - 24**) decreases when compared to the precursor ZnPc-biomolecule conjugates, while similar decreases were observed on either linkage or adsorbing mono- (or tetra-) substituted aminophenoxy Pcs on SWCNTs (complexes, **25 - 28**) due to photo-induced electron transfer from Pc ring (electron donor) to SWCNTs (electron acceptor). However, the Φ_T values for complexes **15**, **19** and **21** increases compared to the precursor ZnPcs as a result of the fast charge recombination process due to highly short-lived radical ion pair produced. Increases were observed in the τ_T values for most ZnPcs derivatives (or ZnPc-biomolecule conjugates) linked to (or adsorbed on) SWCNTs.

The singlet oxygen quantum yields (Φ_Δ) for all the conjugates containing biomolecules (complexes, **5**, **6**, **7**, **9** and **11**) increases compared to the precursor ZnPcs, these increases correspond to the increases in the triplet quantum yields except for **11**. The presence of SWCNTs decreases the Φ_Δ values for all ZnPc-biomolecule-SWCNT conjugates (complexes, **14**, **16**, **17**, **18**, **22 - 24**) and some ZnPc-SWCNT conjugates (complexes, **20**, **25 - 28**). However, the Φ_Δ values for complexes **15**, **19** and **21** increases as compared to the precursor ZnPcs. Decreases or increases in Φ_Δ values correspond to decreases or increases in Φ_T values.

CHAPTER FIVE

5. CYTOTOXICITY TEST AND PHOTODYNAMIC THERAPY ACTIVITY

This chapter describes the cytotoxicity and photodynamic therapy activities of ZnPc-biomolecule conjugates when alone and on adsorption onto single-walled carbon nanotubes on either A375 melanoma or MCF-7 breast cancer cells.

5.1 Cytotoxicity tests and photodynamic therapy activities of ZnMAPc-FA (3), ZnMAPc-FA-SWCNT (14) and SWCNT-FA on A375 melanoma cells and MCF-7 breast cancer cells

The cytotoxicity and PDT effect of ZnMAPc (**1**) alone was not done in this work because this compound is only soluble in organic solvents. However, on conjugating ZnMAPc (**1**) to folic acid (ZnMAPc-FA (**3**)), the conjugate became soluble in aqueous media. Thus, only the cytotoxicity and PDT activity of the ZnMAPc-FA and its SWCNTs conjugate (ZnMAPc-FA-SWCNT, adsorbed (**14**)) were examined. However, based on the increase in singlet oxygen quantum yields on linking FA to ZnMAPc, improved PDT activity is expected for ZnMAPc-FA compared to ZnMAPc in the absence of FA. The FA conjugates were tested on A375 melanoma cells and MCF-7 breast cancer cells for comparison.

5.1.1 Cytotoxicity tests (Dark toxicity)

5.1.1.1 A375 melanoma cells

Cytotoxicity (in the dark) of ZnMAPc-FA (**3**), ZnMAPc-FA-SWCNT (adsorbed) (**14**) or SWCNT-FA were measured by quantifying surviving cells using the NR viability assay 24 h after treatment (incubation of A375 melanoma cell lines with gradient concentration of each complex (5, 10, 20, 40 and 80 μM)). The *in vitro* cytotoxicity viability tests confirmed that the complexes were relatively not toxic at all the experimental concentrations. At 80 μM, 94% of **3** (Fig. 5.1A), 95% of **14** (Fig. 5.1B) and 94% of SWCNT-FA (Fig. 5.1C) were still viable (Table 5.1). Visual observation of the A375 melanoma cells using an inverted microscope Fig. 5.2 (A and B) showed there was no significant difference between the melanoma cells morphology in

the control Fig. 5.2A (absence of complex) and in the presence of complex (Fig. 5.2B) (both without irradiation) indicating that the complexes were relatively not toxic to the cells.

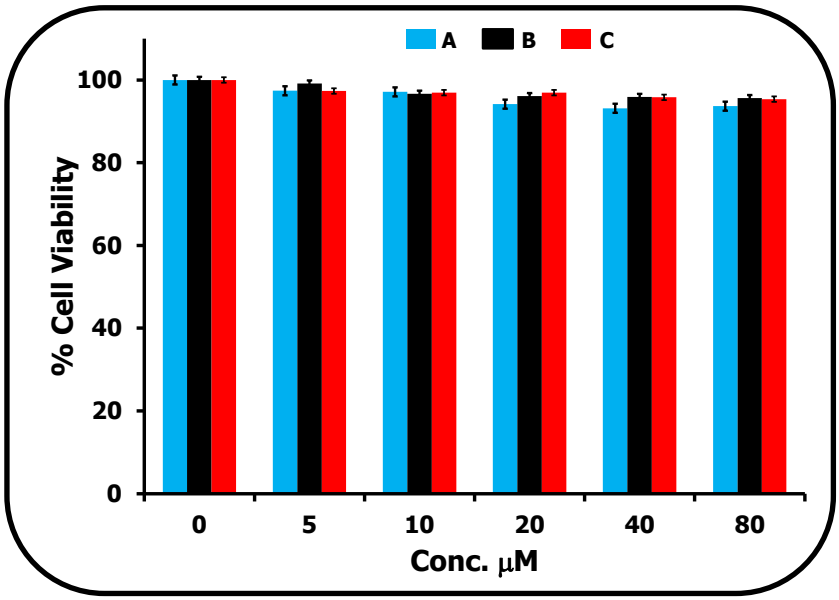

Fig. 5.1: Cytotoxicity (dark toxicity) test of ZnMAPc-FA (**3**) (A), ZnMAPc-FA-SWCNT (adsorbed) (**14**) (B) and SWCNT-FA (C) on A375 melanoma cells.

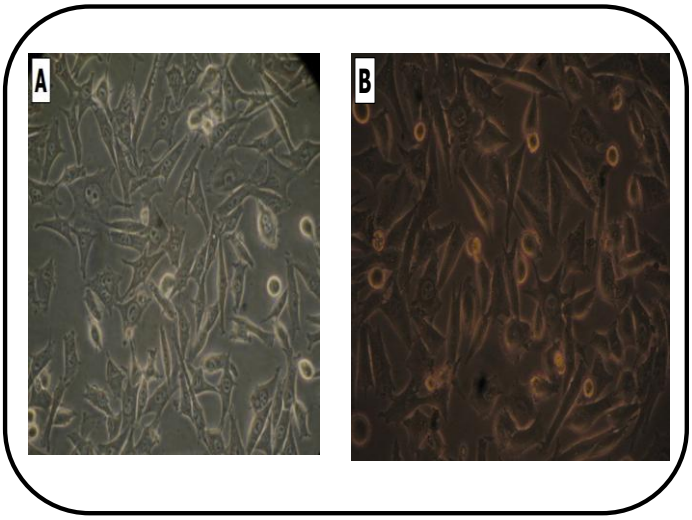

Fig. 5.2: Micrographs of melanoma cells: cells only (A) and cells in the presence of ZnMAPc-FA (**3**) (B) (both without irradiation).

5.1.1.2 MCF-7 breast cancer cells

The cytotoxicity test of **3**, **14** and SWCNT-FA on MCF-7 breast cancer cells also show that the complexes were relatively not toxic at all experimental concentrations (5, 10, 20 and 40 μM). At the highest concentration: 92% of **3** (Fig. 5.3B), 94% of **14** (Fig. 5.3C) and 92% of SWCNT-FA (Fig. 5.3A) (Table 5.1) were still viable, using WST-1 assay. This also confirms that phthalocyanine have low toxicity in the absence of light [10].

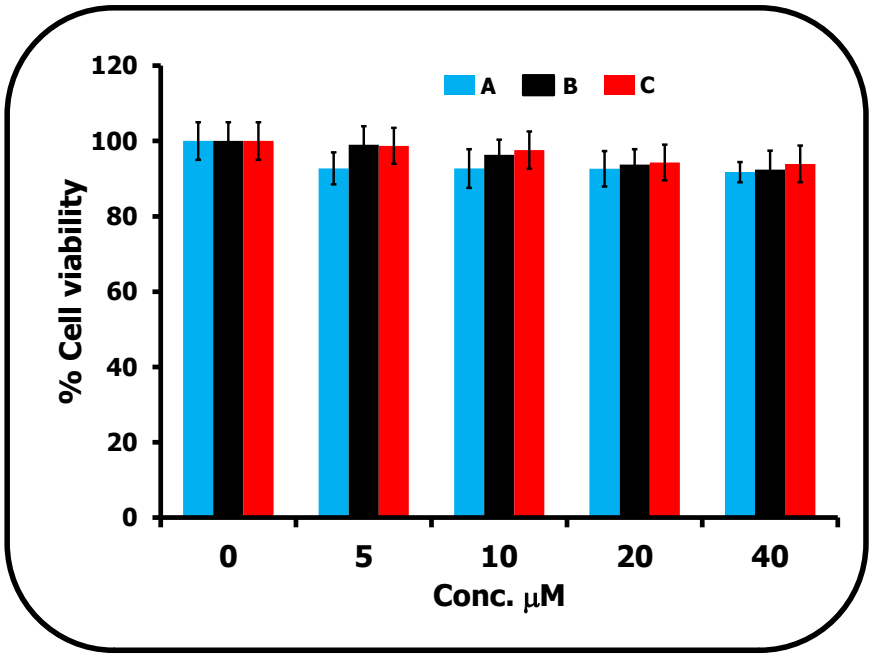

Fig. 5.3: Cytotoxicity (dark toxicity) test of SWCNT-FA (A), ZnMAPc-FA (**3**) (B) and ZnMAPc-FA-SWCNT (adsorbed) (**14**) (C) on MCF-7 breast cancer cells.

5.1.2 Photodynamic therapy activities

5.1.2.1 A375 melanoma cells

The photodynamic therapy activities for **3**, **14** or SWCNT-FA were determined 24 h after treating A375 melanoma cells with 10 μM of each complex, followed by irradiation with laser. Upon irradiation with diode laser at 676 nm, cells viability decreases in a light-dose dependent manner. The *in vitro* phototoxicity tests were quantified using NR viability assay, the results showed that 88% of the cells were viable at 5 J/cm^2 for laser dose treatment (cells only, Fig. 5.4A), showing that in the absence of tested complex there was no significant decrease in cell viability. Fig. 5.4B showed that 77% of the cells were viable at 5 J/cm^2 for SWCNT-FA. SWCNTs absorb in the near infrared region, but absorption extends to the UV region [159]. SWCNTs may induce cell death by a localized PTT effect when irradiated at a wavelength near 950 nm. For A375 melanoma cell lines, a diode laser was used for photo-irradiation and the excitation was at 676 nm where Pcs absorb strongly while SWCNTs absorb weakly, hence the low percentage decrease in cell viability for SWCNT-FA.

PDT activities were observed for **3** and **14** which have strong absorption close to the excitation wavelength (676 nm). On irradiating A375 melanoma cells with a light dose of 5 J/cm^2, 40% and 37% of cells were viable for **3** and **14** respectively, as shown in Fig. 5.4. Thus, complexes **3** and **14** showed PDT activities. The student's t-test was employed as a statistical tool to evaluate the PDT data, the result shows that there is significant difference between the two complexes, **3** and **14** (*$P < 0.05$). The decrease in cell viability of 60% and 63% for **3** and **14** respectively does not correspond to the huge difference between their singlet oxygen quantum yields of 0.48 for **3** and 0.18 for **14** (Table 4.7). This suggests that, though SWCNTs decreased the singlet oxygen

quantum yield of **3**, the PDT activity significantly increased for **14**, possibly due to efficient drug delivery of the SWCNTs present in the nanohybrid.

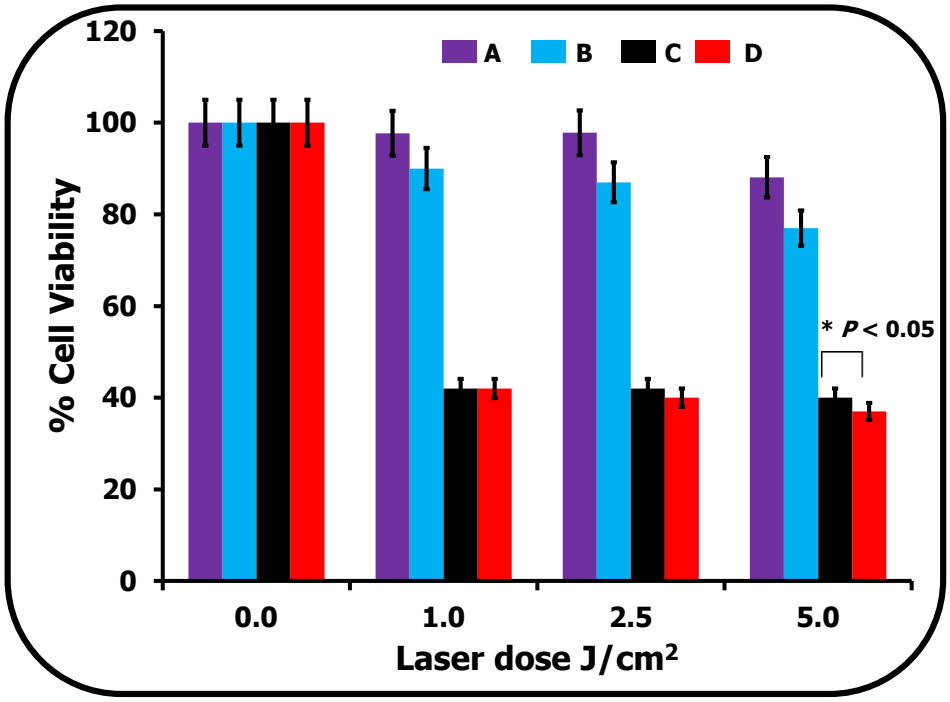

Fig.5.4: Photodynamic test of cells alone (without complex) (A), SWCNT-FA (B), ZnMAPc-FA (**3**) (C) and ZnMAPc-FA-SWCNT (adsorbed) (**14**) (D) on A375 melanoma cells. Statistically, there is significant difference between phototoxicity effects of **3** and **14** (*$P < 0.05$).

5.1.2.2 MCF-7 breast cancer cells

Exposure of MCF-7 breast cancer cells to light in the presence of **3**, **14** and SWCNT-FA resulted in decrease in cells viability in an irradiation-time and concentration dependent manner. The highest decrease in cell viability was observed for the highest concentration of each complex and

longest exposure time, Table 5.1. The PDT effects of **3** and **14** on MCF-7 cells were only observed on exposing the cells to light for 600 s (54 J/cm^2) and 1200 s (112 J/cm^2). The percentage cell viability was 41% (for **3**), 38% (for **14**) at 54 J/cm^2, 15% (for **3**) and 22% (for **14**) at 112 J/cm^2 (Fig. 5.5, Table 5.1).

On comparing the PDT activities of **3** and **14** on A375 melanoma cells and MCF-7 breast cancer cells, complexes **3** and **14** were more efficient on A375 melanoma cells leaving 40% and 37% cells viable at 5 J/cm^2, while at 28 J/cm^2 there was no PDT activity on MCF-7 cancer cells (63% and 64% cell viability were observed for **3** and **14** respectively), Table 5.1. These results show that there are variations in the potency of drugs on different cancer cell lines. The variations depend on different factors: the source of light, the excitation wavelength of the light source, activities of the drug among others.

These factors affected the PDT activities of **3** and **14** on A375 melanoma cells and MCF-7 breast cancer cells. A diode laser light source with excitation at 676 nm close to the Q-band maxima of the Pc was used for A375 melanoma cells, hence the more efficient PDT activity on this cell line. While a quartz lamp light source with excitation from 600 nm (following the use of a glass filter) was used for MCF-7 breast cancer cells. Thus, the variations found in the PDT activities of **3** and **14** on the cancer cell lines.

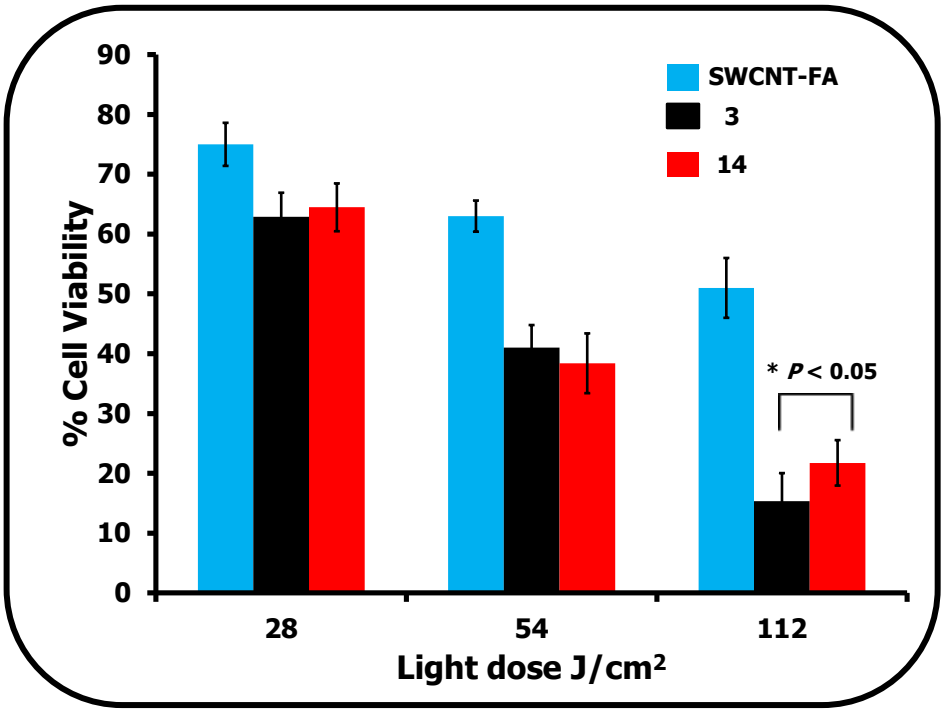

Fig.5.5: Phototoxicity test of SWCNT-FA, ZnMAPc-FA (**3**) and ZnMAPc-FA-SWCNT (adsorbed) (**14**) on MCF-7 cancer cells. Statistically, there is significant difference between phototoxicity effects of **3** and **14** (*$P < 0.05$).

Table 5.1: % Cell viability data for dark (cytotoxicity test) and PDT test for 3, 14 and SWCNT-FA on A375 melanoma cells and MCF-7 cancer cells at the highest concentration

	A375 melanoma cells		MCF-7 breast cancer cells			
ZnPc complexes	**Dark (cytotoxicity) test**	**PDT at 5 J/cm^2**	**Dark (cytotoxicity) test**	**PDT at 28 J/cm^2 (300 s)**	**PDT at 54 J/cm^2 (600 s)**	**PDT at 112 J/cm^2 (1200 s)**
ZnMAPc-FA (**3**)	94 ±2	40 ±5	92 ±5	63 ±5	41 ±5	15 ±5
ZnMAPc-FA-SWCNT (**14**)	95 ±2	37 ±5	94±5	64 ±5	38 ±4	22 ±5
SWCNT-FA	94 ±4	77 ±3	92 ±4	75 ±5	63 ±2	51 ±2

5.2 Cytotoxicity tests and Photodynamic therapy activities of ZnMCPPc and its derivatives on MCF-7 breast cancer cells

The stock concentration of each complex (**4**, **5**, **6**, **7**, **15**, **16**, **17** and **18**) was prepared by dissolving each in DMSO and making the volume up with supplemented media. The effect of DMSO on the cells were investigated by incubating the cells for 24 h with 0.8% (v/v) DMSO in supplemented media (which is the highest percentage of DMSO used for preparing the highest concentration of each complex), control cells were incubated without DMSO in supplemented media. Following this, surviving cells were quantified using the WST-1 cell proliferation assay 24 h after the treatment. 97± 3% of the cells

were still viable as shown in Fig. 5.6. The result shows that 0.8% (v/v) DMSO in supplemented media had negligible effect on the cells.

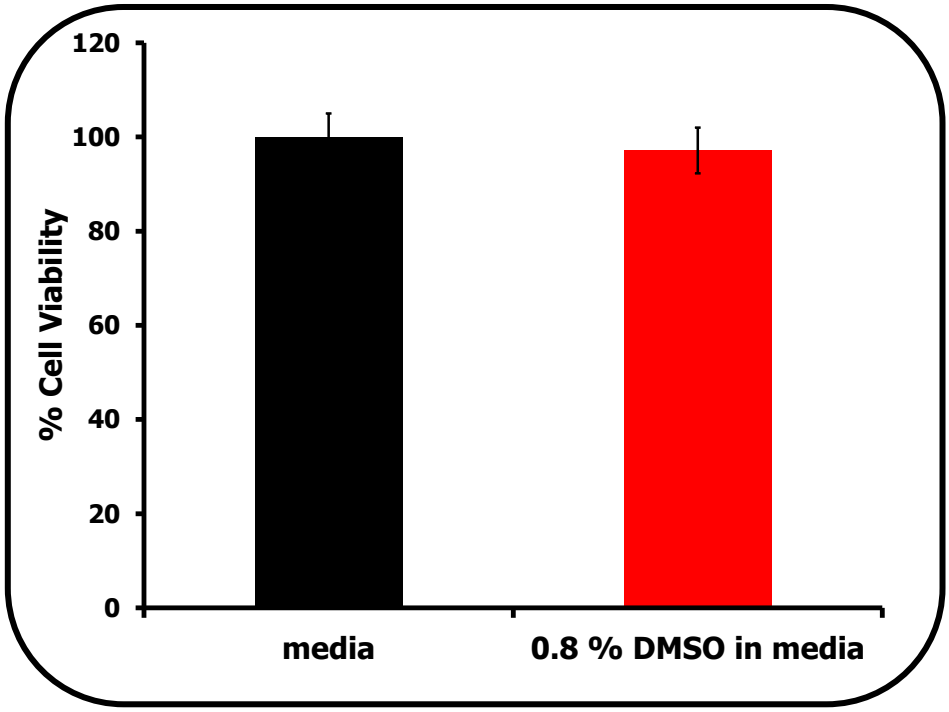

Fig. 5.6: Effect of DMSO on MCF-7 cancer cells.

5.2.1 Cytotoxicity tests of ZnMCPPc and its derivatives on MCF-7 breast cancer cells

The cytotoxicity effects (dark toxicity) of gradient concentration of respective complex; SWCNTs (0.12 - 0.96 μg/ml), SWCNT-AA (2 - 5 μg/ml), **4**, **5**, **6**, **7**, **15**, **16**, **17** and **18** (0 - 40 μM) were tested *in vitro* on MCF-7 breast cancer cells in 100 μl of supplemented media in a 96 well plate for 24 h in the dark. The concentrations of the ZnMCPPc derivatives in the presence of SWCNTs (complexes, **15**, **16**, **17** and **18**) were determined from the Q-band absorption. The concentrations for SWCNT-AA or SWCNT-COOH are in μg/ml while ZnMCPPc derivatives are in μM, since the extinction coefficient of the former is not available.

The cytotoxicity cell viability test of SWCNTs, SWCNT-AA, **4**, **5**, **6**, **7**, **15**, **16**, **17** and **18** (data are shown in Table 5.2) after treating MCF-7 breast cancer cells with the highest concentration of each complex show that they were relatively not toxic to the cells, Table 5.2.

Comparing the dark toxicity data of ZnMCPPc (**4**) and complexes containing spermine (**5**, **16**) (Fig 5.7), complex **5** (ZnMCPPc-spermine) containing spermine increases the dark toxicity of **4** with 75% cell viability to 60% for **5** after incubation in the dark for 24 h. This might be due to the ability of spermine to bind strongly to the DNA of cells through electrostatic interaction. The presence of SWCNTs in **5** (ZnMCPPc-spermine-SWCNT, adsorbed (**16**)) reduces the dark toxicity of spermine leaving 76% cells viable (Fig. 5.7, Table 5.2).

Uridine reduces the dark toxicity of **4** by improving the cell viability of 75% for **4** to 88% (for ZnMCPPc-uridine (**6**)) after cytotoxicity test. There was no significant difference in the cytotoxicity data of **6** and its conjugate with SWCNTs (ZnMCPPc-uridine-SWCNT, adsorbed (**17**)), (Fig. 5.8, Table 5.2).

Ascorbic acid contained in complexes **7** and **18** reduces the cytotoxicity of **4** (Fig. 5.9, Table 5.2) by improving the cell viability. Complex **15** (ZnMCPPc-SWCNT, adsorbed) has similar cytotoxicity effect as **18** (ZnMCPPc-AA-SWCNT, adsorbed). There was significant difference in the cytotoxicity of **4** as compared to **7** and **18** (Fig. 5.9). The role of ascorbic acid in improving cell viability might be due to its nutritional requirements in cell proliferation and its potent reducing properties. AA can protect indispensable molecules in the body (such as, proteins, fats, nucleic acid (deoxyribonucleic acid and ribonucleic acid) from damage by free radicals and reactive oxygen species (ROS) [160-162]. Michels et al [163] also show that dietary antioxidant vitamins and retinol could be protective against breast cancer on the basis of their ability to reduce oxidative DNA damage and their role in cell differentiation.

The improved cell viability in the presence of SWCNTs for complexes **15 - 18** might be due to the ability of SWCNTs to prevent the Pc complexes from direct contact with the cancer cells, since the Pc complexes are adsorbed on it.

Visual observation of the cells, control (Fig 5.10A) or cells in the highest concentration of **18** in supplemented media (Fig. 5.10B) using an inverted microscope show that the cellular morphology of the treated cells remained the same relative to the control.

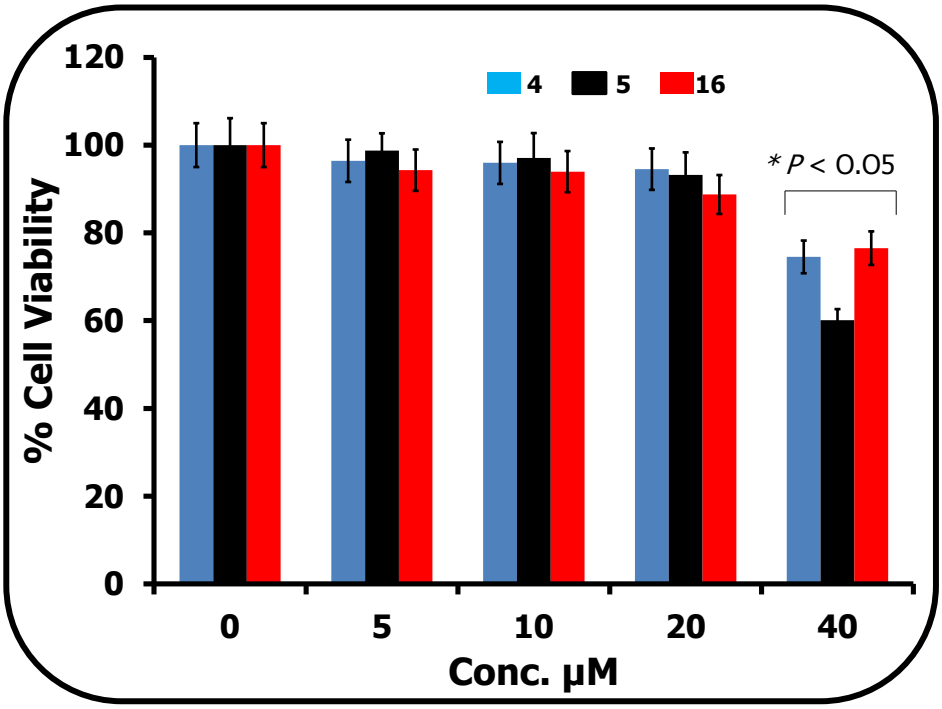

Fig. 5.7: Cytotoxicity test of ZnMCPPc (**4**), ZnMCPPc-spermine (**5**) and ZnMCPPc-spermine-SWCNT (adsorbed) (**16**) on MCF-7 cancer cells. Statistically, there is no significant difference between cytotoxicity test of **4** and **16** (*P > 0.05), while there is significant difference between **4**, **5** and **16** (*P < 0.05).

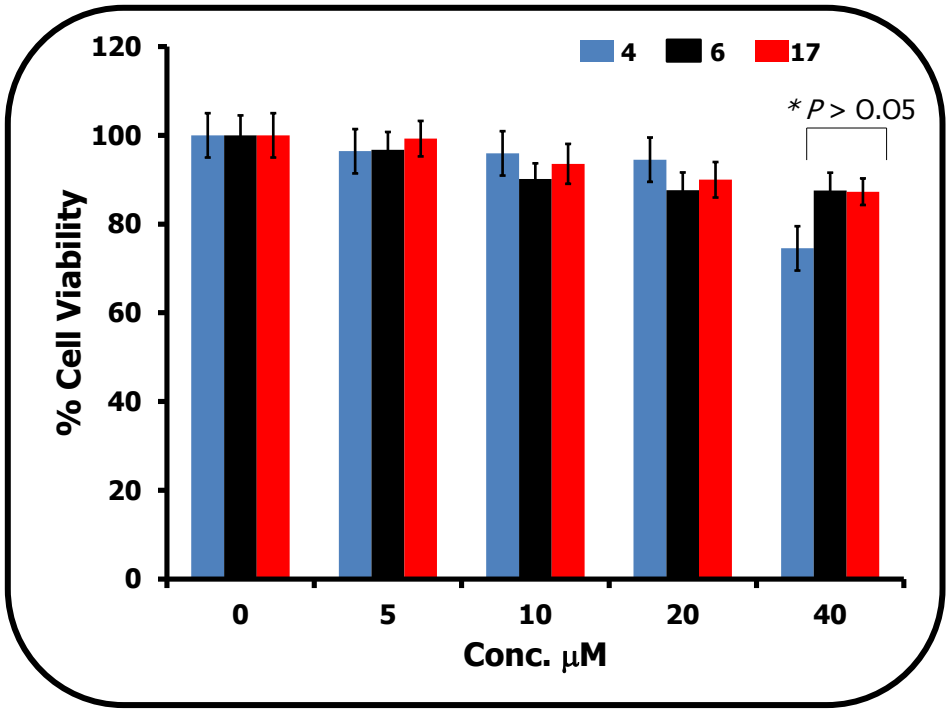

Fig. 5.8: Cytotoxicity test of ZnMCPPc (**4)**, ZnMCPPc-uridine (**6**) and ZnMCPPc-uridine-SWCNT (adsorbed) (**17**) on MCF-7 cancer cells. Statistically, there is no significant difference between cytotoxicity test of **6** and **17** (*$P > 0.05$).

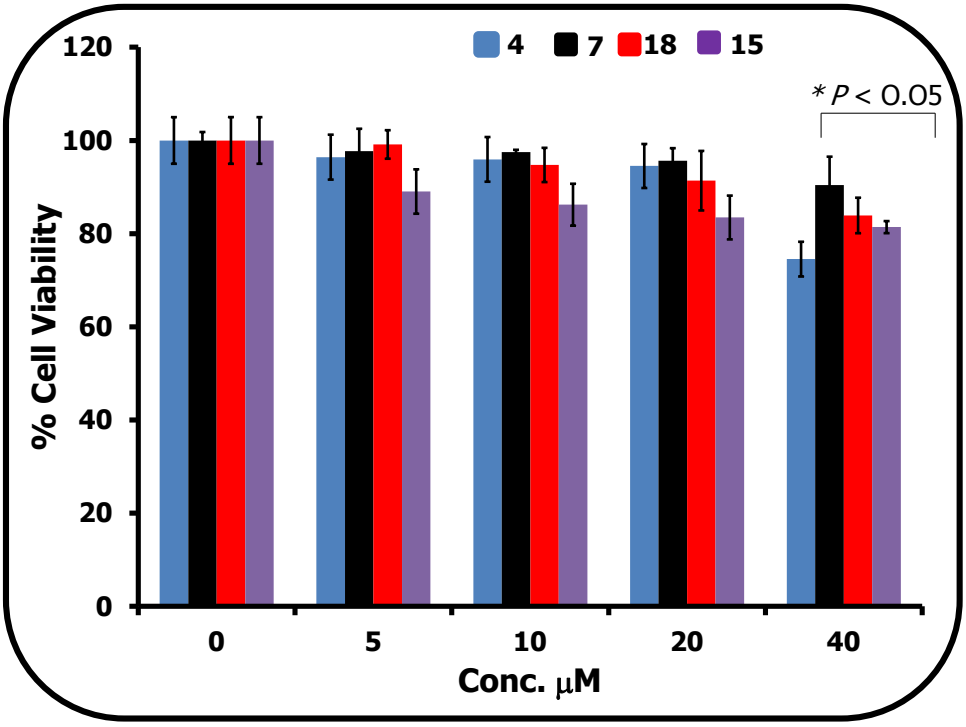

Fig. 5.9: Cytotoxicity test of ZnMCPPc (**4**), ZnMCPPc-AA (**7**), ZnMCPPc-AA-SWCNT (adsorbed) (**18**) and ZnMCPPc-SWCNT (adsorbed) (**15**) on MCF-7 cancer cells. There is significant difference in the cytotoxicity of **4** as compared to **7** and **18** (*P < 0.05).

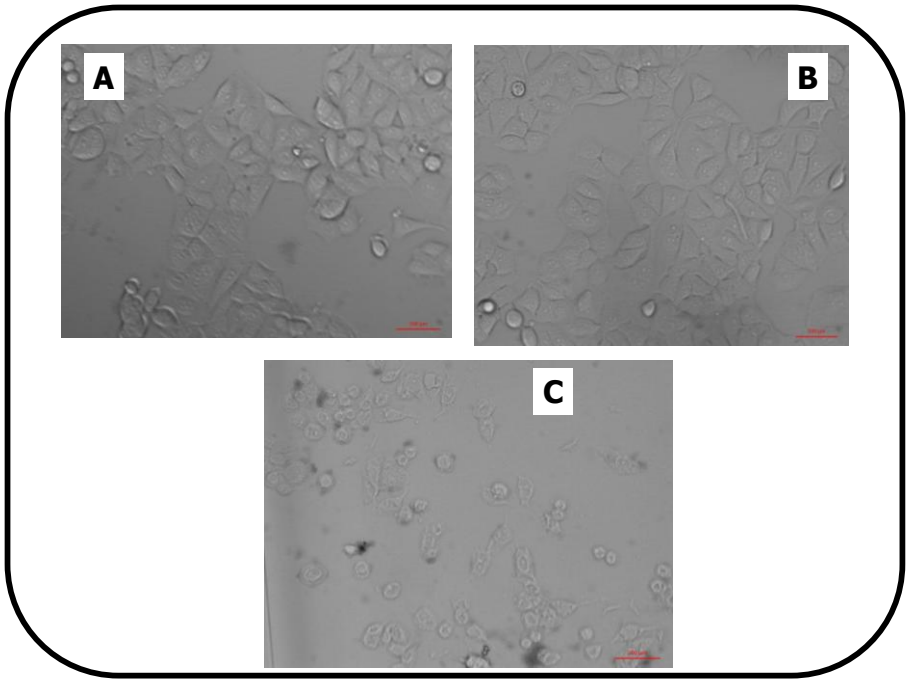

Fig. 5.10: MCF-7 breast cancer cells micrographs: (A) cells only (control), (B) cells in the presence of ZnMCPPc-AA-SWCNT (adsorbed) (**18**) (without irradiation) and (C) cells after PDT (irradiated) and 24 h incubation in fresh culture media. (Images were captured at 5X magnification under bright-field conditions).

5.2.2 Photodynamic therapy activities of ZnMCPPc and its derivatives on MCF-7 breast cancer cells

Exposure of MCF-7 breast cancer cells to light either in the presence of SWCNTs, SWCNT-AA or **4**, **5**, **6**, **7**, **15**, **16**, **17** and **18** resulted in the phototoxicity of the cells through either photodynamic (or photothermal) effect of ZnPc (or SWCNTs) complexes respectively.

Light from a general electric quartz lamp (following the use of a glass filter) was used for photo-irradiation of MCF-7 cancer cells which have been reported to be effective light source in the

photo-irradiation of tumor cells [10,122-125]. A quartz lamp absorbs light from about 600 nm and beyond 1000 nm. This wavelength range includes the wavelength where SWCNTs absorb ~ 950 nm [159], which allows the testing of the PDT and PTT effects of MPc and SWCNTs complexes respectively. Thus, both PDT (Pcs) and PTT (SWCNTs) are expected to be involved in decrease in cell viability. The irradiation time was varied between 300 and 1200 seconds to result in irradiation doses between 28 - 112 J/cm^2.

Visual observation of the treated cells (Fig. 5.10C, cells exposed to light after treatment with complex **18** as an example) relative to the control cells (Fig. 5.10A, without complex and exposure to light) using an inverted microscope showed that the treated MCF-7 cancer cells have lost their cellular morphology indicating their inability to proliferate further.

The percentage cell viability of each complex was quantified using WST-1 assay 24 h following exposure of cells to light at varying time (300 - 1200 s, (28 - 112 J/cm^2)) and incubation of the cells with gradient concentrations of respective complexes (**4**, **5**, **6**, **7**, **15**, **16**, **17**, **18**, SWCNTs and SWCNT-AA). The cell viability decreases in irradiation-time and concentration dependent manner. The percentage cell viability for all the tested complexes at the highest concentration and longest light exposure (1200 s) were lower than 50%, except the complex containing ascorbic acid alone (**7**) (Fig. 5.11) and SWCNT-AA (Table 5.2).

The phototoxicity of ZnMCPPc and its derivatives are in these order: **5** > **16** > **6** > **17** > **15** > **18** > **4** > **7**, these order correspond to the singlet oxygen quantum yield (Φ_Δ) values determined for the complexes, Table 5.2 (except the complexes containing ascorbic acid, **7** and **18**). Generally, all the complexes containing biomolecule showed improved phototoxicity compared to the precursor ZnMCPPc (**4**) except for **7**. The singlet oxygen quantum yields of the complexes were

done in DMSO whereas the cell studies are done in an aqueous environment. The antioxidant activity of AA will be enhanced in aqueous media resulting in decreased PDT activity. The singlet oxygen quantum yields of the Pcs or their conjugates could not be done in aqueous media due to solubility problems.

The PDT effect of **4** (ZnMCPPc) (Fig. 5.11A, Table 5.2) resulted in 36 $\pm$ 2% cell viability after incubating the cells with the highest concentration of **4** and exposure to light for 1200 s. Thus, complex **4** decreases the cell viability of MCF-7 cancer cells by 64% through PDT effect. When MCF-7 cancer cells were treated with the highest concentration of complex **7** (ZnMCPPc-AA) (Fig. 5.11B, Table 5.2) and exposed to light for 1200 s; 62 $\pm$ 5% of the cells were still viable, showing that **7** was not toxic to the cell. On exposing MCF-7 cancer cells to light for 1200 s after incubation with complex **18** (ZnMCPPc-AA-SWCNT) at the highest concentration, 33 $\pm$ 5% of cells were viable (Fig. 5.11C, Table 5.2). The phototoxicity of complex **15** containing ZnMCPPc-SWCNT without AA resulted in 77% decrease in cell viability, leaving 23% of the cells viable (Fig. 5.11D, Table 5.2). The better performance of **15** compared to **18** (Fig. 5.11) could be as a result to increase in cell viability in the presence of AA explained above. The improved decrease in cell viability for **15** and **18** compared to precursor **4** and **7** could be a result of combined PTT (SWCNTs) and PDT (Pc) effects.

Ascorbic acid suppresses cell death in MCF-7 cancer cells and also decreases the PDT effects of ZnMCPPc, Table 5.2. To further investigate the role of ascorbic acid in suppressing cell death, MCF-7 cancer cells were exposed to light for 1200 s after treating the cells with the highest concentration of SWCNTs and SWCNT-AA, the phototoxicity test for SWCNTs and SWCNT-AA left 42% and 60% (Fig. 5.11, Table 5.2) cells viable respectively. Again, this shows that the presence of ascorbic acid in SWCNTs reduces its PTT effects on MCF-7 cancer cells and the

finding supported the earlier report by Subramani et al [164] who stated that AA suppresses cell death induced by tamoxifen in MCF-7 human breast cancer cells. Several reports have also shown that the intake of AA lowers the risk of breast cancer [163,165,166]. The ability of ascorbic acid in suppressing cell death might be due to their ability to reduce oxidative DNA damage and its role in cell differentiation [163]. Statistically, there is no significant difference between complex **7** and SWCNT-AA ($^*P > 0.05$), this indicates that AA has a similar effect in suppressing the PDT and PTT effects of ZnMCPPc and SWCNTs respectively.

Complexes **5** and **16** containing spermine show the highest phototoxicity leaving only 3% and 5% (Fig. 5.12) of cells viable respectively, after PDT. The PDT effects of **5** and **16** correspond with the high Φ_Δ values calculated for these complexes; Φ_Δ value = 0.83 and 0.62 for **5** and **16** respectively, Table 5.2. Statistics of the PDT data at the highest concentration and longest light exposure time (1200 s) show that there is no significant difference between **5** (ZnMCPPc-spermine) and **16** (ZnMCPPc-spermine-SWCNT, adsorbed), this indicates that though SWCNTs lowers the singlet oxygen quantum yield of **5**, the phototoxicity of the complexes were relatively the same. The phototoxicity of **5** and **16** might be due to the ability of spermine to bind strongly to DNA through electrostatic interaction. Reports have also shown that spermine increases PDT effects [167,168]. Lamarche et al [167] reported on the PDT activity of porphyrin-spermine conjugate against K562 human chronic myelogenous leukemia cells. Higher uptake of different porphyrins into human glioma T98G cells in the presence of polyamine was reported by Bhupathiraju et al [168], with however, low PDT activity. Porphyrins have low absorption in the visible region where cells are transparent, while Pcs absorb strongly in this region. MPc-spermine complexes reported in this work exhibited very high singlet oxygen quantum yields, resulting in improved PDT efficiency on MCF-7 breast cancer cells (Fig. 5.12, Table 5.2).

The uridine containing complexes (**6**, **17**) were more phototoxic than the AA containing complexes. Complexes **6** and **17** left 16% and 20% cells viable at the highest concentration and longest light exposure time (1200 s), Fig. 5.13. Although, the presence of SWCNTs in **17** (ZnMCPPc-uridine-SWCNT, adsorbed) tend to lower the phototoxicity of **6** (ZnMCPPc-uridine), statistically, there was no significant difference in the phototoxicity of **6** and **17** ($^*P > 0.05$). The phototoxicity of **6** and **17** might be due to the anticancer properties of uridine [39-43] and the ability of nucleoside to generate singlet oxygen at photo-excited state [158].

The phototoxicity of complexes **16** and **17** containing SWCNTs were slightly lower compared to the precursor Pc **5** and **6** respectively (Table 5.2). These complexes were expected to be more efficient due to combine therapy of PDT and PTT. The reduce phototoxicity of these complexes might be due to screening effect where SWCNTs sterically prevent the direct and fast interaction of molecular oxygen (O_2) with the Pc molecule attached to SWCNTs [169].

The least phototoxicity was observed in complex **7** containing AA. Complex **15** (ZnMCPPc-SWCNT, adsorbed) and **18** (ZnMCPPc-AA-SWCNT, adsorbed) showed the importance of combination drug therapy, with the presence of SWCNTs improving the phototoxicity of **4** (ZnMCPPc) and **7** (ZnMCPPc-AA) respectively, (Table 5.2). SWCNTS in complex **18** might have reduced the antioxidant properties of ascorbic acid.

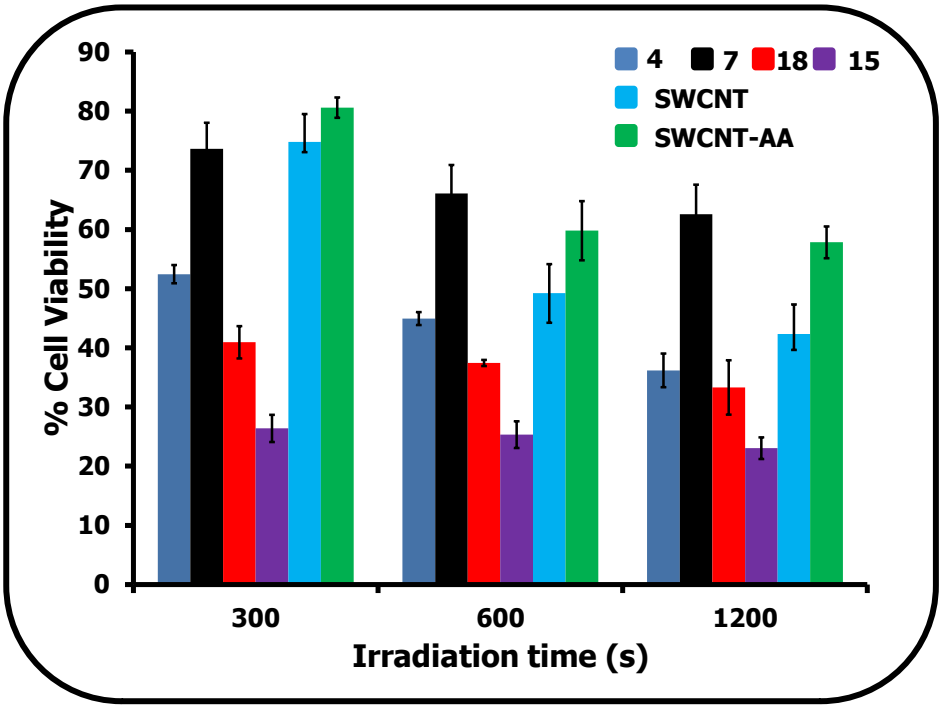

Fig.5.11: Phototoxicity test of ZnMCPPc (**4**), ZnMCPPc-AA (**7**), ZnMCPPc-AA-SWCNT (adsorbed) (**18**) ZnMCPPc-SWCNT (adsorbed) (**15**), SWCNT and SWCNT-AA on MCF-7 cancer cells, at the highest concentration for each complex. Statistically, there is significant difference between phototoxicity effects of **4** and other complexes (*$P < 0.05$), however, there is no significant difference between complexes **7** and SWCNT-AA (*$P > 0.05$).

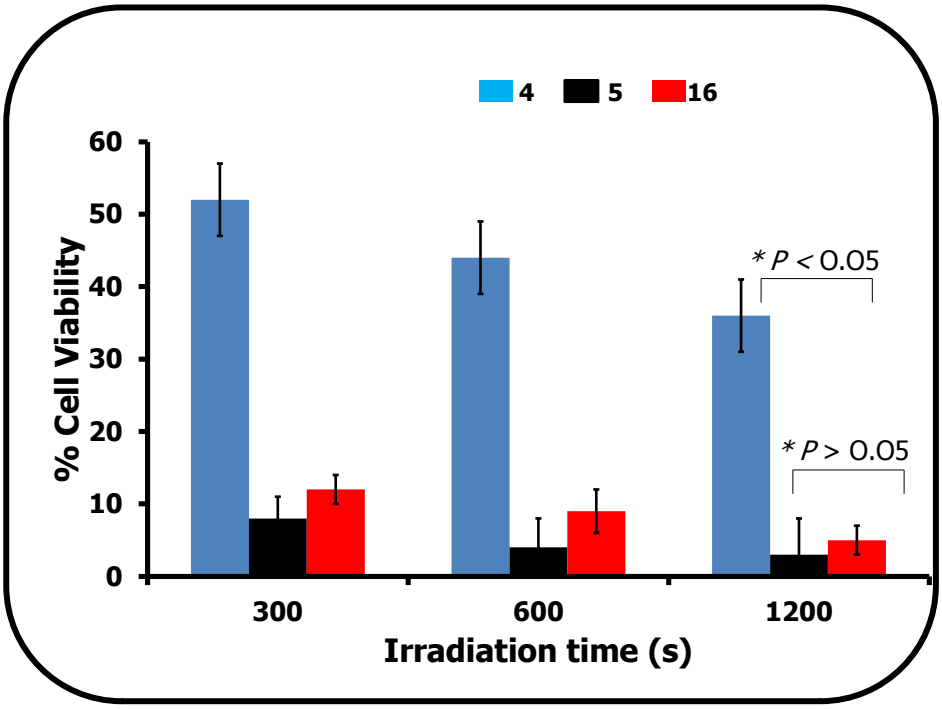

Fig. 5.12: Phototoxicity test of ZnMCPPc (**4)**, ZnMCPPc-spermine (**5**) and ZnMCPPc-spermine-SWCNT (adsorbed) (**16**) on MCF-7 cancer cells, at the highest concentration for each complex. Statistically, there is significant difference between phototoxicity effects of **4** and complexes containing spermine; **5** and **16** (*P < 0.05) and there is no significant difference between complexes **5** and **16** (*P > 0.05).

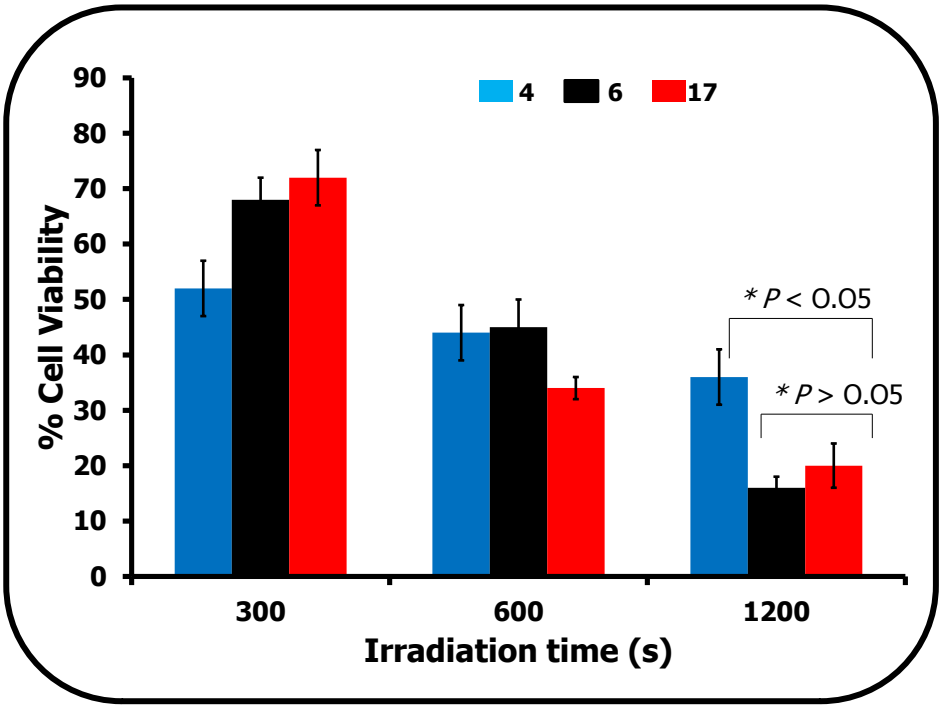

Fig. 5.13: Phototoxicity test of ZnMCPPc (**4**), ZnMCPPc-uridine (**6**) and ZnMCPPc-uridine-SWCNT (adsorbed) (**17**) on MCF-7 cancer cell, at highest concentration of each complex. Statistically, there is significant difference between phototoxicity effects of **4** and complexes containing uridine; **6** and **17** (*$P < 0.05$) and there is no significant difference between complexes **6** and **17** (*$P > 0.05$).

Table 5.2: % Cell viability data for dark (cytotoxicity test) and PDT test for all tested complexes on MCF-7 cancer cells at the highest concentration

ZnPc complexes	Φ_Δ	Dark (cytotoxicity) test	irradiation time 300 s (28 J/cm^2)	irradiation Time 600 s (54 J/cm^2)	irradiation time 1200 s (112 J/cm^2)
SWCNT-FA	-	79±3	75±4	51 ±2	63±2
SWCNT-AA	-	90 ±3	80 ±2	58 ±5	59 ±3
SWCNTs	-	76±4	75±3	49 ±5	42 ±5
ZnMAPc-FA (**3**)	0.48	92 ±2	63±5	41±5	15±5
ZnMCPPc (**4**)	0.20	75±2	52±5	44±5	36 ±5
ZnMCPPc-spermine (**5**)	0.83	60 ±4	8 ±3	4 ±4	3 ±5
ZnMCPPc-uridine (**6**)	0.49	88±4	68±4	45±5	16 ±2
ZnMCPPc-AA (**7**)	0.65	94 ±5	73 ±4	66 ±5	62 ±5
ZnMAPc-FA-SWCNT (ad) (**14**) [from **3**]	0.18	94±5	64 ±5	38 ±4	22±5
ZnMCPPc-SWCNT (ad) (**15**) [from **4**]	0.47	81 ±2	25±2	26 ±2	23 ±2
ZnMCPPc-spermine-SWCNT (ad) (**16**) [from **5**]	0.62	76 ±3	12 ±2	9 ±3	5±2
ZnMCPPc-uridine-SWCNT (ad) (**17**) [from **6**]	0.44	87 ±3	72±5	34 ±2	20 ±4
ZnMCPPc-AA-SWCNT (ad) (**18**) [from **7**]	0.52	84 ±3	40 ±3	37 ±2	33 ±5

ad = adsorbed, Φ_Δ= singlet oxygen quantum yield.

5.3 General conclusion

The cytotoxicity test and photodynamic therapy activities of some ZnPc-biomolecule conjugates when alone and on adsorption onto SWCNTs on either A375 melanoma cells or MCF-7 breast cancer cells have been presented.

ZnMAPc-FA (**3**), ZnMAPc-FA-SWCNT (adsorbed) (**14**) and SWCNT-FA were tested on both A375 melanoma and MCF-7 breast cancer cells. The complexes were relatively not toxic to both cell lines when they were incubated in the dark. There were variations in the phototoxicity of the complexes on both cell lines. Complexes **3** and **14** were more efficient on A375 melanoma cells leaving 40% and 37% cells viable at 5 J/cm^2; this was due to the diode laser light source used and the excitation wavelength (676 nm) which was close to the Q-band maxima of the Pc. A quartz lamp light source with excitation from 600 nm was used for MCF-7 breast cancer cells. At 28 J/cm^2, 63% and 64% cell viability were obtained for **3** and **14** respectively, indicating that there was no phototoxicity at this light dose. Phototoxicity was only observed from 54 J/cm^2 for MCF-7 breast cancer cells.

ZnMCPPc (**4**), ZnMCPPc-spermine (**5**), ZnMCPPc-uridine (**6**), ZnMCPPc-AA (**7**), ZnMCPPc-SWCNT (adsorbed) (**15**), ZnMCPPc-spermine-SWCNT (adsorbed) (**16**), ZnMCPPc-uridine-SWCNT (adsorbed) (**17**), ZnMCPPc-AA-SWCNT (adsorbed) (**18**), SWCNT-AA and SWCNTs were tested on MCF-7 breast cancer cells. The cytotoxicity cell viability test for all the complexes were higher than 50%, these indicate that these complexes were relatively not toxic to the cells without light. The phototoxicity cell viability tests show that the presence of spermine and uridine improves the PDT effects of ZnMCPPc. The complexes containing spermine (**5**,**16**) show the highest phototoxicity, these correspond with the high singlet oxygen quantum yields obtained for these complexes. Ascorbic acid (AA) in complexes **7** and **18** suppresses the PDT

effects of these ZnPc complexes, similar effect was observed in the PTT effects of SWCNTs due to its antioxidant activity in aqueous media.

The phototoxicity results for ZnPc-biomolecule-SWCNT conjugates were not consistent with the lower singlet oxygen quantum yields obtained due to the presence of SWCNTs as compared to the ZnPc-biomolecule conjugates alone. The phototoxicity of the ZnPc-biomolecule-SWCNT conjugates were relatively the same as that of the precursor ZnPc-biomolecule conjugates.

CHAPTER SIX

6. GENERAL CONCLUSIONS AND FUTURE PROSPECTS

This chapter summarizes the results obtained for the studies conducted and reported in this thesis and future prospects.

6.1 General conclusions

The synthesis of zinc phthalocyanine (ZnPc) derivatives covalently linked to pyrene and different biological molecules (such as: folic acid, spermine, uridine, ascorbic acid or bovine serum albumin) of importance in photodynamic therapy (PDT) for cancer treatment are presented in this work. The ZnPc derivatives alone were either linked to (or adsorbed onto) single-walled carbon nanotubes (SWCNTs); a drug delivery agent and an anticancer agent which could kill cancer cells through photothermal therapy (PTT). All the ZnPc-biomolecule conjugates were adsorbed onto SWCNTs.

The different derivatives of ZnPcs (or ZnPc-biomolecule-) SWCNTs conjugates when alone or in combination were characterized using combination of different spectroscopic techniques. The functional groups of all the complexes were confirmed using Fourier transform infrared (FTIR) spectroscopy. Nuclear magnetic resonance (NMR) spectroscopy was used to assign the protons signature of all the synthesized ZnPc-derivatives (ZnMAPc-Py (**2**) and ZnMAPc-FA (**3**) from ZnMAPc (**1**), ZnMCPPc-spermine (**5**), ZnMCPPc-uridine (**6**) and ZnMCPPc-AA (**7**) from ZnMCPPc (**4**) and ZnTCPPc-AA (**9**) from ZnTCPPc (**8**), except the complex with BSA (**11**)). Elemental analysis and mass spectroscopy were used to confirm the respective mono- or tetra-substituted conjugates.

The presence of SWCNTs in complexes **14** - **28** were confirmed using combination of spectroscopic techniques: FTIR, XRD, TEM and Raman spectroscopy. The characteristic signatures of carbon at (002) and (111) were observed for the complexes containing SWCNTs has obtained by XRD. The TEM images of all the complexes (**14** - **28**) showed a long tube-like substance suggesting the presence of SWCNTs in these complexes. Characteristics Raman peaks of SWCNTs which are centered at 2500 cm^{-1} (G*), 1590 cm^{-1} (G-band (tangential mode) sp^2)

and 1270 cm^{-1} (D-band (disorder, breathing mode) sp^3) were observed in all the complexes containing SWCNTs (linked or adsorbed). All the synthesized complexes (**1** - **28**) were of different structural composition and thermal stability as shown by the thermogravimetric analysis.

All the studied complexes showed a monomeric Q-band as shown by the absorption spectra using UV-visible spectroscopy. The Q-band of the ground state absorption spectra of ZnMAPc-Py (**2**) and ZnMAPc-FA (**3**) were broad due to aggregation. The emission spectra of all the studied complexes (**1** - **28**) were mirror images of the excitation and absorption spectra.

The photophysical and photochemical properties of all the derivatives of ZnPc- (or ZnPc-biomolecule-) SWCNTs conjugates when alone or in combination were studied. The fluorescence quantum yields (Φ_F) of the ZnPc-biomolecule conjugates remain relatively the same as compared to the precursor ZnPcs. However, high Φ_F values were observed for complexes containing substituents such as folic acid and bovine serum albumin that have intrinsic fluorescence properties. The ZnPc-pyrene conjugate also showed high fluorescence quantum yield, as a result of the high fluorescing properties of pyrene. Mono-exponential fluorescence decay curves (indicating one life-time) were obtained for complexes, **1** - **10** and **12**, while complexes **11** and **13** exhibited bi-exponential decay profiles (indication two life-times).

The presence of SWCNTs in the ZnPc derivatives reduces the fluorescence quantum yields for most of the complexes due to photo-induced electron transfer mediated process from the electron-donating phthalocyanine ring to the electron accepting SWCNTs which rapidly deactivates the photo-excited phthalocyanine. Bi-exponential fluorescence decay profiles were observed for all the complexes containing SWCNTs except for mono-substituted carboxy phenoxy ZnPc derivatives.

The triplet quantum yields (Φ_T) of most conjugates (in the absence of SWCNTs) increased when compared to the precursor Pcs. Extended π conjugation resulted in the increase of the Φ_T value for ZnMAPc-py (**2**), while the phenyl bridge connecting the ZnMCPPc (**4**) to respective biomolecule; spermine in **5**, uridine in **6**, ascorbic acid in **7** and **9** (**9** is from ZnTCPPc) resulted in increases in the Φ_T values. Phenyl bridge supports the SOCT-ISC mechanism.

Decreases were observed in the Φ_T values of the ZnPc-biomolecule conjugates in the presence of SWCNTs (**14**, **16 - 18**) and in complexes **20**, **25 - 28**, this is due to photo-induced electron transfer from the Pc ring (electron donor) to SWCNTs (electron acceptor). The Φ_T values for complexes **15**, **19** and **21** increases when compared to the precursor Pcs this is as a result of the fast charge recombination process due to highly short-lived radical ion pair produced.

The singlet oxygen quantum yields (Φ_Δ) of all the synthesized ZnPc-biomolecule conjugates increases when compared to the precursor Pcs these correspond to increases in the Φ_T values. While decreases or increases were observed in the Φ_Δ values in the presence of SWCNTs corresponding to decreases or increases in the Φ_T values.

All the complexes tested on A375 melanoma cells (or MCF-7 breast cancer cells) were relatively not toxic at all the experimental concentrations when the cells were incubated for 24 h in the dark. On exposing the cells to light at varying time after treating the cells in the dark with varying concentrations of respective complexes, the cells viability decreases in an irradiation-time and concentration dependent manner for all the complexes except the ones containing ascorbic acid. From the experiments, ascorbic acid was shown to suppress cell death either through PDT (or PTT) for ZnPc derivatives (or SWCNTs) respectively due to its ability to reduce oxidative DNA damage as a result of its potent reducing properties. The phototoxicity of the conjugates containing SWCNTs was relatively the same as that of the precursor ZnPc-

biomolecule conjugates. This suggests that, although SWCNTs decreases the singlet oxygen quantum yield of the ZnPc complexes, however it improve the phototoxicity of the nanohybrid through its PTT effects.

The findings from this work show the importance of combination therapy which gives the advantage of a dual modality drug protocol, where the ZnPc derivatives are the PDT agents and SWCNTs is the PTT agent.

6.2 Future prospects

Femtosecond laser flash photolysis will give more insight on the kinetics of the photo-induced electron transfer (PET) process from the ZnPcs (or ZnPc-biomolecule conjugates) to the SWCNTs in the nanohybrid of ZnPc-SWCNT (or ZnPc-biomolecule-SWCNT). Electrochemical characterization will also prove useful information on the energy potential of the complexes involve in PET.

The excellent singlet oxygen quantum yield of the low symmetry ZnPcs derivatives in the presence of biological molecule is of particular importance in photodynamic therapy (PDT) and the preliminary cytotoxicity and PDT results show that the complexes are potential PDT agents. Detailed *in vitro* and *in vivo* experiments of these complexes on different cancer cell lines will be required to advance ongoing research on the treatment of cancer. In addition, spermine which resulted in 95% decrease in cell viability after PDT should be incorporated into MPc complexes that are presently in clinical trials. More research on water soluble Pc-ascorbic acid complexes will help investigate the effect of ascorbic acid in reducing the PDT efficiency of Pc. Detailed experiments on the screening effect of SWCNTs that reduces the PDT efficiency of Pc complexes will help advance the science of combination therapy of PDT and PTT.

REFERENCES

[1] I.J. Macdonald, T.J. Dougherty, J. Porphyrins Phthalocyanines, **5** (2001)105.

[2] I. Rosenthal, Photochem. Photobiol., **53** (1991) 859.

[3] R. Bonnett, B.D. Djelal, A. Nguyen, J. Porphyrins Phthalocyanines, **5** (2001) 652.

[4] J.D. Spikes, J. Photochem. Photobiol., B **6** (1990) 259.

[5] S.G. Brown, C.J. Tralau, P.D. Colendge-Smith, D. Akdemir, T.J. Wieman, Br. J. Cancer, **54** (1987) 43.

[6] E.A. Lukyanets, J. Porphyrins Phthalocyanines, **3** (1999) 424.

[7] N.L. Oleinick, A.R. Antunez, M.E. Clay, B.D. Rihter, M.E. Kenney, Photochem. Photobiol., **57** (1993) 242.

[8] T. Nyokong, in: J.H. Zagal, F. Bedioui, J.P. Dodelet (Eds.), N4-Macrocyclic Metal Complexes, Springer, New York, 2006. K.C. Hwang, J. Chem. Soc. Chem. Commun. **2** (1995) 173.

[9] D. Dini, M. Hanack, in: K.M. Kadish, K.M. Smith, R. Guilard (Eds.), The Porphyrin Handbook: Physical Properties of Phthalocyanine-based Materials, vol. **17**, Academic Press, USA, 2003, pp 22-31.

[10] R. Bonnett, Chemical Aspects of Photodynamic Therapy, Gordon and Breach Science Publishers, Amsterdam, 2000.

[11] P. Zimcik, M. Miletin, J. Ponec, M. Kostka, Z. Fiedler, J. Photochem. Photobiol., A **155** (2003) 127.

[12] I. Okura, Photosensitization of Porphyrins and Phthalocyanines, Gordon and Breach Publishers, Germany, 2001.

[13] K.C. Hwang, J. Chem. Soc. Chem. Commun. **2** (1995) 173.

[14] D.B. Mawhinney, V. Naumenko, A. Kuznetzova, Y.T. Yates, J. Am. Chem. Soc. **122** (2000) 2383.

[15] S. Banerjee, T. Hemraj-Benny, S.S. Wong, Adv. Mater. **17** (2005) 17.

[16] K.B. Shelimov, R.O. Esenaliev, A.G. Rinzler, C.B. Huffman, R.E. Smalley, Chem. Phys. Lett. **282** (1998) 429.

[17] L. Edwards, M. Gouterman, J. Mol. Spectrosc. **33** (1970) 292.

[18] A. Henrikson, M. Soundbom, Theor. Chim. Acta **27** (1972) 213.

[19] M. Gouterman, in The Porphyrins, Part A. Physical Chemistry, D. Dolphin (Ed) Academic Press, New York, Vol. **3** (1978) pp 1-165.

[20] C.G. Claessens, U. Hahn, T. Torres, Chem. Rec. **8** (2008) 75.

[21] C.C. Leznoff in: Phthalocyanines Properties and Applications. C.C. Leznoff, A.B.P. Lever, (eds.), VCH, Weinheim. Chapter one, Vol **1** (1989-1996), pp 3-54.

[22] A. Wang, L. Long, C. Zhang, Tetrahedron **68** (2012) 2433.

[23] M.S. Rodríguez-Morgade, G. de la Torre, T. Torres, in The Porphyrin Handbook, K.M. Kadish, K.M. Smith, R. Guilard (Eds.), Academic Press, Elsevier Science, Vol. **15** (2003) Chapter 99.

[24] W.A. Nevin, W. Liu, S. Greenberg, M.R. Hempstead, S.M. Marcuccio, M. Melnik, C.C. Leznoff, A.B.P. Lever. Inorg. Chem. **26** (1987) 891.

[25] T.J. Dougherty, C.J. Gomer, B.W. Henderson, G. Jori, D. Kessel, M. Korbelik, J. Moan, Q. Peng, Review in Photodynamic therapy. J. Natl. Cancer Inst. **90** (1998) 889.

[26] A.P. Castano, T.N. Demidova, M.R. Hamblin, Photodiagn. Photodyn. Ther. **1** (2004) 279.

[27] J. Morgan, A.R. Oseroff, Adv Drug Delivery Rev. **49** (2001) 71.

[28] I.A. Patito, C. Rothmann, Z. Malik, Biol Cell. **93** (2001) 285.

[29] N. Oleinick, Photodyn. News **1** (1998) 6.

[30] E. Ben-Hur, I. Rosenthal, Photochem. Photobiol., **42** (l985) 129.

[31] L.C. Hartmann, G.L. Keeney, W.L. Lingle, T.J. Christianson, B. Varghese, D. Hillman, A.L. Oberg, P.S. Low, Int. J. Cancer **121** (2007) 938.

[32] E. Cameron, A. Campbell, Chem. Biol. Interact. **9** (1974) 285.

[33] E. Cameron, L. Pauling, Proc. Natl. Acad. Sci. U.S.A. **73** (1976) 36859.

[34] E. Cameron, L. Pauling, Proc. Natl. Acad. Sci. U.S.A. **75** (1978) 4538.

[35] M.J. González, E.M. Mora, N.H. Riordan, H.D. Riordan, P. Mójica, Cancer prevent. Int. **3** (1998) 215.

[36] Q. Chen, M.G. Espey, M.C. Krishna, J.B. Mitchell, C.P. Corpe, G.R. Buettner, E. Shacter, M. Levine, Proc. Natl. Acad. Sci. U.S.A. **102** (2005) 13604.

[37] M.J. González, J.R. Miranda-Massari, E.M. Mora, A. Guzmán, N.H. Riordan, H.D. Riordan, J.J. Casciari, J.A. Jackson, A. Román-Franco, Integ Cancer Ther **4** (2005) 32.

[38] B. Nikolić, J. Stanojević, B. Vuković-Gačić, D. Simić, J. Knežević-Vukčević, Food Technol. Biotechnol. **44** (2006) 449.

[39] J. Pliml, F. Sorm. C. Czech, Chem Commun., **29** (1964) 2576.

[40] F. Sorm, J. Vesely, Neoplasma **15** (1968) 339.

[41] K.L. Grove, Y-C. Chene, Cancer Res., **56** (1996) 4187.

[42] S. Nagar, R.P. Remmel, Oncogene, **25** (2006) 1659.

[43] C. Guillemette, R.C. Millikan, B. Newman, D.E. Housman, Cancer Res., **60** (2000) 950.

[44] V.D. Haakensen, M. Biong, O.C. Lingjærde, M.M. Holmen, J.O. Frantzen, Y. Chen, D. Navjord, L. Romundstad, T. Lüders, I.K. Bukholm, H.K. Solvang, V.N. Kristensen, G. Ursin, A-L. Børresen-Dale, Å. Helland, Breast Cancer Res., **12:R65 (**2010) 1.

[45] X.M. He, D.C. Carter, Nature **358** (1992) 209.

[46] E. Frei, Diabetol. Metab. Synd. **3** (2011) 1.

[47] R.J. Bergeron. Acc. Chem. Res. **19** (1986) 105.

[48] I.S. Blagbrough, S, Carrington, A.J. Geall. J. Pharm. Sci. **3** (1997) 223.

[49] J.P. Behr. Acc. Chem. Res. **26** (1993) 274.

[50] N. Schmid, J-P Behr. Tetrahedron Lett. **36** (1995) 1447.

[51] U. Bachrach. Function of Naturally Occurring Polyamines; Academic Press: New York, 1973, pp 63.

[52] C.W. Tabor, H. Tabor. Annu. Rev. Biochem. **53** (1984) 49.

[53] M. Zhang, T. Murakami, K. Ajima, K. Tsuchida, A.S.D. Sandanayaka, O. Ito, S. Lijima, M. Yudasaka, PNAS **105** (2008) 14773.

[54] S. Banfi, E. Caruso, L. Buccafurni, R. Ravizza, M. Gariboldi, E. Monti. J. Organomet. Chem. **692** (2007) 1269.

[55] E. Friso, G. Roncucci, D. Dei, M. Soncin, C. Fabris, G. Chiti, P. Colautti, J. Esposito, L. De Nardo, C.R. Rossi, D. Nitti, F. Giuntini, L. Borsetto, G. Jori, Photochem. and Photobiol. Sci., **5** (2006) 39.

[56] B. Natalia, R. Vittar, J. Awruch, K. Azizuddin, V. Rivarol, Int J Biochem Cell Biol **42** (2010) 1123.

[57] T. Stuchinskaya, M. Moreno, M.J. Cook, D.R. Edwards, D.A. Russell, Photochem. Photobiol. Sci., **10** (2011) 822.

[58] N. Nombona, K. Maduray, E. Antunes, A. Karsten, T. Nyokong, J. Photochem. Photobiol. B: Biol. **107** (2012) 35.

[59] J. Shao, J. Xue, Y. Dai, H. Liu, N. Chen, L. Jia, J. Huang, Eur J. Cancer **48** (2012) 2086.

[60] S. Wang, J. Wang, J-Y. Chen, J. Mater. Chem. B **2** (2014) 1594.

[61] P. Khoza, E. Antunes, J.Y. Chen, T. Nyokong, J. Lumin. **134** (2013) 784.

[62] A. Borgatti-Jeffreys, S.B. Hooser, M.A. Miller, M.D. Lucroy, Am J Vet Res. **64** (2007) 399.

[63] J. Huang, N. Chen, J. Huang, E. Liu, J. Xue, S. Yang, Z. Huang, J. Sun. science in china (series B) **44** (2001) 113.

[64] H.L.L.M van Leengoed, V. Cuomo, A.A.C. Versteeg, N. van der Veen, G. Jori, W.M. Star, Br J Cancer 69 (1994) 840.

[65] S. D'Souza, E. Antunes, C. Litwinski, T. Nyokong, J. Photochem. Photobiol. A: Chem. **220** (2011) 11.

[66] R. Gabrio, D. Donata, M. Filippis, D. Paola, F. Lia, N. Daniele, European patent application No. 2441386C, Filed on 21/03/2001.

[67] M.D.K. Nazeeruddin, R. Humphry-Baker, M. Grätzel, D. Wöhrle, G. Schnurpfeil, G. Schneider, A. Hirth, N. Trombach, J. Porphyrins Phthalocyanines **3** (1999) 230.

[68] K. Sakamoto, E. Ohno, Prog, Org. Coat. **31** (1997) 139.

[69] S. D'Souza, E. Antunes, T. Nyokong, Inorg. Chim. Acta. **367** (2011) 173.

[70] O. Tsaryova, A. Semioshkin, D. Wohrle, V.I. Bregadze, J. Porphyrins Phthalocyanines **9** (2005) 268.

[71] N. Nakashima, Y. Tomonari, H. Murakami, Chem. Lett. **31** (2002) 638.

[72] X. Wang, Y. Liu, W. Qiu, D. Zhou, J. Mater. Chem., **12** (2002) 1636.

[73] D. Kaya, O. Pekcan, Y. Yılmaz, Phys. Rev. E: Stat., Nonlinear, Soft Matter Phys., **69** (2004) 016117.

[74] M.S. Frahn, R.D. Abellon, W.F. Jager, L.H. Luthjens, J.M. Warman, Nucl. Instrum. Methods Phys. Res., Sect. B, **185** (2001) 241.

[75] T. Nyokong, E. Antunes, in The Handbook of Porphyrin Science, ed. K.M. Kadish, K.M. Smith and R. Guilard, World Scientific, Singapore, 2010, ch. 34, vol 7.

[76] M. Ouyang, J-L. Huang, C.M. Lieber, Acc. Chem. Res. **35** (2002) 1018.

[77] N. Nakashima, Int. J. Nanoscience **4** (2005) 119.

[78] C.A. Dyke, J.M. Tour, J. Phys. Chem. A **108** (2004) 11151.

[79] R.H. Baughman, A.A. Zakhidov, W.A. de Heer, Science **297** (2002) 787.

[80] S. Hampel, D. Kunze, D. Haase, K. Kramer, M. Rauschenbach, M. Ritschel, A. Leonhardt, J. Thomas, S. Oswald, V. Hoffmann, B. Buchner, Nanomedicine **3** (2008) 175.

[81] Y. Zhang, Z. Shi, Z. Gu, S. Iijima, Carbon **38** (2000) 2055.

[82] H. Murakami, N. Nakashima, J. Nanosci. Nanotechnol. **6** (2006) 16.

[83] A. Star, Y. Liu, K. Grant, L. Ridvan, J.F. Stoddart, D.W. Steuerman, M.R. Diehl, A. Boukai, J.R. Heath, Macromolecules **36** (2003) 553.

[84] D. Tasis, N. Tagmatarchis, A. Bianco, M. Prato, Chem. Rev. **106** (2006) 1105.

[85] A. Zerda, J-W. Kim, E.L. Galanzha, S.S. Gambhir, V.P. Zharov. Contrast Media Mol Imaging **6** (2011) 346.

[86] Y. Lin, L.F. Allard, Y.P. Sun, J. Phys. Chem. B **108** (2004) 3760.

[87] B. Ballesteros, S. Campidelli, G. de la Torre, C. Ehli, D.M. Guldi, M. Prato, T. Torres, Chem. Commun. **0** (2007) 2950.

[88] N.W.S. Kam, M. O'Connell, J.A. Wisdom, H. Dai, Proc. Natl. Acad. Sci. U.S.A. **102** (2005) 11600.

[89] P. Chaudhuri, S. Soni, S. Sengupta Nanotechnology **21** (2010) 025102.

[90] Z. Jablonski, Phys. **94** (1935) 38.

[91] P.W. Atkins, in Physical Chemistry, P.W. Atkins (Ed.), Oxford University Press, Oxford, 6th Edition, (1998) Chapter 17.

[92] K. Ishii, N. Kobayashi, in The Porphyrin Handbook, K.M. Kadish, K.M. Smith, R. Guilard, (Eds.), Elsevier Science, New York, Vol. **16** (2003) Chapter 102.

[93] J. Fu, X.Y. Li, D.K.P. Ng, C. Wu, Langmuir **18** (2002) 3843.

[94] T.W.J. Gadella Jr, R.M. Clegg, T.M. Jovin, Biomaging **2** (1994) 139.

[95] A. Ogunsipe, J-Y. Chen, T. Nyokong, New. J. Chem. **28** (2004) 822.

[96] H.C. Gerritsen, R. Sanders, A. Draaijer, Proc. SPI **2329** (1994) 260.

[97] A.G. Ryder, S. Power, T.J. Glynn, J.J. Morrison, Proc. SPI **4529** (2001) 102.

[98] T. Förster, Discuss. Faraday Soc. **27** (1959) 7.

[99] J.R. Lakowicz, in Principles of Fluorescence Spectroscopy, Kluwer Academic, New York, 2nd Ed. (1999), p 35.

[100] J. Turro, in Modern Molecular Photochemistry, The Benjamin/Cummings Publishing Co., Inc., New York (1978).

[101] X-F. Zhang, Y. Dia, F. Zhang, J. Photochem. Photobiol. A **203** (2009) 216.

[102] P. Kubat, J. Mosinger, J. Photochem. Photobiol. A: Chem. **96** (1993) 93.

[103] T.H. Tran-Thi, C. Desforge, C. Thiec, J. Phys. Chem. **93** (1989) 1226.

[104] D. Wöhrle, O. Suvorova, R. Gerdes, O. Bartels, L. Lapok, N. Baziakina, S. Makarov, A. Slodek, J. Porphyrins Phthalocyanines **8** (2004) 1020.

[105] M. Niedre, M.S. Patterson, B.C. Wilson, Photochem. Photobiol. **75** (2003) 382.

[106] H. Li, T.F. Guarr, J. Chem. Soc. Chem. Commun. (1989) 832.

[107] N.A. Kuznetsova, N. Gretsova, O. Yuzhakova, V. Negrimovsky, O. Kaliya, E. Luk'yanets, Russ. J. Gen. Chem. **71** (2001) 36.

[108] M.S. Patterson, S.J. Madsen, R. Wilson, J. Photochem. Photobiol. B: Biol. **5** (1990) 69.

[109] P. Modisha, E. Antunes, J. Mack, T. Nyokong, Int. J. Nanosci. **12** (2013) 1350010.

[110] Y. Li, T. M. Pritchett, J. Huang, M. Ke, P. Shao, W. Sun, J. Phys. Chem. A. **112** (2008) 7200.

[111] X-F. Zhang, H-J. Xu, J. Chem. Soc. Faraday Trans. **89** (1993) 3347.

[112] D.S. Lawrence, D.G. Whitten, Photochem. Photobiol. **64** (1996) 923.

[113] A. Ogunsipe, T. Nyokong, J. Photochem. Photobiol. A: Chem., **173** (2005) 211.

[114] M. Durmus, T. Nyokong, Spectrochim. Acta Part A, **69** (2008) 1170.

[115] A.M. Bello, E. Poduch, M. Fujihashi, M Amani, Y. Li, I. Crandall, R. Hui, P.I. Lee, K.C. Kain, E.F. Pai, L.P. Kotra, J. Med. Chem. **50** (2007) 915.

[116] W. Spiller, H. Kliesch, D. Wohrle, S. Hackbarth, B. Roder and G. Schnurpfeil, J. Porphyrins Phthalocyanines, **2** (1998) 145.

[117] A. Fashina, E. Antunes, T. Nyokong, New J. Chem. **37** (2013) 2800.

[118] J. Liu, A.G. Rinzler, H. Dai, J.H. Hafner, H. Jason, R.K. Bradley, P.J. Boul, A. Lu, T. Iverson, K. Shelimov, H. Konstantin, C.B. Huffman, F. Rodriguez Macias, S. Young Seok, R.T. Randall, D.T. Colbert, T. Daniel, R.E. Smalley, Science **280** (1998) 1253.

[119] W. Chidawanyika, T. Nyokong, Carbon **48** (2010) 2831.

[120] E. Beorenfreund, J.A. Puerner. J. Tissue Cult. Meth. **9** (1985) 7.

[121] G. Repetto, A. del Peso, J.L. Zurita, Nat Protoc. **3** (2008) 1125.

[122] M. Alexiades-Armenakas, Clin in Dermatol **24** (2006) 16.

[123] R.R. Allison, G.H. Downie, R. Cuenca, X-H. Hu, C.J.H. Childs, C.H. Sibata, Photodiagonsis photodyn Ther. **1** (2004) 27.

[124] D. Dave, U. Desai, N. Despande, J. Orofac Ress. **29** (2012) 82.

[125] P. Wolf, E. Rieger, H. Kerl, J. Am. Acad. Dermatol. 28 (1993) 17.

[126] S. Gaspard, P. Maillard, Tetrahedron **43** (1987) 1083.

[127] A.Y. Tolbin, V.E. Pushkarev, G.F. Nikitin, L.G. Tomilova, Tetrahedron Lett. **50** (2009) 4848.

[128] İ. Özcesmeci, A. Gelir, A. Gül, Dyes Pigm., **92** (2001) 954.

[129] J. Bartelmess, B. Ballesteros, G. de la Torre, D. Kiessling, S. Campidelli, M. Prato, T. Torres, D.M. Guldi, J. Am. Chem. Soc., **132** (2010) 16202.

[130] T. Nyokong, H. Isago, J. Porphyrins Phthalocyanines, **8** (2004) 1083.

[131] X. Yang, W. Deng, L. Fu, E. Blanco, J. Gao, D. Quan, X. Shuai, J. Biomed. Mater. Res. A **86** (2008) 48.

[132] R. Schneider, F. Schmitt, C. Frochot, Y. Fort, N. Lourette, F. Guillemin, J. Muller, M. Barberi-Heyob, Bioorg. Med. Chem. **13** (2005) 2799.

[133] N. Nombona, W. Chidawanyika, T. Nyokong, Polyhedron **30** (2011) 654.

[134] H. Murakamia, G. Nakamurab, T. Nomuraa, T. Miyamoto, N. Nakashima, J. Porphyrins Phthalocyanines **11** (2007) 418.

[135] B. Ballesteros, G. de la Torre, C. Ehli, G.M. Aminur Rahman, F. Agullo-Rueda, D.M. Guldi, T. Torres, J. Am. Chem. Soc. **129** (2007) 5061.

[136] M.S. Dresselhaus, G. Dresselhaus, A. Jorio, J. Phys. Chem. C **111** (2007) 17887.

[137] E.P. Dillon, C.A. Crouse, A.R. Barron, ACS Nano **2** (2008) 156.

[138] S. Hussain, P. Jha, A. Chouksey, R. Raman, S.S. Islam, T. Islam, P.K. Choudhary, Harsh, Journal of Modern Physics, **2** (2011) 538.

[139] K. Yang, M. Gu, Y. Guo, X. Pan, G. Mu, Carbon **47** (2009) 1723.

[140] A. Sivanesan, S.A. John, Electrochim. Acta **53** (2008) 6629.

[141] S. Sapra, D.D. Sarma, Pramana- J. phys., **65** (2005) 565.

[142] I. Stamatina, A. Morozan, A. Dumitru, V. Ciupina, G. Prodan, J. Niewolski, H. Figiel, Physica E. **37** (2007) 44.

[143] Y. Zhang, X. Sun, L. Pan, H. Li, Z. Sun, C. Sun, B.K. Tay, J. Alloys Compd., **480** (2009) L17.

[144] A.W. Snow, J.R. Griffith, N.P. Marullo, Macromolecules **17** (1984) 1614.

[145] B-P. Jiang, L-F Hu, D-J. Wang, S-C. Ji, X-C. Shen, H. Liang, J. Mater. Chem. B, **2** (2014) 7141.

[146] B. Valeur, in Molecular Fluorescence: Principles and Applications, Wiley-VCH, Weinheim, Germany, 2001.

[147] A. Papadopoulou, R.J. Green, R.A. Frazier, J. Agric. Food Chem. **53** (2005) 158.

[148] X-F. Zhang, X. Li, L. Niu, L. Sun, L. Liu, J. Fluoresc. **19** (2009) 947.

[149] M.T. Colvin, A.B. Ricks, A.M. Scott, D.T. Co, M.R. Wasielewski, J. Phys. Chem. A **116** (2012) 1923.

[150] T. Suzuki, K. Obi Chemical Physics Letters **246** (1995) 130.

[151] J.R. Darwent, P. Douglas, A. Harriman, G. Porter, M-C. Richoux, Coord. Chem. Rev. **44** (1982) 83.

[152] I. E. Borissevitch, T. T. Tominaga, C. C. Schmitt, J. Photochem. Photobiol. A: Chem. **114** (1998) 201.

[153] G. Bottari, G. de la Torre, D.M. Guldi, T. Torres, Chem. Rev., **110** (2010) 6768

[154] G. Bottari, J.A. Suanzes, O. Trukhina, T. Torres, J. Phys. Chem. Lett., **2** (2011), 905.

[155] A. Sastre, A. Gouloumis, P. Vázquez, T. Torres, V. Doan, V.B.J. Schwartz, F. Wudl, L. Echegoyen, J. Rivera, Org. Lett., **1** (1999), 1807.

[156] X. Shu, S. Diego, R.Y. Tsien, L. Jolla, United States patent application No. US 2013/0330718 A1, Filed on 12/12/2013.

[157] M. Gracanin, C. Hawkins, D. Pattison, M.J. Davies, Free Radical Biol. Med. **47** (2009) 92.

[158] A. Wright, W.A. Bubb, C.L. Hawkins, M.J. Davies, Photochem. Photobiol. **76** (2002) 35.

[159] A. Hartschuh, H.N. Pedrosa, J. Peterson, L. Huang, P. Anger, H. Qian, A.J. Meixner, M.Steiner, L. Novotny, T. D. Krauss, Chem. Phys. Chem. **6** (2005) 1.

[160] J. Combs, F. Gerald, The Vitamins. 4th ed. Burlington: Elsevier Science; 2012.

[161] J.W. Erdman, I. MacDonald, S.H. Zeisel, International Life Sciences Institute. Present knowledge in nutrition. 10th ed. Ames, Iowa: International Life Sciences Institute; 2012.

[162] A.C. Carr, B. Frei, Am. J. Clin. Nutr. **69** (1999) 1086.

[163] K.B. Michels, L. Holmberg, L. Bergkvist, H. Ljung, Å. Bruce, A. Wolk, Int. J. Cancer: **91** (2001) 563.

[164] T. Subramani, S.K. Yeap, W.Y. Ho, C.L. Ho, A.R. Omar, S.A. Aziz, N.M. Rahman, N.B. Alitheen, J Cell Mol Med **18** (2014) 305.

[165] S. Zhang, D.J. Hunter, M.R. Forman, B.A. Rosner, F.E. Speizer, G.A. Colditz, J.E. Manson, S.E. Hankinson, W.C. Willett, J. Natl. Cancer Inst. **91** (1999) 547.

[166] N. Roswall, A. Olsen, J. Christensen, L.O. Dragsted, K. Overvad, A. Tjonneland, Eur J Cancer Prev. **19** (2010) 360.

[167] F. Lamarche, V. Sol, Yi-M. Huang, R. Granet, M. Guilloton and P. Krausz, J. Porphyrins Phthalocyanines, **6** (2002) 130.

[168] N.V.S.D.K. Bhupathiraju, M.G.H. Vicente, Bioorg. Med. Chem., **21** (2013) 485.

[169] E. I. Sagun, E. I. Zenkevich, V. N. Knyukshto, A. M. Shulga, D.A. Starukhin and C. von Borczyskowski, Chemical Phys., **275** (2002) 211.